SOME STUDIES ON MACHINING CHARACTERISTICS OF WIRE ELECTRO DISCHARGE MACHINING OF Ti$_{50}$Ni$_{50\text{-}X}$Co$_{X}$ (X=1, 5 AND 10 AT. %) SHAPE MEMORY ALLOYS

Thesis

Submitted in partial fulfillment of the requirements for the degree of

DOCTOR OF PHILOSOPHY

By

HARGOVIND SONI

DEPARTMENT OF MECHANICAL ENGINEERING

NATIONAL INSTITUTE OF TECHNOLOGY KARNATAKA

SURATHKAL, P.O. SRINIVASNAGAR, MANGALORE-575 025

SEPTEMBER, 2018

D E C L A R A T I O N

I hereby *declare* that the Research Thesis entitled **"SOME STUDIES ON MACHINING CHARACTERISTICS OF WIRE ELECTRO DISCHARGE MACHINING OF $Ti_{50}Ni_{50-X}Co_X$ (X=1, 5 AND 10 AT. %) SHAPE MEMORY ALLOYS"** which is being submitted to the **National Institute of Technology Karnataka, Surathkal** in partial fulfillment of the requirements for the award of the Degree of **Doctor of Philosophy** in **Department of Mechanical Engineering** is a *bonafide report of the research work carried out by me.* The material contained in this Research Thesis has not been submitted to any University or Institution for the award of any degree.

Register Number   : **148057ME14F16**

Name of the Research Scholar: **Hargovind Soni**

Signature of the Research Scholar:

Department of Mechanical Engineering, National Institute of Technology Karnataka, Surathkal

Place: NITK, Surathkal

Date: 17/09/2018

C E R T I F I C A T E

This is to *certify* that the Research Thesis entitled **"SOME STUDIES ON MACHINING CHARACTERISTICS OF WIRE ELECTRO DISCHARGE MACHINING OF $Ti_{50}Ni_{50-X}Co_X$ (X=1, 5 AND 10 AT. %) SHAPE MEMORY ALLOYS"** submitted by **Mr. Hargovind Soni** (**Register Number: 148057ME14F16**) as the record of the research work carried out by him, is *accepted as the Research Thesis submission* in partial fulfilment of the requirements for the award of degree of **Doctor of Philosophy.**

Research Guides

Dr. Narendranath S.
Professor & Head
Dept. of Mech. Engg.

Dr. Ramesh M R
Associate Professor
Dept. of Mech. Engg.

Chairman - DRPC

Date:

Dedicated to …….

My beloved father and my family members

&

All of my teachers and colleagues who encouraged me with positive thoughts….

ACKNOWLEGEMENT

(HARGOVIND SONI)

CHAPTER	CONTENTS	Page No.

LIST OF FIGURES

LIST OF TABLES

ABBREVIATIONS

Symbols	Definitions
SMAs	Shape memory alloys
WEDM	Wire electro discharge machining
EDM	Electro discharge machining
VAM	Vacuum arc melting
Ton	Pulse on time
Toff	Pulse off time
SV	Servo voltage
WS	Wire speed
SF	Servo Feed
GRA	Grey relational analysis
RSM	Response surface methodology
MRR	Material removal rate
SR	Surface roughness
DOE	Design of Experiments
ANN	Artificial Neural Network
μs	Micro Second
SV	Servo voltage
Mu	Machine Unit
M/min	Meter /minute
μm	Microns
Mm^3/min	Millimetre^3/minute

CHAPTER 1

INTRODUCTION

In this Chapter, introduction of shape memory alloys, conventional machining, non-conventional machining of shape memory alloys, machining process parameters, machining responses, optimization techniques, characterization and prediction techniques are presented.

1.1 SHAPE MEMORY ALLOY

Materials capable to regain their original shape when temperature or load is increased or decreased are called shape memory alloys (SMAs). These materials are attractive for many applications in several fields due to their excellent properties such as shape memory effect and pseudo elasticity (Wei et al. 1998). TiNi based shape memory alloys are most popular shape memory alloys because they are having two way shape memory effect and exhibit more corrosion resistance (Jiang et al. 2014; Liu et al. 2005). Shape memory alloys materials exhibit a thermomechanical behavior induced by the occurrence of phase transformations. They are having two types of phase transformation one is austenite phase with cubic crystal structure and second is martensitic phase with monoclinic crystal structure (Ibrahim, Elbagoury, and Fouad 2011; Kong et al. 2011; Wang et al. 2005). Phase transformation from the austenite phase to martensitic phase in these alloys does not occur by diffusion of the atom but rather by shear lattice distortion, such kind of transformation called as martensitic transformation. Each martensitic crystal formed can have a different orientation direction called a variant. The assembly of martensitic variants can exist in two forms: twined martensite (M^t), which is formed by a combination of self-accommodated martensitic variants, and de-twinned or reoriented martensite with a specific variant (M^d). Shape memory alloys are widely used in aircraft applications, robotics applications and medicine applications etc.

1.2 TYPE OF SHAPE MEMORY ALLOYS

There are three types of shape memory alloys namely TiNi based, Copper-based and Iron-based shape memory alloys. Table 1.1 exhibits the Introduction of all three alloys.

Table 1.1 Types of shape memory alloys (Wei et al. 1998).

Shape memory alloys	Introduction
TiNi based	TiNi shape memory alloys developed by Buehler and his staff in 1960. TiNi based shape memory alloys are most popular for various applications such as biomedical, robotics, aerospace etc. because these alloys show strong shape memory effect, two-way shape memory effect, pseudoelastic behavior, corrosion resistance and biocompatibility under the right situations.
Copper-based	Cu- based alloys are a good alternative to TiNi based alloy due to their excellent thermal and electrical conductivity. Cu based alloys create less hysteresis than TiNi, with the transformation temperatures in Cu-based alloys highly dependent on the composition. Cu- based shape memory alloys are relatively economical than TiNi based shape memory alloys
Iron-based	Iron-based shape memory alloys (FeNiCoTi and FemnSi) are purely ferrous alloys. These alloys having great potential in civil engineering structures and exhibit shape memory effect after the specific thermomechanical treatment. Fe–Mn–Si alloys have a temperature transformation hysteresis (~ 150°C) and a higher elastic stiffness than TiNi based alloys. They also exhibit a good workability, corrosion resistance and weldability (A.Cladera, B.Weber, C.Leinenbach, C.Czaderski, M.Shahverdi 2014).

1.3 PROPERTIES OF SHAPE MEMORY ALLOYS

Shape memory alloys having excellent properties such as shape memory effect, pseudo elasticity and cyclic behaviour. Table 1.2 indicates the properties and their effects.

1.3.1 Shape memory effects

Shape memory alloys exhibit the shape memory effects when it is deformed while in the twinned martensite phase and then unloaded while at a temperature below austenite start. When it is subsequently heated above austenite finish, the shape memory alloy will regain its original shape by transforming back into the parent austenite phase. Sometime these alloys exhibit the two-way shape memory effects. Moreover, these alloys show repeatable shape changes without applied mechanical load when subjected to a cyclic thermal load; this behavior is called two-way shape memory effects (Lagoudlas 2008).

1.3.2 Pseudoelasticity

Pseudo elasticity is from the reversible motion of domain boundaries during the phase transformation, rather than just bond stretching or the introduction of defects in the crystal lattice (thus it is not true super elasticity but rather pseudo elasticity). Even if the domain boundaries do become pinned, they may be reversed through heating. Thus, a pseudo elastic material may return to its previous shape (hence, shape memory) after the removal of even relatively high applied strains. One special case of pseudo elasticity is called the Bain Correspondence. This involves the austenite/martensite phase transformation between a face-centered crystal lattice (FCC) and a body-centered tetragonal crystal structure (BCT). Superelastic alloys belong to the larger family of shape-memory alloys. When mechanically loaded, a superplastic alloy deforms reversibly to very high strains (up to 10%) by the creation of a stress-induced phase. When the load is removed, the new phase becomes unstable and the material regains its original shape. Unlike shape-memory alloys, no change in temperature is needed for the alloy to recover its initial shape.. Initially, the material is in the austenitic phase. The simultaneous transformation and de-twinning of the martensitic variants start at a point and results in fully transformed and de-twinned

martensite. Upon unloading, the reverse transformation starts. Finally, at the end of the loading path the material is again in the austenitic phase.

Table 1.2 Shape memory alloy properties and their effects (Goryczka et al. 2005).

S. No.	Properties	Effects
1	Shape memory effect	The material can be used as an actuator, providing force during shape recovery
2	Pseudoelasticity	The material can be stressed to provide large, recoverable deformations at relatively constant stress levels
3	Hysteresis	Allows for dissipation of energy during a pseudoelastic response
4	High actuation stress (400–700 MPa)	Small component cross-sections can provide substantial forces
5	High actuation strain (8%)	Small component lengths can provide large displacements
6	High energy density (~1200 J/kg)	A small amount of material required to provide substantial actuation work
7	Three-dimensional actuation	Polycrystalline SMA components fabricated in a variety of shapes, providing a variety of useful geometric configuration
8	Actuation frequency	The difficulty of quickly cooling components limits use in high frequency applications
9	Energy efficiency (10–15%)	Amount of thermal energy required or actuation is much larger than mechanical work output
10	Transformation-induced plasticity	Plastic accumulation during cyclic response eventually degrades material and leads to failure

1.4 APPLICATIONS OF SHAPE MEMORY ALLOYS

1.4.1 Aerospace

Due to increase demand for multi-functionality and reliability in the aerospace industry, shape memory alloys are attractive material for scientist across the world in this area for aerospace applications. Shape memory effect and pseudo elasticity properties are attractive these materials in wing aircraft, spacecraft, and rotorcraft areas (Jani et al. 2014).

1.4.2 Medicine

Shape memory alloys are used in medical applications due to pseudoelasticity; shape memory effects, biocompatibility, and corrosion resistance (Petrini and Migliavacca 2011). Table 1.3 indicates the applications of shape memory alloys for biomedical applications due to pseudoelasticity and shape memory effects. Fig. 1.1 exhibit medical application where Fig. 1.1 a and Fig. 1.1b SMA orthodontic wires, Fig. 1.1c Palatal arches and Fig. 1.1d Orthodontic distracters.

Table 1.3 Medical application of Shape memory alloys (Petrini and Migliavacca 2011).

Application	Pseudoelasticity	Shape memory effects
Orthodontic field	Wires, distractors, palatal arches, endodontic files.	Wires
Vascular field	Venous filters, devices for closing ventricular septal defects, self-expandable vascular stents, stent-graft, percutaneous devices to treat valvular diseases	Venous filters, devices for closing ventricular septal defects
Neurosurgical Field Surgical field	Coils, stents, micro guidewires.	Mini-invasive surgical instruments
Orthopaedic field	Intraspinal implants, intramedullary nails	Staples or plates, devices for correcting scoliosis, spinal

		vertebrae spacer, intramedullary nails, devices for physiotherapy
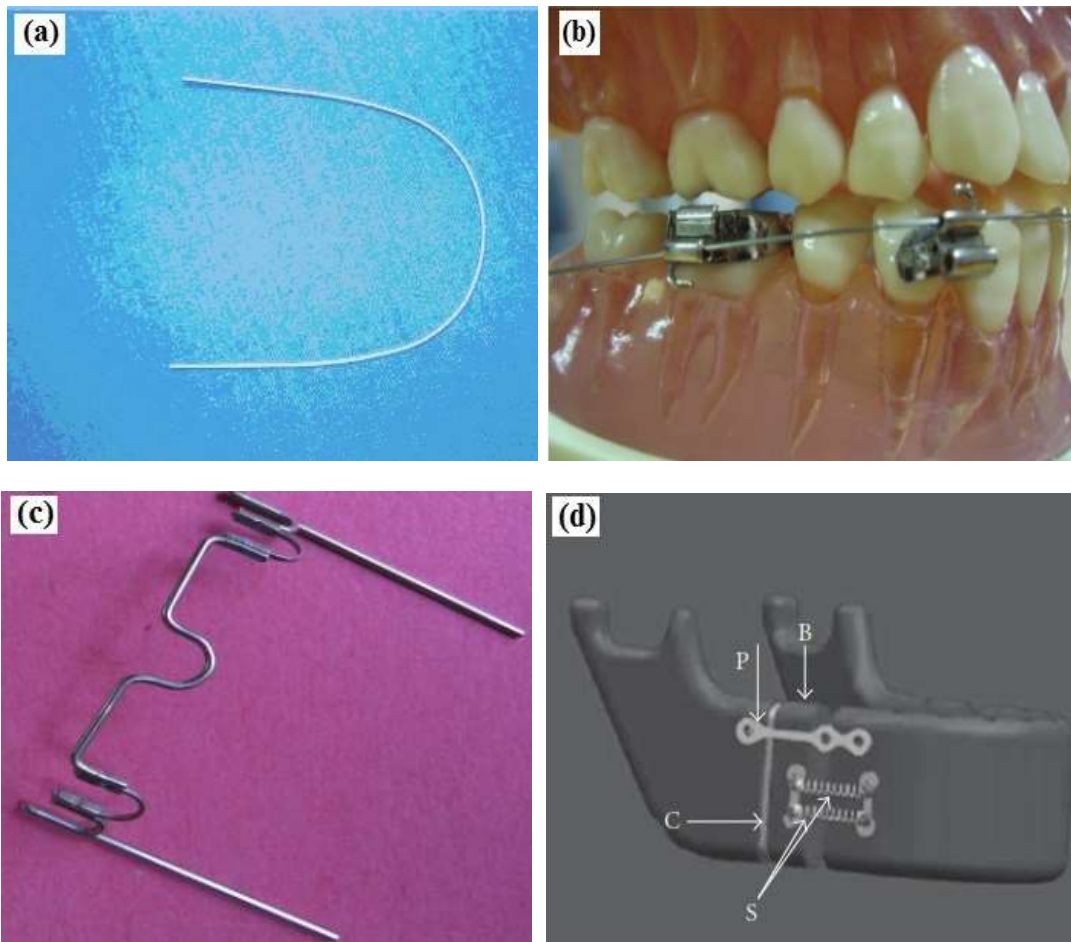
Figure 1.1 SMA orthodontic wires (a and b), Palatal arches (c) and
Orthodontic distracters (d) (Petrini and Migliavacca 2011).

1.5 MACHINING OF SHAPE MEMORY ALLOYS

Machining of shape memory alloys is very difficult through conventional machining because they may affect the internal properties of shape memory alloys. Therefore non-conventional machining can be used for machining of such kind of alloys such as wire electro-discharge machining, electrochemical machining, laser beam machining and water jet machining etc. Wire electro-discharge machining achieving high

precision and quality of cut of surface and, therefore, this method is a most suitable process to be machined for all conductive machining (Ablyaz and Muratov 2017). To achieve high precision and surface quality through any machining process their input process parameters play a very important role during the machining. Moreover, wire electro discharge machining has been classified into various physical characteristics which can be seen in Fig 1.2. However they have divided into different types of machine features affecting the performance measures, machining capacity and auxiliary facilities (Ho et al. 2004).
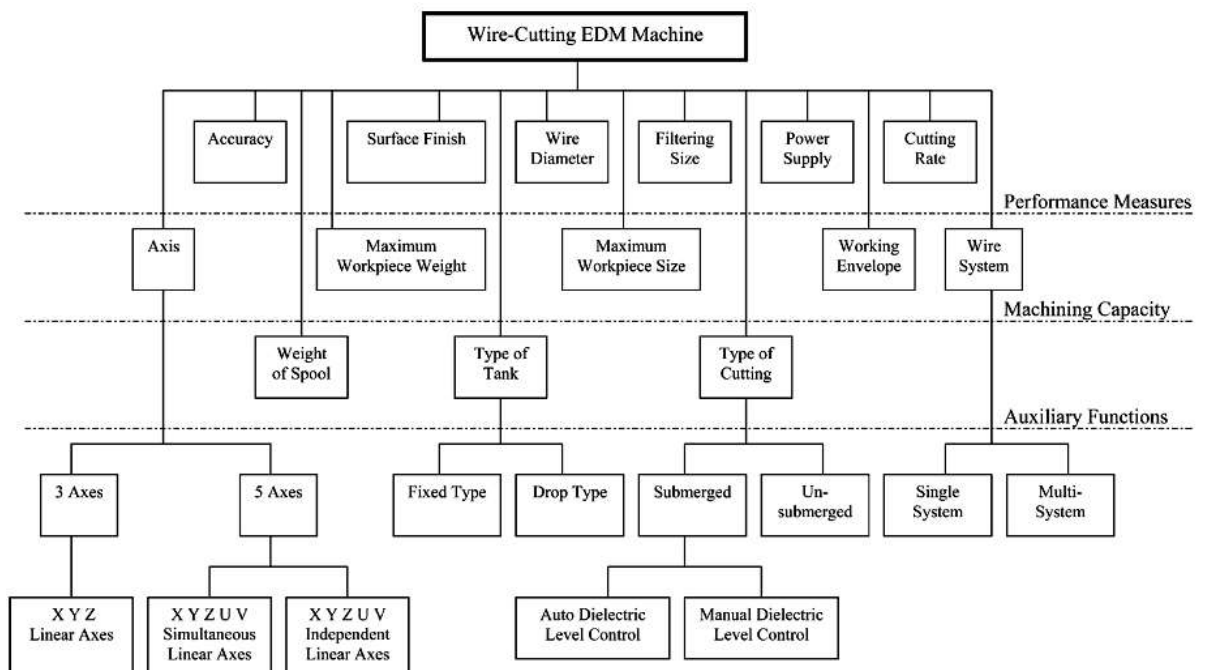
Figure 1.2 Classifications of wire electro discharge machining (Ho et al. 2004).

1.5.1 Working principle of WEDM

Wire electro-discharge machining is a thermoelectric process, which removes the materials from the workpiece surface through spark erosion in machining zone. In wire electro-discharge machining wire is used as a tool electrode and workpiece make anode, mostly deionized water used as a dielectric fluid which continuously flows in the machining area through the nozzle. Wire and workpiece both are connected by DC power supply maintaining constant gap. The size of this gap may be the half of the wire diameter and also this gap called spark gap. During the WEDM process wire

such as brass wire, zinc coated brass are used as a tool and workpiece materials should be conductive. Fig. 1.3 exhibits the working principle of WEDM process. There are three important parts of WEDM which are as follows.

- Generator
- Servo system
- Dielectric system
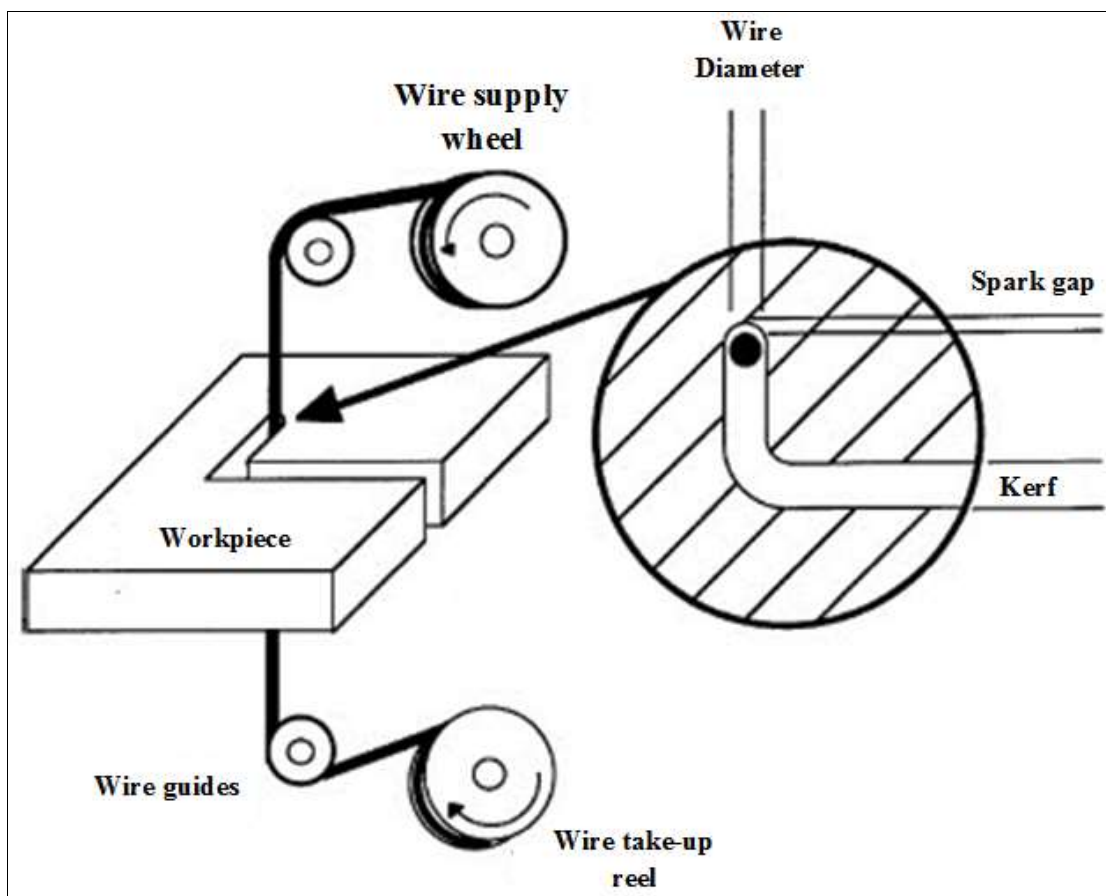
Figure 1.3 Working principle of WEDM (Ghodsiyeh et al. 2013).

1.5.1.1 Generator

In the EDM process, electrical energy in the form of short duration impulses is required to be supplied to the machining gap. For this purpose, specially designed generators are employed. The generators for spark erosion are distinguished according to the way in which the voltage is transformed and the purpose is controlled and also

on the basis of the characteristics of discharge. Modern EDM machines employ controlled pulse generators which enable easy variation of spark frequency and intensity of the discharge. The pulse generators are invariably provided with an electronic interrupter which could switch high current flows.

1.5.1.2 Servo system

The servo system controls the gap between the tool and workpiece in EDM. The servo gets its input signal from the difference between a selected reference voltage and the actual voltage across the gap. The signal is amplified and the tool, as it wears a little, is advanced by the hydraulic control. A short circuit across the gap causes the servo to reverse the motion of the tool until the correct gap is established. The essential requirements of a servo system for use in EDM is (a) to locate the tool accurately in relation to the work surface, (b) high sensitivity to change in gap conditions, (c) low inertia, (d) quick response and (e) maintenance of constant gap (Liao et al. 1997).

1.5.1.3 Dielectric fluid

Deionized water used as dielectric fluid mostly during wire electro-discharge machining because of its desirable thermal properties such as low viscosity and pollution free working for WEDM and deionized water has no fire hazard, high cooling rate result in higher material removal rate. Low viscosity helps in efficient flow with high cooling rate yields very thin recast layer, therefore, deionized water is used to as dielectric fluid. Other than deionized water kerosene also used as dielectric fluid during wire electro-discharge machining. The important requirements of a dielectric fluid to be used in WEDM process- are mentioned below.

- Remain electrically non-conducting until the required breakdown voltage has been reached.
- Should have high dielectric strength.
- Rapidly quench the spark or demonize the spark or spark gap after the discharges have occurred.
- Have a good degree of fluidity.

1.5.2 Process parameters of WEDM

Process parameters of WEDM play important role in controlling the machining process and to achieve higher material removal rate with better surface roughness. Since WEDM process parameters influence machining characteristics, this section is dedicated to detailed explanation of influence of process parameters on machining responses. Some important process parameters are follows:

1.5.2.1 Pulse on time

Pulse on time is the time interval of spark allowed per cycle. Pulse on time is most important parameters for wire electro-discharge machining. Higher values of pulse on time give higher material removal rate (Soni et al. 2017) but more frequent wire breakage seems at the higher values of this parameter hence the range 100-129 μs of this parameter will be different for different materials. This parameter should be optimized for a particular material.

1.5.2.2 Pulse off time

Pulse off time (Toff) indicates the duration of time in microsecond (μs), between two simultaneous sparks. The range of this parameter is 0-63 μs during wire electro-discharge machining which is applied in steps of 1 unit, moreover, the voltage is absent during this part of the cycle. Material removal rate and surface roughness are decreased with increase in pulse off time, which is due to decrease in spark intensity as more time is required for flowing dielectric fluid leading to low MRR. At high pulse off time, most of the molten metal is flushed away from the machined surface and reduce the formation of craters and micro globules hence leading to low surface roughness (Manjaiah et al. 2015).

1.5.2.3 Servo voltage

Servo voltage is another important process parameter for wire electro discharge machine which sends signals to servo system through gap voltage sensor to control a predetermined gap between tool and workpiece. The range of the servo voltage is 1-100 V in wire EDM. The increase in servo voltage, results in decrease of materials removal rate and surface roughness because increase in servo voltage results in larger

spark gap thereby reducing the spark intensity and eventually lesser amount of material is removed from the surface of the workpiece which leads to lower MRR (Kumar et al. 2017).

1.5.2.4 Wire feed

Wire feed indicate the speed at which the wire-electrode travels along the wire guide path and is fed continuously for sparking. The range of this parameter is 1-15 m/min as perused WEDM for present work. For better machining performance and stability wire feed should be set to the maximum.

1.5.2.5 Spark gap

The distance between the tool and workpiece is called the spark gap in the WEDM process. Generally, the size of this gap is half of the wire diameter in wire electro discharge machine. Fig. 1.4 exhibits the systematic diagram of spark gap of machining zone in wire electro discharge machining. The arc column diameter increases with the passage of time and was equal to the diameter of the generated discharge crater (Ojha et al. 2010).
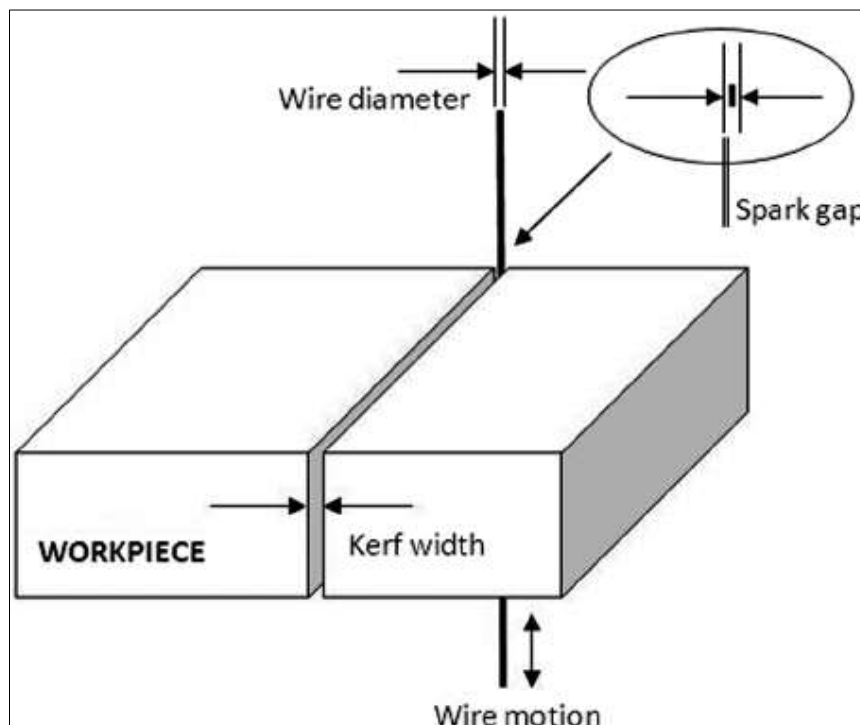
Figure 1.4 Schematic view of discharge gap (Karthikeyan et al. 1997).

1.5.2.6 Servo feed

Servo feed setting decides the servo speed. The servo speed, at the set value of servo feed, can vary in proportion to the gap voltage (normal feed mode) or can be held constant while machining (with constant feed mode).

1.5.2.7 Peak current

The peak current (IP) exhibit the maximum value of the current passing through the electrodes for the given pulse. Machining at higher values of peak current leads to the generation of higher heat energy.

1.6 APPLICATIONS OF WIRE ELECTRO DISCHARGE MACHINING

Wire electro discharge machining is used for machining of all conductive and semi conductive materials in many areas which are following-

- Semiconductor applications, Aerospace, Electronics and Medical
- Die & Tool making industries.
- For cutting the hard Extrusion Dies
- In making Fixtures, Gauges & Cams
- Cutting of Gears, Strippers, Punches and Dies
- Manufacturing hard Electrodes.
- Manufacturing micro-tooling for Micro-EDM, Micro-USM and such other micromachining applications.

1.7 DESIGN OF EXPERIMENT (DOE)

Design of experiment plays an important role in Design for Reliability (DFR) programs, allowing the simultaneous investigation of the effects of various factors and thereby facilitating design optimization. Some important DOE methods are response surface design, Taguchi design, and full factorial, but in the present study response surface design method is used to create an experimental plan.

1.8 OPTIMIZATION TECHNIQUES

Optimization techniques are important to obtain a combination of process parameters for the expected outputs. There are two types of optimization techniques first is single objective optimization techniques and another is multi-objective optimization techniques. When objectives are two and more, multi-objective optimization

techniques are used for optimization of process parameters. There are many multi-objective optimization techniques available such as Grey relational analysis, entropy measurement, generate algorithm response surface method, teaching-learning optimizations techniques etc. But in the present study hybrid combination of multi-objective optimization techniques such as grey relational analysis, entropy measurement and response surface methodology is used to find the best combination of process parameters.

1.8.1 Grey relational analysis and entropy measurement method

Grey relational analysis (GRA) is developed by Julong Deng (1989) therefore it is also known as Deng's Grey model. GRA is a most popular grey system which uses a specific concept of information. In GRA there are two systems one is black and another is a white system where black system indicates no information data in the system while white shows the perfect information data in the system. However, GRA is a practical analytical optimization method which provides suitable tools for examining a rank of order of multiple objects with resemblance from an objective. GRA requires limited information to estimate the behavior of an uncertain system and discrete data problem. If the sequence range is large, the factors are effaceable therefore data pre-processing is an important step to manage the factors of GRA. The range of data pre-processing is from zero to one. For the data pre-processing, there are three conditions of normalization namely higher the best, lower the best and nominal the best, user can choose any conditions according to their requirement during the study. In the present study higher the better is used in the normalization of MRR and another one is lower the better for normalization of SR. In GRA, the weights of each quality characteristics are determined. Entropy measurement method is an objective weighting method. Discrete type of entropy is used in grey entropy measurement for properly conduct weighting analysis and calculating grey relational grade.

1.8.2 Response surface methodology

Response surface methodology (RSM) investigates the communication between many illustrative variables and one or more response variables. The most essential application of this approach is to utilize a series of designed experiments to get best

response. Commonly a second-degree polynomial model is used in this approach. Even though these models are just a prediction, such a model is easy to estimate and apply. RSM is used in the present work as a design of experiment method for design the experimental plan and analysis of grey relational grade in the optimization technique.

1.8.3 Artificial neural network

An artificial neural network (ANN) is an information-processing system that has certain performance characteristics in common with biological neural networks. Generally, an ANN is made up of some neurons connected together via links. Among various neural network models, the feed-forward neural network based on back-propagation is the best general-purpose model (Pant et al. 2014). An artificial neural network approach is an effective tool to predict process parameters; it can generate the outputs for a set of inputs that are within the range of the original inputs during the training phase. ANN will be used for prediction the material removal rate and surface roughness in the present study.

THESIS OUTLINE

The thesis consists of six chapters.

CHAPTER -1

In this Chapter, introduction of shape memory alloys, machining of shape memory alloys, conventional machining, non-conventional machining of these alloys, machining process parameters, machining responses, optimization techniques, characterization and prediction techniques are presented.

CHAPTER -2

This chapter presents critical review of the published literature relevant to the present study. Comprehensive review of the existing literature on TiNiCo shape memory alloy, machining of shape memory alloys, machining performances and machined surface characterization. Major focus of literature is on advanced machining (Wire electro discharge machining) of shape memory alloys, parametric optimization of process parameters and error analysis during the machining was also debated.

CHAPTER -3

This chapter contains description of experimental equipments and procedures adopted for development of TiNiCo shape memory alloy, WEDM machining at optimized process parameters and characterization of machined surface.

CHAPTER -4

This chapter describes the WEDM machining characteristics. Results are discussed critically in view of the existing literature. Machining has been carried out as per L-33 orthogonal array and measured the responses such as material removal rate and surface roughness for all three alloys ($Ti_{50}Ni_{49}Co_1$, $Ti_{50}Ni_{45}Co_5$, and $Ti_{50}Ni_{40}Co_{10}$ shape memory alloys). Multi objective optimization technique (grey relational analysis) was adopted for optimization of process parameters, and machined surface characterization was performed on machined surface at optimized process parameters.

CHAPTER -5

It is observed that pulses on time and servo voltage are most influential process parameters for machining of TiNiCo shape memory alloys. Therefore in the present

chapter two parameter approach has been adopted to observe deeply the effect of pulses on time and servo voltage on the machining of different compositions of TiNiCo shape memory alloys. The machined surface characterization is carried out at lower and higher values of responses. Machining as per L-25 orthogonal array has been carried out and machining performance MRR and SR are measured. Moreover, in this chapter error analysis has been carried out considering two parameter approach during the machining of all three alloys. This chapter presents the comparison between experimental and predicted values. Prediction was done using artificial neural network approach.

CHAPTER -6

This chapter summarizes the conclusions from the results found within the present research. Also the scope for future work in the area of TiNiCo alloy and key contributions of present study are presented in this chapter.

CHAPTER 2

LITERATURE REVIEW

This chapter contains a comprehensive review of the literature with a special reference to TiNiCo shape memory alloy, WEDM machining, machining performances, parametric optimization to obtain the best optimization of process parameters and machined surface characterization. The objectives of the present work have been formulated after critical analysis of the literature towards the end of this chapter.

2.1 SHAPE MEMORY ALLOYS

NiTi-based shape memory alloys (SMAs) are unique class of shape memory material which recover their original shape when temperature and load are varied. Due to their excellent properties, SMAs are being used in many biomedical and engineering applications (Lekston et al. 2012; Nam et al. 1990). SMA shows outstanding properties such as super elasticity, shape memory effect, corrosion resistance, high specific strength, biocompatibility, greater ductility and elastic modulus (Manjaiah et al. 2015). Due to excellent biocompatibility, TiNi based shape memory alloys are used for biomedical applications such as bone staple, stone extraction baskets, cardiovascular stents, catheter guide wires and other biomedical devices (Dadbakhsh et al. 2016). The properties of SMAs can be increased by adding a third element in TiNi replacing Ni with Co, Cu, Ag, Au, Hf, Zr and Cr etc. Substitution of Cu for Ni in TiNi alloys is known to produce a stable shape memory effect, reduce the transformation stresses, narrow temperature hysteresis, and composition insensitivity compared with the TiNi binary alloys. Moreover the addition of Cu (Up to 10 at. %), the transformation hysteresis is much smaller than for binary alloy at the expense of the total transformation strain which is reduced to nearly 4.0% in NiTi (Lekston et al. 2012). By adding Hf in TiNi high temperature shape memory alloys can be developed which are referred to as materials with a phase transformation temperature higher than 100°C, have increasingly gained interest in the robotic, automotive and aerospace fields (Kim et al. 2016). Zr is another element which can be suitable in developing high temperature shape memory alloys. McCluskey et al.(2014) reported that

martensitic start (Ms) temperature of ternary alloy films found to increase with increasing Zr content when it is higher than 10 at%. The highest Ms temperature attained was ~170°C for films containing 19.5 at% Zr. Moreover Critical stress against plastic deformation increases with increasing Zr content up to 10 at%. Although further increase in Zr content resulted in embrittlement of the alloy films, Ti32.3Ni48.2Zr19.5 film showed a shape memory effect with recoverable strain of ~1.3% under a constant stress of 250 MPa. This suggests that the TiNiZr alloy film can be a candidate for cantilever type micro-actuators. Similarly addition of Ag in to TiNi can improve antibacterial properties (Zheng et al. 2011). It is reported that adding certain noble elements such as Pd, Pt and Au can slightly decrease the SMA's hysteresis at certain precise concentrations (Shi et al. 2014). The addition of Cr has attracted much attention because it not only adjusts the transformation temperatures but also results in improvement of mechanical properties, such as yield stress, stiffness and workability fatigue life (Tong et al. 2014).

2.2 TiNiCo ALLOY

In 1971, elastic properties of TiNiCo shape memory alloy wires were evaluated by Andreasen to develop TiNi-based shape memory alloys for medical application (Y.J Huang et al. 2014). JING Rui-rui et al. (2007) studied on the influences of Co-addition on phase transformation behaviour and mechanical properties, they were reported that a substitute for Ni, with Co in to NiTi alloys can marginally decrease the martensite transformation temperature and R Phase transformation are accordingly separated. $Ti_{50}Ni_{48}Co_2$ alloy exhibits good ductility with a lower stress plateau caused by stress-induced martensite, martensite reorientation and also the addition of Co resulted in higher yield strength. A fracture elongation of more than 20% was obtained for $Ti_{50}Ni_{48}Co_2$ (Zheng et. al. 2004). It is shown (Drugacz et al. 1995 and J. Rui- rui et al. 2004) that when compared to binary alloys, the addition of Co in NiTi alloy increases the loading plateaus and workability. It is observed that $Ti_{50}Ni_{50-x}Co_x$ (x=1-2) alloys exhibit about 30 % higher modulus, loading plateau, and unloading plateau as compared to the binary alloy. Drugacz et al. (2002) evaluated the biocompatibility performance of TiNiCo alloys and reported that no reactivity occurred during cytotoxicity and hemolysis test. The application of TiNiCo

alloy, clamps for surgical treatment of mandible fractures facilitates treatment while ensuring stable fixation of the bone fragments. No pathologic tissue reactions to the implants were observed in either humans or animals.

2.3 MACHINING OF SHAPE MEMORY ALLOYS

The high ductility, severe work hardening and unique pseudoelastic behaviour in TiNi SMAs cause their machining to be quite complicated (Weinert et al. 2004) and it is difficult to machine TiNi alloy using traditional machining such as mechanical drilling, cutting and shaping. Non-traditional machining processes exhibit an excellent ability for machining of shape memory alloys. The machining of SMAs is relatively important and integral part in the production of components for utilization in engineering applications.

2.3.1 Traditional machining

The machining of shape memory alloys through conventional machining such as milling, turning, drilling is very difficult due to their poor performance such as poor surface finish, dimensional accuracy and also affects the internal properties (pseudoelasticity, shape memory behaviour etc.) of shape memory alloys. Due to high reactivity of titanium alloy with the cutting tools, low heat conductivity, high strength at elevated temperatures and low elastic modulus result in increased temperatures at the tool-chip interface there by workpiece distortions and rapid tool wear are likely to occur (Zailania et al. 2016). The high tool wear rate and poor surface quality during the traditional machining of TiNi shape memory alloy which reduce the applications of shape memory alloys (Kaynak et al. 2013). Kowalczyk et al. (2017) and Markopoulos et al. (2015) observed the difficulties of conventional machining of TiNi shape memory alloys and reported that traditional machining affect internal properties such as pseudoelastic behaviour and ductility. Hassan et al. (2014) reported the presence of surface defects in Ni-Ti alloy during traditional machining processes in the forms of feed marks, surface drag, debris of microchips, surface plucking, tearing surface, material cracking, surface cavities, adhered material particles, chip layer formation, deformed grains, slip zones, laps (material folded onto the surface), and lay patterns few of them has shown in Figure 2.1.

2.3.2 Non-traditional machining

Non-traditional machining process are advanced machining processes which remove the material from surface of workpiece without contact between tool and workpiece therefore tool wear can be minimized. The difficulties in conventional machining of TiNi alloys can be overcome by effectively machining through non-conventional machining process such as laser machining, water jet machining (WJM), Electro discharge machining (EDM) and Wire Electro discharge machining (WEDM). WEDM is an advanced method that has revolutionized in the field of cutting tool, die and mould making industries. Some WEDM machining based literature is reported in Table 2.1.
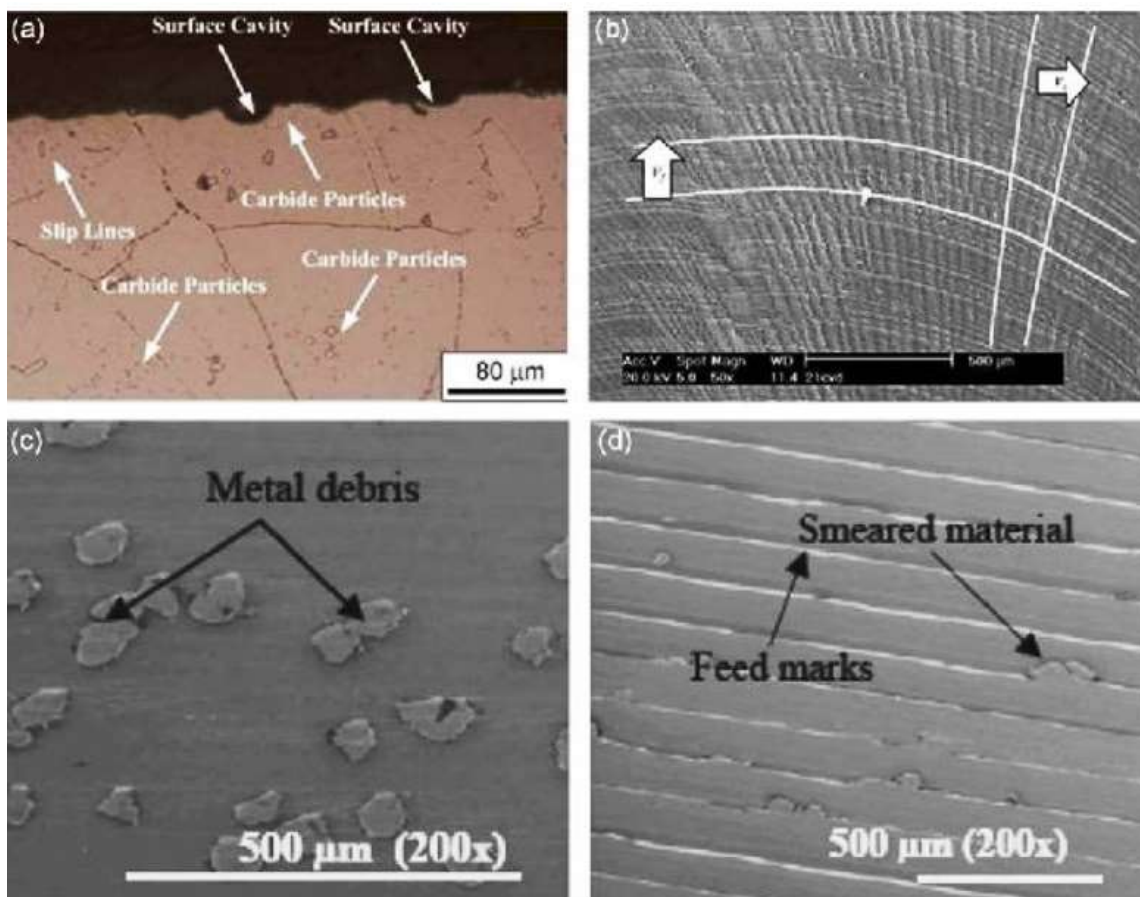
Figure 2.1 Surface Damages in Machining of Nickel-Titanium Alloys: (a) Metallographic microstructure after turning process (b) Lay pattern after dry milling process (c) Metal debris after turning process and (d) Smeared material and feed marks after turning process (Hassan et al. 2014).

WEDM is an essential machine in several manufacturing processes in industries, which gives importance to precision and accuracy. Several researchers have attempted to improve the performance characteristics namely the surface roughness, cutting speed, dimensional accuracy and material removal rate. But the full potential utilization of this process is not completely solved because of its complex and stochastic nature and more number of variables involved in this operation (Spedding and Wang, 1997). Scott et al. (1991) developed mathematical models to predict material removal rate and surface finish while machining D-2 tool steel at different machining conditions. It was found that there is no single combination of levels of the different factors that can be optimal under all circumstances. Tarng et al. (1995) formulated a neural network model and simulated annealing algorithm in order to predict and optimize the surface roughness and cutting velocity of the WEDM process in machining of SUS-304 stainless steel materials. Spedding and Wang (1997) attempted to model the cutting speed and surface roughness of EDM process through the response-surface methodology and artificial neural networks (ANNs). A feed-forward back-propagation neural network based on a central composite rotatable experimental design is developed to model the machining process. Liao et al. (1997) performed an WEDM machining study using SKD11 alloy steel and established mathematical models relating the machine performance like MRR, SR and gap width with various machining parameters and then determined the optimal parametric settings for WEDM process applying feasible-direction method of non-linear programming. Bitonto et al. (1989) presented a simple cathode erosion model for EDM process. This point heat-source model accepts power rather than temperature as the boundary condition at the plasma/cathode interface. A constant fraction of the total power supplied to the gap is transferred to the cathode over a wide range of currents. The model identifies the key parameters of optimum pulse time factor and erodibility in terms of thermo-physical properties of cathode material. Shankar Singh et al. (2004) reported the results of an experimental investigation carried out to study the effects of machining parameters such as pulse current on material removal rate, radial over cut, electrode wear, and surface roughness in electric discharge machining of EN-31 tool steel hardened and tempered to 55 HRC. The work material was EDMed with copper, copper tungsten, brass and aluminium electrodes by varying the

pulsed current at reverse polarity. Investigations indicate that the output parameters of EDM increase with the increase in pulsed current and the best machining rates are achieved with copper and aluminium electrodes. Copper is comparatively a better electrode material as it gives better surface finish, low diametric over cut, high MRR and less electrode wear for EN-31 work material. The periodic component of the surface texture is identified and an auto regressive (AR) model is used to describe its stochastic component. Huang et al. (1999) investigated experimentally the effect of various machining parameters on the gap width, SR and the depth of white layer on the machined work piece (SKD11 alloy steel) surface. Anish Kumar et al. (2013) presented WEDM as an adequate process to machine high strength temperature resistant pure titanium (grade-2) with good surface finish and dimensional accuracy.

Table 2.1 Literature survey based on Wire electro discharge machining process applied to different material.

No.	Authors	Material	Brief Contribution
1	(Hsieh et al. 2009)	$Ti_{35.5}Ni_{49.5}Zr_{15}$ and $Ti_{50}Ni_{49.5}Cr_{0.5}$ alloys	Machined alloys exhibited a good shape recovery.
2	(Geng & Zhong 2010)	45 steel	The result shows that topography of the WEDM surface exhibits strong fractal characteristics within a certain scale.
3	(Antar et al. 2011)	720 nickel based super alloy and Ti-6Al-2Sn- 4Zr-6Mo titanium alloy	Reported surface finish ~ 0.6μm (Ra), with near neutral residual stresses and almost zero recast were produced following two trim passes.
4	(Dhobe et al. 2013)	Tool steel	Microstructural changes and the droplets forming recast layer are found to influence the surface roughness, hardness, and white layer thickness of the wire electro-discharge machined surface of the tool steel.
5	(Guo et al. 2013)	$Ni_{50.8}Ti_{49.2}$	It is reported that very high strength and specific heat are responsible for large flank wear and fast tribo-chemical crater wear. The austenitic white layer in cutting is caused by deformation, while the twinned martensitic white layer is caused by quenching in EDM.

6	(Manjaiah et al. 2015)	TiNiCu	Harder surface has been noticed near the machined surface which was about 59% increase with respect to the base material for longer pulse on time due to the recast layer thickness and the formation of oxides.
7	(Pramanik et al. 2015)	6061 aluminium alloy	It is observed that the higher wire tension facilitates steady machining process, which generates low wear in wire electrode and better surface finish
8	(Tian et al. 2015)	Stainless steel based	It was noted that WEDM can be used to generate a recast layer on stainless steel surface.
9	(Sharma et al. 2015)	Inconel 706	Observed the reduction in micro voids and micro globules at lower value of pulse on time and higher values of servo voltage. Thicker recast layer was noticed at higher value of pulse on time and lower value of servo voltage.
10	(Manjaiah et al. 2015)	$Ti_{50}Ni_{45}Cu_5$	The globule of appendages formed around the craters and the intensity of the crater was evident for the higher surface roughness with an increase in peak current and pulse-on time during WEDM
11	(Pramanik et al. 2016)	Al-based metal matrix composites	It was found that initial circular shaped wire deformed during the machining process as curved front and rear edges and two straight side edges irrespective of cutting conditions and workpiece materials.

12	(Pramanik et al. 2016)	6061 aluminium alloy	The effect of wire tension on MRR is much more significant at longer pule-on-time compare to that at shorter pule-on-time.
13	(Srinivasa Rao et al. 2016)	Aluminium	Microscopic examination exposed absence of surface cracks on aluminium surface at all the machining conditions.
14	(Saha & Mondal 2016)	Nano Carb 110 has	The result implies that servo voltage has the greatest effect on the multiple-criteria quality characteristics of brass wire and discharge pulse time for zinc-coated brass wire, respectively.
15	(Soni et al. 2017)	TiNiCo	Pulses on time and servo voltage are found as the most influential process parameters in achieving the good machinability with TiNiCo shape memory alloys.
16	(Sun et al. 2017)	Carbon steel rod	They found the good surface quality with Ra of 0.59 mm and high dimensional precision with surface profile accuracy of 3.22 mm of machined component.
17	(Kuppuswamy & Yui 2017)	NiTi	Machining behaviour characterized in terms of low cutting forces and reduced burr size was achieved at 15 m/min of cutting speed when the NiTi alloy under goes a transition from B2 phase to B19 phase.

18	(Arikatla et al. 2017)	Ti-6Al-4V	The WEDMed surface topography shows dominant micro voids, thick white layer, heat affected zone and micro cracks at high pulse on time and pulse current and these are low at low pulse on time and pulse current during trim cuts.
19	(Kumar et al. 2017)	Nimonic-90	Topography of machined surface suggests that high discharge energy results in overlapped and deep craters of large size diameters and high thickness of recast layer whereas low discharge energy results into fine surface with minimum recast layer.
20	(Daneshmand et al. 2017)	NiTi-60	The increase in the material removal rate is observed through the use of Al2O3 powder and tool rotation along with increasing current intensity, pulse on time and voltage.
	(Roy et al. 2017)	TiNiCu	Thicker recast layer has been found with higher MRR and SR at higher pulse on time.
21	(Mouralova et al. 2018)	Ti- 6Al-4V alloy	The analysis of the surface morphology has shown that the surface of all investigated samples bears traces typical of material to have been completely molten and subsequently rapidly cooled; as a result, numerous fine surface micro fissures and cracks got created.

2.4 MATERIAL REMOVAL RATE (MRR)

The material removal rate, is an important process factor in manufacturing, approximately increases in linear proportion with the discharge energy in EDM-process, and achieves commercially interesting values by using an electrode made of copper and tungsten (W. Theisen, and A. Schuermann 2004). H C Lin et al. (2001) investigated the effect of input parameters on MRR during the machining of TiNi based SMAs through EDM and they found that MRR significantly relates to the electro discharge energy mode. It increases monotonically with increasing pulse current, but appears an optimal pulse duration, saying τ_p= 6-12 μs at I_p=12A to have a maximum value. Besides, it has a reverse relationship to the product of melting temperature and thermal conductivity of TiNi SMAs, therefore a longer pulse duration τ_p and a lower pulse current Ip should be selected to have a precise EDM machining. It has been reported that increased the pulse current I_p will increase the current density. Figure 2.2 shows the MRR versus the pulse duration τ_p at various pulse currents I_p for the $Ti_{49}Ni_{51}$ alloy.
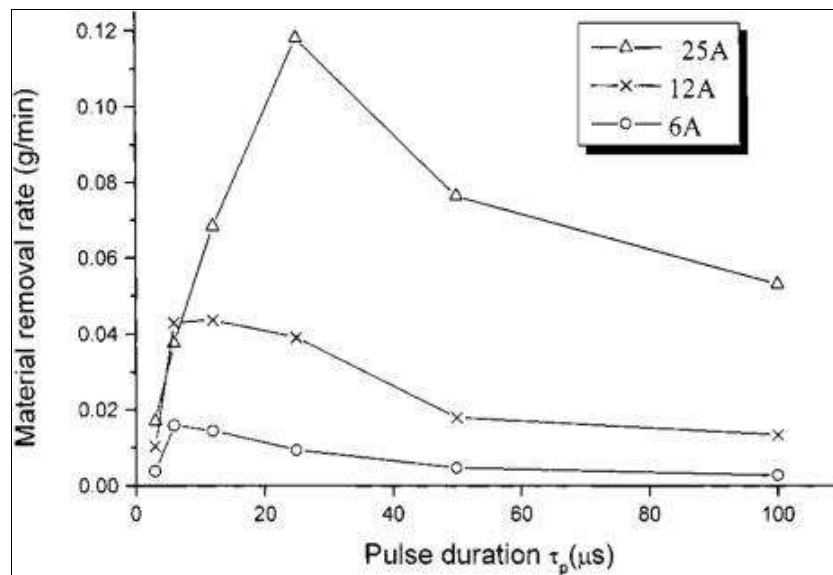
Figure 2.2 MRR versus the pulse duration τ_p at various pulse currents IP for the $Ti_{49}Ni_{51}$ alloy (H C Lin et al 2001).

Manish Kumar et al. (2014) investigated that Pulse on Time (Ton) and Pulse off Time (Toff) are the most significant machining parameter for controlling the MRR. During

WEDM, MRR depends on the electrode material, melting temperature of the electrode and electrode wear rate. The discharge energy increases with growing pulse duration. The MRR varies with dielectric fluid. The MRR increases linearly with pulse on duration and when kerosene is used as dielectric fluid, MRR increases till the optimum point and further reduce. Moreover electrode wear rate (EWR) also increases with the pulse on time duration, but when using deionized water the EWR is relatively less compared with kerosene (Chen et al. 1999). Yilmaz et al. (2010) investigated the effect of single and multi- channel electrodes made of copper and brass material on MRR.   The single channel copper electrode has higher MRR compared to multichannel copper and brass electrode. Manjaiah et al. (2017) reported during the WEDM of TiNiCu shape memory alloys that MRR is increases with increasing in pulse on time while MRR is decreases with increasing servo voltage and pulse off time. The reason behind the increasing of MRR is that spark intensity is high at higher pulse on time. Fig. 2.3 exhibits the effects of important process parameters of WEDM on MRR during the machining of Inconel 706 alloy. It is observed from the graph that MRR is increases with increased pulse on time while decreases with increased pulse off time (Fig. 2.3b) and servo voltage (2.3c). The spark intensity is reduce in both cases when servo voltage and pulse off time are increased and at the same time spark intensity will be high at higher pulse on time. The trend of MRR was not constant with respect to wire feed (Fig. 2.3d) and flushing pressure (2.3f) because of machining error. The servo feed (Fig. 2.3e) do not have much effect on MRR during the WEDM process (Sharma et al. 2015).
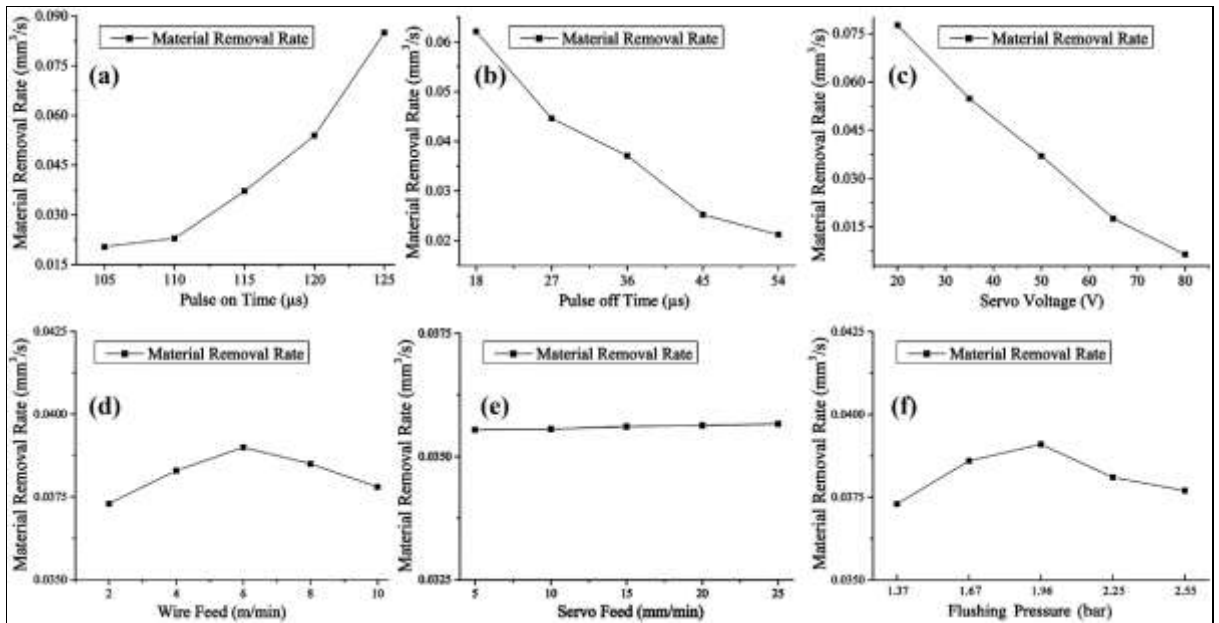
Figure 2.3 Effect of WEDM process parameters on MRR (Sharma et al. 2015).

2.5 SURFACE INTEGRITY

Surface integrity is another parameter which is influenced by the machining situations and indicates the machined surface and subsurface (D.K. Aspinwall 2008). It is a major contributing factor in processing and performance of the part. The surface integrity constitutes surface roughness, surface morphology, hardness, residual stresses and recast or white layer formation. During the non-conventional machining, the MRR is less compare to the conventional machining. The surface quality obtained with the non-conventional machining is high compare to the conventional machining and surface is comparatively less affected by phenomena such as defects, plastic deformation, phase transformation, micro cracks, work hardened layer and residual stress (F. Nourbakhsh et al.2013).

2.5.1 Surface roughness

Surface roughness in the machining process which is depends on the machining process parameters, type of machining tool, fraction and deformation between tool and workpiece. The selection of process parameters play important role for producing surface quality through any machining process. Sharma et al. (2015) found that pulse on time and servo voltage are most influential process parameters during WED

machining of Inconel 706 for turbine disk application. Manjaiah et al. (2015) found that surface roughness increase with increase in pulse on time while surface roughness decrease with increase in servo voltage. Kumar et al. (2012) reported that increase in the pulse duration increases the feed rate of wire electrode and extending the pulse duration to allow greater discharge energy, melt and penetrate into the surface of work-piece forms the deeper craters. Raj. D et al. (2015) investigated that pulse on time and pulse off time are the important parameters that influences the surface roughness while servo feed is found to be almost ineffective. Surface roughness is also influenced by the wire speed. When the wire speed is lower, the melting of material is more due to higher energy and higher MRR causes the higher surface roughness. Spark gap is also important parameter for surface roughness, which is directly proportional to pulse on time. When the pulse on time increase from 20 μs to 25 μs, spark gap increases (K. Basil, and J. Paul 2013). The order of the importance for the controllable factors to the average surface roughness mentioned in sequence, i e. pulse off time, pulse on time, spark gap, and finally the current (N.Z. Khan et al. 2014). In the fig. 2.4, it can be clearly seen that large number of craters or voids has been created due to high pulse-on time. But as the pulse on time decreases the numbers of voids are less. As the pulse-off time increases the height of the crater gets decreased which is the main reason behind the lower surface roughness.
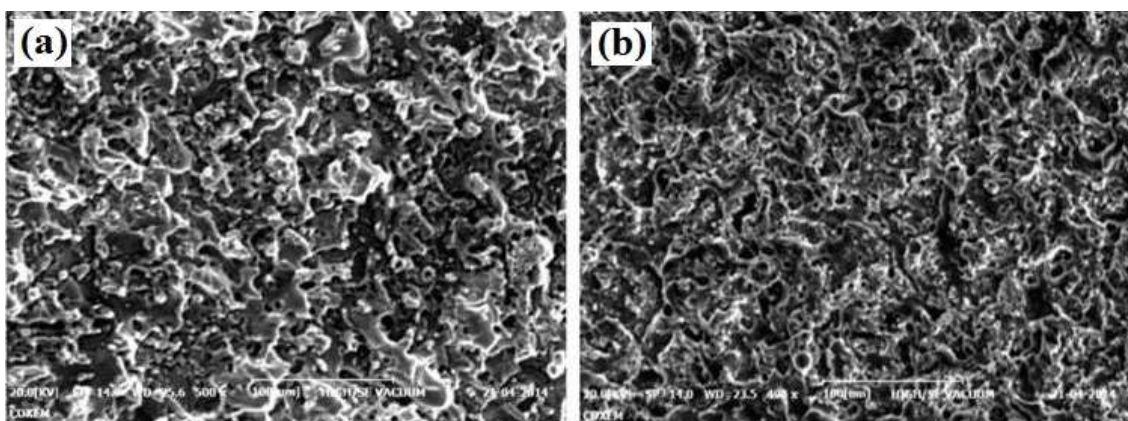
Figure 2.4 (a) SEM image of machined surface: Pulse-on time =0.75μ s, Pulse-off time=10.2 μ s, Wire feed rate=2 (b) SEM image of machined surface: Pulse-on time=0.5μ s, Pulse-off time=17μ s, Wire feed rate=3 (Amrish Raj.D et al. 2015)

Fig. 2.5 shows that the roughness of the machined surface under increasing current intensity becomes more and more significant, due to enlarged craters and cracks formed on the machined surface. This is because at high current intensity more amount of spark has been produced in the machining zone results in some of the melted material has been removed through dielectric fluid rest of the melted material deposited in the form of craters and cracks on the machined surface. (W. Theisen. et al. 2004).
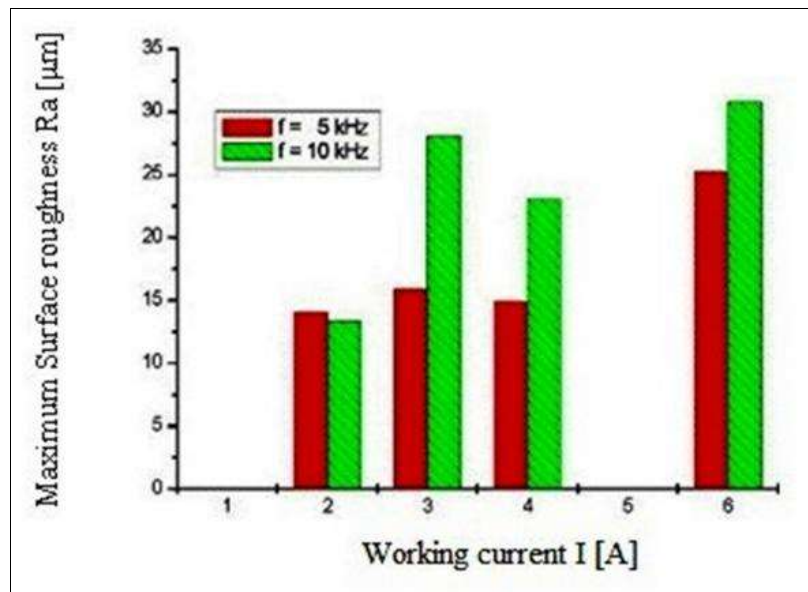
Figure 2.5 Development of the surface roughness depending on the working current and the frequency (W. Theisen. et al. 2004).

2.5.2 Surface topography

Surface topography controls friction and transfer layer formation during machining. It can be either isotropic or anisotropic which is communally measured by the diamond stylus profile meter. Puri et al. (2005) observed during the WEDM, the surface topography of the machined surface mainly influenced by the sparking frequency and the crater size determined by the electrical discharge energy contained in a pulse. The work piece material which gets melted is not completely removing during the process. The surface topography presented in Fig. 2.6 reveals that the surface roughness of D2 (air-hardening, high carbon, high chromium tool steel) and H13 materials (chromium- molybdenum-vanadium alloyed steel) is caused by an uneven structure or

surface, globules of debris, shallow craters, pockmarks, voids and cracks. These effects become more pronounced as the pulse current and pulse-on duration increase (H.T. Lee et. al. 2003). Similarly Manjaiah et al. (2015) found that servo voltage and pulse on time are influential parameters. Figure 2.7 reflect the machined surface topography at higher pulse on time and lower values of servo voltage. Fig. 2.7a and Fig. 2.7c exhibit the surface topography at 120μs pulse on time and 20V servo voltage while Fig. 2.7b and Fig. 2.7d reveals the surface topography at 120μs pulse on time and 80V servo voltage. These figure it is inferred that, surface roughness was high in both wires (brass and zinc coated) at higher values of pulse on time while at higher servo voltage roughness of machined surface is low with both wire condition (brass and zinc coated).
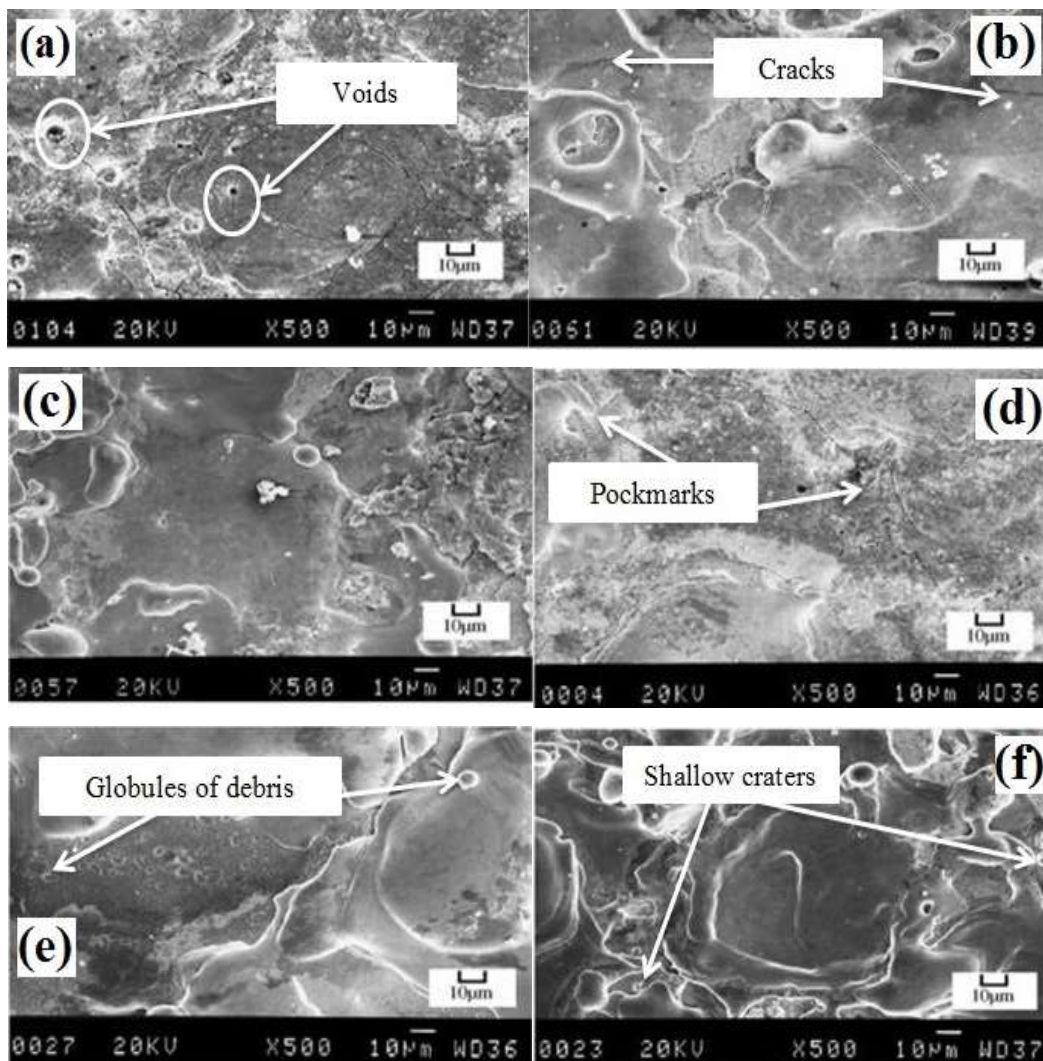
Figure 2.6 SEM photographs of electro discharge machined surface of D2 and H13 tool steel (a) D2 surface topography (4 A/15 μs); (b) D2 surface topography (16 A/15 μs); (c) D2 surface topography (16 A/6 μs); (d) H13 surface topography (4 A/15 μs); (e) H13 surface topography (16 A/15 μs); (f) H13 surface topography (16A /6 μs) (H.T. Lee et. al. 2003).
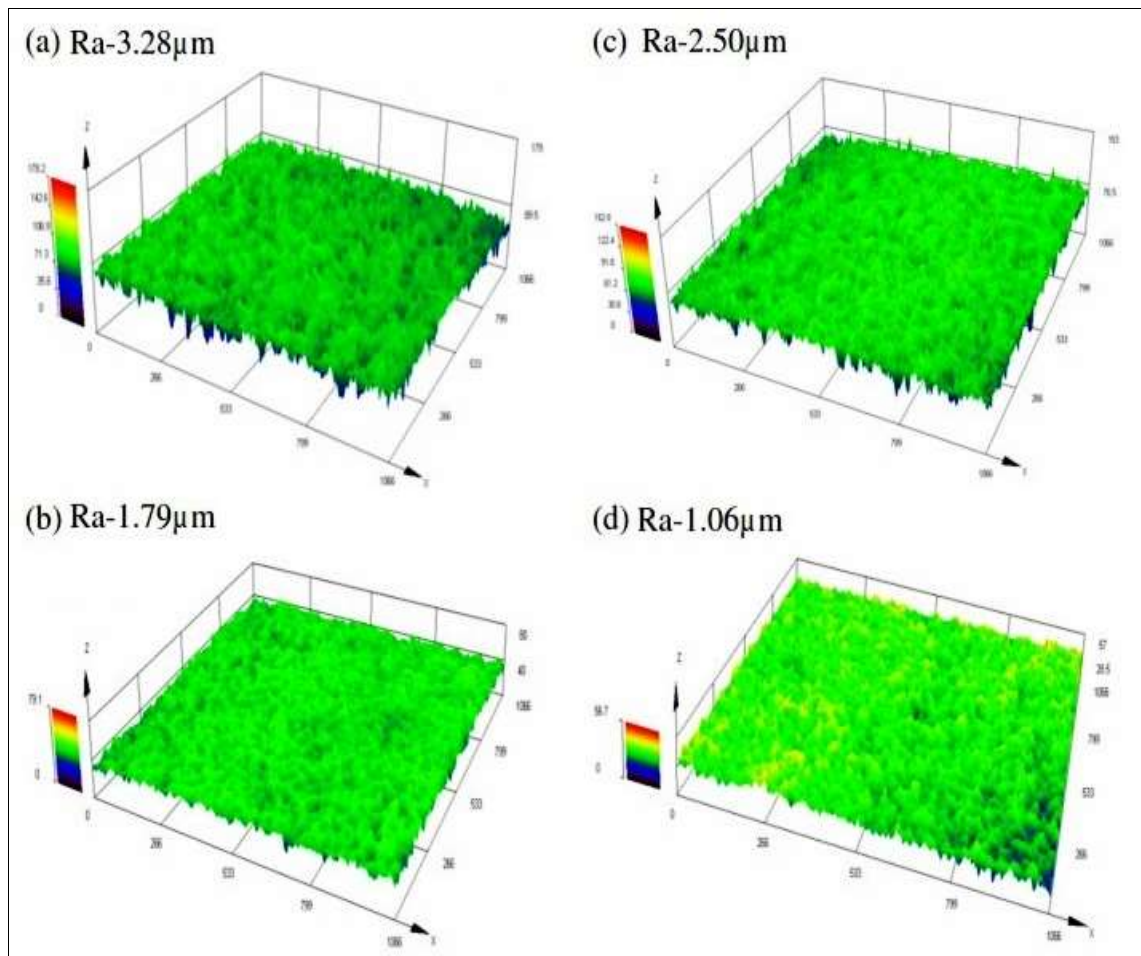
Figure 2.7 3D surface profile of Ti50Ni40Cu10 machined surface for higher and lower servo voltage (a and b) brass; (c and d) Zinc coated brass wire (Manjaiah et al. 2015).

2.5.3 Surface metallurgy

Metallurgical transformation involves micro structural changes caused by temperature cycles; these cycles may consist of phase transformations, recrystallization, alloy depletion, decarburization, and re-solidified or redeposited material on the machined

surface (Suffi et al. 2010). Surface metallurgy of a wire-cut electro-discharge machined surface is concerned with the subsurface characteristics, which are usually termed as altered material zones (AMZ). These alterations, caused by the thermal energy of spark discharges, are generally in the form of micro cracks, spalling, and change in hardness, residual stresses, and metallurgical transformations and of course, heat affected zone (Puri et al. 2005). Machined surface of the work piece always undergoes various kinds of metallurgical alterations (Ekmeckci et al. 2011). Hsieh et al. (2013) studied on the machined surface and they found that the XRD patterns of the EDMed surface for the $Ti_{35.5}Ni_{48.5}Zr_{16}$ and $Ni_{60}Al_{24.5}Fe_{15.5}$ alloys are shown in Fig. 2.8, the formation of TiO, NiO and ZrO_2 oxides is ascribed to the high activity of Ti, Ni and Zr atoms with dielectric fluid during the machining. These oxides are responsible for forming harder surface on the machined surface.
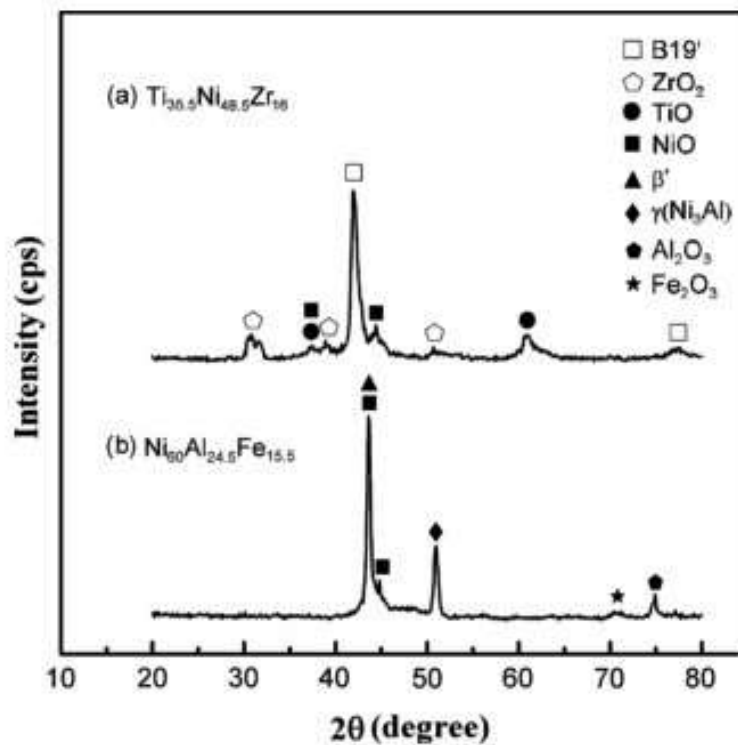
Figure 2.8 The XRD patterns of the EDMed surface layer for: (a) $Ti_{35.5}Ni_{48.5}Zr_{16}$ alloy and (b) $Ni_{60}Al_{24.5}Fe_{15.5}$ alloy (Hsieh et al. 2013).

34

2.6 HARDNESS

H.C. Lin, et al. (2005) investigated the WEDM characteristics of Fe–30Mn–6Si and Fe– 30Mn–6Si–5Cr SMAs. They observed machined surface hardening effect arises from the formation of the $Cu_{0.83}Si_{0.17}$ compound, η'-(Cu, Si) and (Fe, Cr) solid solutions in the re-cast layer. Fig.2.9 shows the specimen's hardness at various distances from the WEDM surface. Increase in the pulse on-time leads to increase in both the surface roughness and the micro-hardness (N.Z. Khan et al. 2014).

Chen et al. (2007) reported increase in machined surface hardness with the higher pulse duration and peak current. This hardening effect is because of formation of oxides Cr_2O_3, ZrO_2, TiO_2, $TiNiO_3$, carbide like TiC in the recast layer. It is mainly during use of copper electrode and kerosene as dielectric fluid during the EDM of TiNi based ternary alloy. Similar observations are reported by authors Hsieh et al. (2009) during the EDM of TiNiCr and TiNiZr alloys.
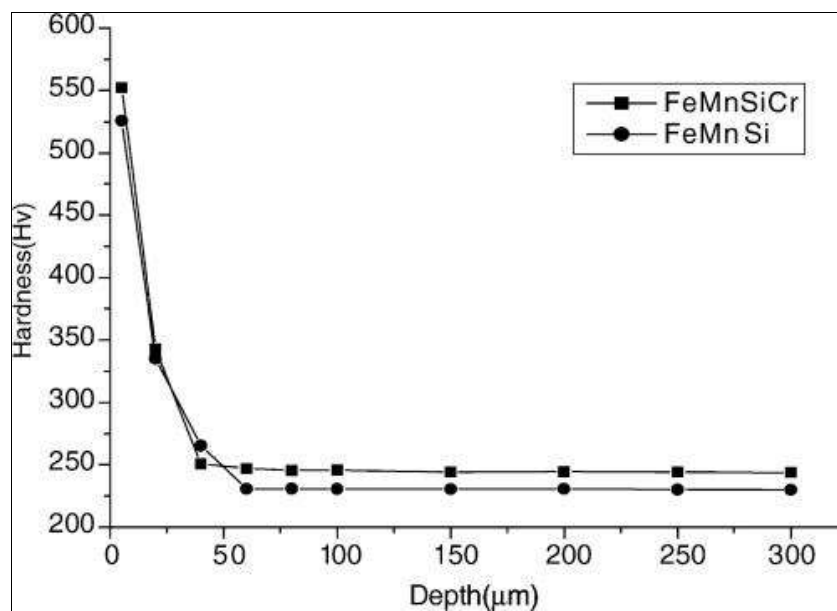
Figure 2.9 Hardness at various distances from the WEDM surface (N.Z. Khan et al. 2014).

2.7 RECAST LAYER FORMATION

The recast layer thickness increases with increasing peak current, pulse on-time and dielectric flushing (Bhattacharya et al. 2007). The average recast layer thicknesses

increases with increase in pulse energy, higher discharge current and longer duration of pulse-on. The changes in pulse on-time durations is more significant factor than changes in the peak current for variation in the recast layer thickness and it is observed that the majority of cracks terminated with in the recast layer or at the interface of the recast layer without affecting sub surface (Lee H.T. et al. 2003). The use hydrocarbon-based dielectric fluid leading to micro cracks on recast layers due to presence of excessive amount of carbon (Ekmekci, et al. 2007). The effect of process parameters on metal removal rate, re-cast layer and surface finish was studied with statistical models of the EDM process and the pulse current is critical factor affect the surface finish (Hung N.P. 1994). The white layer is composed mainly of martensite and retained austenite, with some dissolved carbide (R. Bormann et al. 1991). The white layer formed on D2 tool steel and H13 tool steel is presented in Figs 2.10 (a) and (b) respectively.
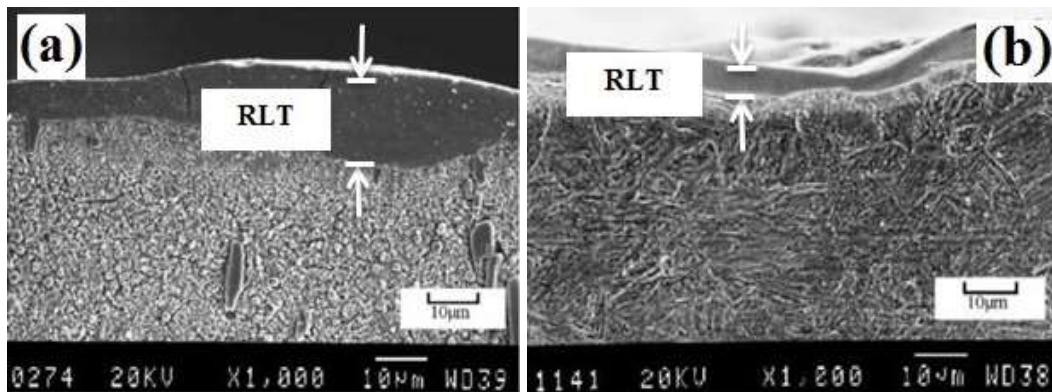
Figure 2.10 SEM photographs of (a) D2 tool steel white layer (12 A/15 μs) and (b) H13 tool steel white layer (4 A/12 μs) (H.T. Lee et. al. 2003).

To increase the life of the tool or product, the recast layer is generally removed, particularly for applications in which the part is subjected to cyclical stress (aero engine components) or fluctuating loads (forging and punching tools/dies). This is achieved either by hand polishing, etching or heat treatment. Alternatively, burnishing or shot peening is employed in order to impose a compressive residual stress regime. However, such processes are supplementary and may increase cost and time. With operations in which repeated high levels of mechanical impact are not a factor, the EDM recast layer can be beneficial in providing increased abrasion and

corrosion resistance. Lin et al. (2005) reported that the re-cast layer of Fe–30Mn–6Si is much thicker than that of Fe–30Mn–6Si–5Cr SMAs after WEDM. The re-cast layer consists of the γ-austenite, $Cu_{0.83}Si_{0.17}$ compound, η′-(Cu, Si) and (Fe, Cr) solid solutions, and Zn phase. The WEDM Fe–30Mn–6Si and Fe–30Mn–6Si–5Cr SMAs still exhibit a good shape recovery, but a slight degradation of shape recovery occurs due to the depression of the re-cast layer. The degradation of shape recovery is more obvious for the WEDM Fe–30Mn–6Si SMA due to its thicker re-cast layer.

2.8 RESIDUAL STRESSES

Residual stresses are those stresses that remain once a body is at rest and at equilibrium with its surroundings without mechanical loading (Withers 2001). EDM generates residual stresses; this is mainly due to the non-homogeneity of heat flow and metallurgical transformations (Dijcket et al. 1974). An increase of their magnitude is observed at the surface layer with increasing pulse energy. Since the integrity of the EDM surface is degraded by the unstable arcing which always occurs during the machining process, the quality of an EDM product is evaluated in terms of surface integrity, which is characterized by the surface roughness, presence of surface cracks, and the residual stresses. The residual material re-solidifies on the machined surface to form a hard skin on the work piece. Thus, an extreme fast heating, melting and vaporization is followed by a fast cooling of the work piece material in the sparking zone during the process of material removal. This causes a massive change in both on the surface topography as well as in the surface metallurgy of the work piece (Puri, et al. 2005). It has been observed that WEDM process creates generally tensile residual stress on the machined surface. Figure 2.11 that the machine surface stress is in tensile nature but compressive residual stress has been noticed after the 150µm distance from the machined surface (Ghanem et al. 2011).
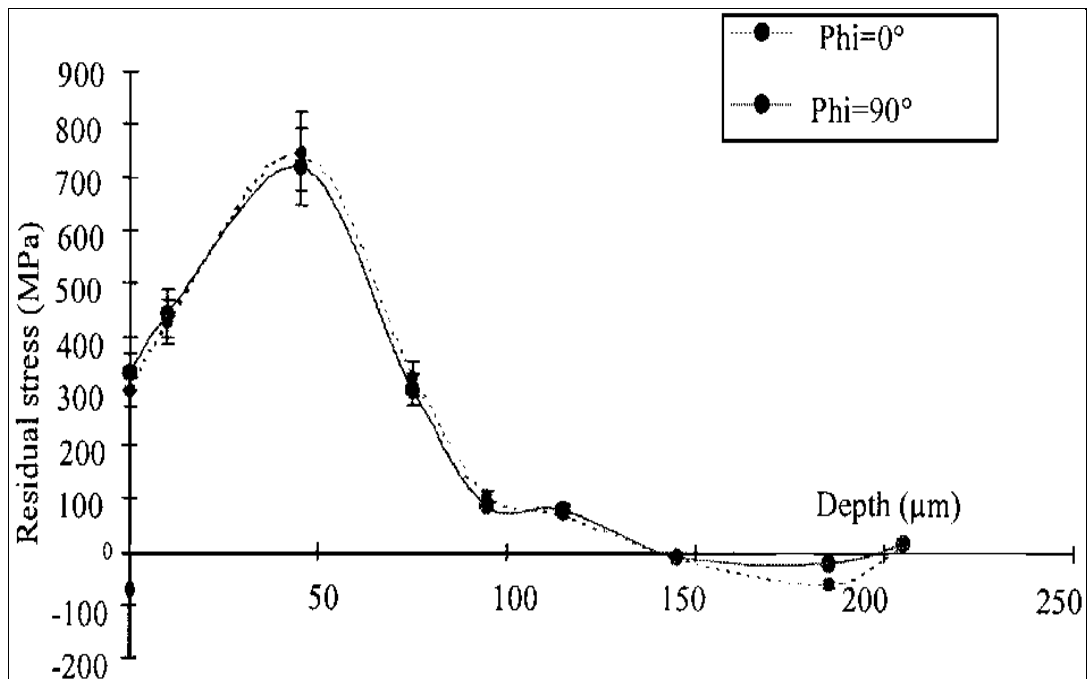
Figure 2.11 Variation of residual stress on the machined specimens (Ghanem et al. 2002)

Literature survey based on the process parameters of WEDM process are presented in Table 2.2. Effects of process parameters on machining responses such as MRR and SR have been discussed in the above literature survey. However machined surface characterization based literature survey were also discussed. Further literature survey reveals the mathematical modelling and optimization techniques.

Table 2.2 Literature survey based on the process parameters of WEDM process

No.	Authors	Work material	Process parameters	Dielectric Fluid	Tool material	Tool diameter
1	(Kuriakose & Shunmugam 2004)	Ti6Al4V	Time between two pulses, Pulse duration, Servo control reference voltage, Maximum servo-speed variation, Wire speed, Wire tension and Injection pressure	Deionized water	Zinc-coated brass	0.25 mm
2	(Ramakrishnan & Karunamoorthy 2006)	Tool steel	Pulse on time, wire tension, delay time, wire feed speed and Ignition current intensity	Deionized water of	Zinc coated brass	0.25mm
3	(Aspinwall et al. 2008)	Ti–6Al–4V	Current, Voltage, On/Off time and Frequency	Deionised water	zinc coated brass	200 mm
4	(Singh & Garg 2009)	Hot die steel (H-11)	Pulse on time , Pulse off time, Gap voltage, Peak current, Wire feed and Wire tension	De-ionized water	Brass wire	0.25 mm
5	(Hsieh et al. 2009)	$Ti_{35.5}Ni_{49.5}Zr_{15}$ and $Ti_{50}Ni_{49.5}Cr_{0.5}$	Wire electrode, Pulse duration, Pause duration, Duty factor, Gap voltage, and Flushing pressure.	De-ionized water	Brass	0.25mm
6	(Antar et al. 2011)	Ti-6Al-2Sn-4Zr-6Mo (hereafter	Voltage, Ignition current, On-time, Off-time, Flushing pressure, Wire speed, Wire tension and Wire offset	De-ionised water	Brass wire	0.25 mm
7	(Jangra et al. 2012)	Cemented	Peak current, Pulse-on time, Micro-second, Pulse-	Distilled water	Zinc coated	0.25mm

		tungsten carbides (WC)	off time, Micro- second, Wire speed, Wire tension, Servo voltage and Dielectric flow.		brass wire	
8	(Sivaprakasam et al. 2013)	Aluminium Matrix Composite (A413-9% B4C)	Voltage, Capacitance, Feed rate and Symbol	Commercial grade EDM oil	Zinc coated copper wire	70μm
9	(Shandilya et al. 2013)	SiCp/6061 Al MMC	Servo Voltage, Pulse-on time, Pulse-off time and Wire feed rate	Deionized water	Diffused brass wire	0.25 mm
10	(Kumar et al. 2013)	Pure titanium	Pulse on time, pulse off time, peak current, spark gap voltage, wire feed and wire tension were	Deionized water	Brass wire	0.25 mm
11	(Goswami & Kumar 2014)	Nimonic 80A	Pulse-on time, pulse-off time, spark gap set voltage, peak current, wire feed and wire tension.	De-ionized water	Brass wire	0.25 mm
12	(Shivade & Shinde 2014)	D3 tool steel	Pulse-on time, Pulse-off time, Peak current and Wire speed	De-ionized water	Brass wire	0.25 mm
13	(Azhiri et al. 2014)	Al/SiC metal matrix composite	Pulse on time, pulse off time, gap voltage, discharge current	Mineral oil-based dielectric	Copper and brass	0.1 mm
14	(Luo et al. 2014)	YG15 steel	Pulse-on time, Pulse-off time, Cutting feed rate, Wire tension, Wire speed and Water pressure	De-ionised water	Brass wire Brass wire	0.25 mm
15	(Saha & Mondal 2016)	Nano Carb 110	Discharge pulse time, Discharge stop time, Servo voltage, Wire tension and Wire feed rate	Deionized water	Brass and zinc-coated	0.25 mm

				brass	
16	(Kumar et al. 2016)	Pure titanium	Pulse on time, Pulse off time, Peak current, Spark gap voltage, Wire feed and Wire tension	Deionised water	Brass	0.25 mm
17	(Ayesta et al. 2016)	Inconel 718	Intensity, Pulse off time, Voltage and Servo voltage	Deionized water	Brass wire	0.25mm
18	(Soundararajan et al. 2016)	A413 alloy	Dielectric medium, wire feed, wire tension, servo voltage, flushing pressure, servo feed, peak voltage Pulse on time, Pulse off time and Peak Current.	De-mineralized water	Zinc coated brass wire	0.25 mm
19	(Chalisgaonkar & Kumar 2016)	Pure titanium	Pulse on time, Pulse off time, peak current, wire feed rate, wire tension and Servo voltage.	De-ionized water	Zinc-coated and uncoated brass wire	0.25 mm
20	(Sharma et al. 2016)	Inconel 706	Polarity, Discharge current, Discharge voltage, Servo feed, Flushing pressure, Current speed, Dwell time and Corner control factor	De-ionized water	Brass wire	0.25 mm
21	(Mouralová et al. 2016)	Tool steel X155CrVMo12-1	Grinding wheel ,Wheel speed, Table speed Cross feed, Down feed and Number of pass	deionized water	Brass wire	0.25 mm
22	(Chen et al. 2017)	SKD-11	Pulse on time, pulse off time, reference voltage, wire speed and Magnetic induction intensity.	Deionized water	Copper wire	0.25 mm

2.9 MATHEMATICAL MODELING

Optimization techniques play important role in the achieving the best result for a given problem under given circumstances. Any optimization is possible through exact algorithms to find an optimal solution. The model exhibits the relationship among decisions, constraints and objectives. Some researchers correlating their experimental results with modelling techniques, and they developing equations for the output responses from the input parameters. In this section literature survey discussed based on the modelling and optimization techniques to optimize the WEDM process parameters. However to investigate the experimental error, based on the error analysis literatures have been included.

Chakravorty et al. (2012) investigated different principal component analysis (PCA) based techniques using L18 orthogonal array to optimize EDM processes and it was observed that PCA based proportion of quality loss reduction (PQLR) method yielded best results . Sahaet al. (2013) reported that Neuro-Genetic technique has potential in finding several optimal input machining conditions which can satisfy wide requirements of a process engineer and help in efficient utilization of WEDM in industry. Nayak et al. (2015) presented a multi response optimization approach to determine the optimal process parameters in wire electrical discharge machining process during taper cutting operation using new metaheuristic algorithm, called as Harmonic search algorithm. Vundavilli et al. (2012) studied on the optimization techniques to obtain the best process parameters of WEDM, They used genetic algorithm (GA) and Particle swarm optimization (PSO) and found that both the optimization approaches show similar trend in pareto optimal fronts but PSO produce optimal front in less time compared to GA. Pradhan (2013) studied the effect of process parameters on MRR, tool wear ratio (TWR) and overcut (OC) of EDM with AISI D2 tool steel. The experimental results obtained were optimized using grey relational analysis (GRA), and the weights of the responses were determined using PCA. Gauriand Chakraborty (2009) discussed about some modifications in the PCA-based approach and two sets of experimental data published by the past researchers were analysed using this modified approach. It was observed that the PCA based grey

relation analysis has been successfully used for multi-objective optimization (Khan et al. 2010 and Lu et al. 2009).

2.9.1 Response surface methodology (RSM)

BOX and Wilson Suggested RSM in 1951 to explore the relationship between several explanatory variables and one or more response variables. The most essential application of this approach is to utilize a series of designed experiments to get best response. Commonly a second-degree polynomial model is used in this approach. Even though these models are just a prediction, such a model is easy to estimate and apply, even when little is known about the process (Hewidy et al. 2005). Kumar et al. (2017) developed empirical models for material removal rate and wire wear ratio, in terms of six prominent WEDM process parameters for the machining of pure titanium by using response surface methodology. They noticed that optimum setting of process parameters can be adjusted in order to minimize the wire wear ratio, Palani et al. (2013) optimized the Micro WEDM process parameters such as voltage, capacitance, and feed rate on machining for the better material removal rate (MRR), kerf width (KW), and surface roughness (SR) by using response surface methodology for the machining of Aluminum Matrix Composite (A413-9% B4C. The better MRR, KW and SR have been found at the optimized process parameters.

2.9.2 Grey relational analysis (GRA) method

Deng (1989) proposed a Grey relational analysis approach. Grey relational analysis is a multi-objective optimizations technique which helps in decision-making process and guides the selection of best combination of process parameters to rank the materials with respect to several criteria (Joseph et al. 2006). Lin et al. (2002) adopted the grey relational analysis and the Fuzzy-based Taguchi method for optimising the EDM process. They optimized EDM process parameters such as pulse on time, duty factor, and discharge current to find the best machining responses (electrode wear ratio, material removal rate, and surface roughness). Grey relational analysis method was found more straightforward than Fuzzy-based Taguchi method. However grey relational grade indicate the best combination of process parameters based on the rank of process parameters (Lin et al. 2004). Similarly Anand et al. (2014) examined

WEDM process parameters (pulse-on time, pulse-off time, peak current and wire speed) to fine best machining time, MRR, gap current and dimensional deviation by using grey relational analysis method. Taguchi Design of experiment method was used for experimental plan to conduct the machining on D3 tool steel. During their study they have been proved that the potential of GRA to optimized process parameters successfully for multi-objective characteristics.

2.9.3 Entropy measurement method

Entropy measurement method is an objective weighting method. Discrete type of entropy is used in grey entropy measurement for properly conduct weighting analysis (Mineta et al. 2011). Pradhan (2013) have been optimized the EDM process parameters (pulse current, pulse duration & pulse off time) for maximum MRR and minimum SR and tool wear ratio during the machining of D2 steel. He has used a combination of multi-objective optimization techniques such as grey relational analysis, response surface methodology and entropy measurement methods. Where the entropy measurement method used for determined the percentage weightage of the grey relational coefficients and finally Grey relational grades. Similarly Rao et al. (2008) the process parameters of laser cutting process which minimized the kerf width, kerf taper, and kerf deviation together during laser cutting of a thin sheet of SUPERNI 718 nickel-based super alloy.

The review of literature based on optimization techniques are given in Table 2.3. It has been observed from the literature that the combination of RSM & GRA with entropy measurement method is rarely used and these combinations of optimization techniques give good setting of process parameters. Therefore in the present study will be used the combination of these three optimization techniques for optimal setting of WEDM process parameters. The roll of each optimization technique can be seen in Fig. 2.12. Further literature is based on the error analysis has been discussed.
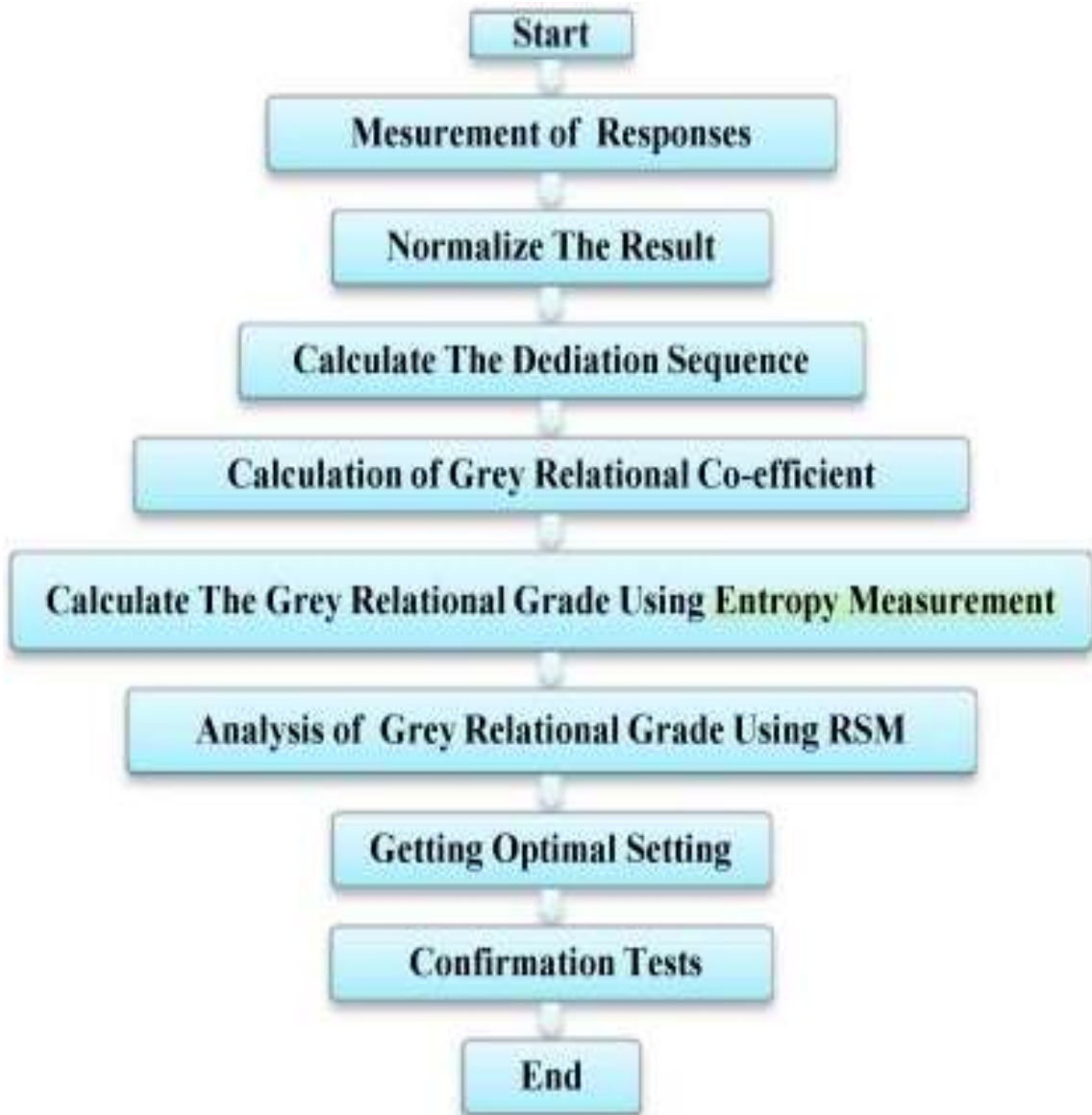
Figure 2.12 Flow chart for optimization techniques (Pradhan 2013).

Table 2.3 Literature survey on optimization techniques

No.	Authors	Material	Modelling/Optimization techniques	Type of optimum results	Process	Machining responses
1	(Hewidy et al. 2005)	Inconel 601	Response surface methodology (RSM).	Multi Response	WEDM	SR and MRR
2	(Ramakrishnan & Karunamoorthy 2006)	Tool steel	Taguchi's robust design	Multi Response	WEDM	Wire wear ratio, MRR and SR
3	(Rao & Yadava 2009)	Nickel-based super alloy (SUPERNI 718)	Grey relational analysis with entropy measurement	Multi Response	WEDM	MRR and SR
4	(Çaydas et al. 2009)	AISI D5 tool steel	Principal component analysis (PCA), Adaptive neuro-fuzzy inference system (ANFIS)	Multi Response	WEDM	White layer thickness (WLT) and the average surface roughness
5	(Datta & Mahapatra 2010)	ROBOFIL 100 high	Response surface methodology and Grey relational analysis theory	Multi Response	WEDM	MRR, SR and Kerf width
6	(Singh et al. 2010)	Tungsten carbide-cobalt composite	Grey relational analysis	Multi Response	Conventional grinding and EDM	MRR, wheel wear rate and average surface

						roughness
7	(Sharma el al. 2012)	High-strength low-alloy steel	Response surface method and Anova	Multi Response	WEDM	Cutting speed and dimensional deviation
8	(Jangra et al. 2012)	Cemented tungsten carbides	Grey relational analysis and entropy measurement method	Multi Response	WEDM	MRR, SR, Angular error and Radial overcut.
9	(Shrivastav et al. 2012)	Copper-iron-graphite composite	Artificial neural network, genetic algorithm, and grey relational analysis	Multi Response	Electric Discharge Diamond Grinding	MRR and high wheel wear rate
10	(Zhang et al. 2013)	SKD11	Response Surface methodology and Genetic Algorithm	Multi Response	WEDM	MRR and SR (Ra)
11	(Saha et al. 2013)	Metal matrix composite (MMC)	Neuro-Genetic technique	Multi Response	WEDM	Cutting speed and Kerf width
12	(Sharma et al. 2013)	High-strength low-alloy steel	Response surface methodology	Multi Response	WEDM	Cutting speed and Dimensional deviation
13	(Sivaprakasam et al. 2013)	Aluminum Matrix Composite (A413-9%	Response Surface Methodology	Multi Response	Micro-WEDM	MRR, Kerf width and SR

		B4C)				
14	(Kumar et al. 2013)	Pure titanium	Response surface methodology and Box–Behnken design	Multi Response	WEDM	Machining rate, SR, Dimensional deviation and Wire wear ratio
15	(Pradhan 2013)	AISI D2 tool steel	Response surface methodology, grey relational analysis and entropy measurement	Multi Response	WEDM	MRR and SR
16	(Goswami & Kumar 2014)	TiNi	Grey relational analysis	Multi Response	WEDM	MRR and Wire wear ratio
17	(Azhiri et al. 2014)	Al/SiC metal matrix composite (MMC)	Adaptive neuro-fuzzy inference system, Grey relational analysis	Multi Response	WEDM	Cutting velocity and SR
18	(Sivaprakasam et al. 2014)	Ti6Al4V	Genetic Algorithm	Multi Response	Micro WEDM	MRR, Kerf width and SR
19	(Shivade & Shinde 2014)	AISI D3 tool steel	Grey relational analysis method	Multi Response	WEDM	MRR, Dimensional deviation, Gap current and Machining time
20	(Saedon et al. 2014)	Titanium alloy	ANOVA; Grey relational analysis	Multi Response	WEDM	SR, Cutting rate and MRR
	(Varun et al. 2014)	EN 353 work	Grey relational analysis with	Multi	WEDM	MRR, SR, and

			genetic algorithm	Response		cutting width
21	(Kumar et al. 2015)	Metal matrix composites	Grey relational analysis	Multi Response	WEDM	Kerf and Roughness
22	(Bijeta et al. 2015)	TiNi	Harmonic search algorithm	Multi Response	WEDM	MRR and Roughness
23	(Adalarasan et al. 2015)	Al6061/SiCp/Al2O3	Grey based response surface method	Multi Response	WEDM	kerf width, surface finish and cut edge slope
24	(Bhuyan et al. 2015)	Al-18wt.%SiCp metal matrix composite	VIKOR and Entropy Weight method	Multi Response	EDM	MRR, TWR, Radial over cut and SR
25	(Soundararajan et al. 2016)	A413 alloy	Response surface methodology	Multi Response	WEDM	Cutting velocity, Kerf width , MRR and SR
26	(Saha & Mondal 2016)	NanoCarb 110	Taguchi · Principle Component Analysis and Response surface methodology	Multi Response	WEDM	MRR, Machining time and Ra (μm)
27	(Dhuria et al.2016)	Ti–6Al–4V	Entropy-based grey relational analysis	Multi Response	Ultrasonic machining	MRR and Tool wear rate
28	(Chen et al. 2017)	SKD-11	Support vector regression and Particle swarm optimization	Multi-Objective	WEDM	MRR and Surface quality

2.10 PREDICTION OF WEDM RESPONSES

The various techniques used for prediction of WEDM responses such as artificial neural network (ANN), response surface methodology (RSM), grey prediction, adaptive neuro-fuzzy inference system, feed forward back propagation neural network, multiple regression analysis , group method data handling technique, box–behnken design etc. Lee & Liao (2007) used Grey prediction technique to predict the cutting speed of WEDM process. Present literature shows the prediction of main WEDM performances such as material removal rate and surface roughness by using various prediction techniques.

2.10.1 Prediction of MRR and SR

Ramakrishnan & Karunamoorthy (2008) predicted WEDM responses such as material removal rate and surface roughness by using artificial neural network (ANN) as a prediction tool for the machining of Inconel 718 alloy. Similarly others are adopted artificial neural network method for prediction of WEDM responses such as Rao et al. (2010) predicted material removal rate during the machining of Aluminium BIS-24345 alloy, Ugrasen et al. (2014) predicted dimensional accuracy, surface roughness and material removal rate for machining of Stavax material and Surya et al. (2017) predicted surface roughness and material removal during the machining of Aluminum 7075. However some other prediction techniques were implemented for WEDM responses, ANN-linear regression mathematical model was used for prediction of surface roughness, waviness and material removal rates of WEDM on Udimet- L605 (Singh Nain et al. 2017). In this order Akkurt (2013) adaptive neuro-fazzy inference system method for prediction surface roughness during the machining of Tool steel. While Pant et al. (2014) used feed forward back propagation neural network method for surface roughness for the machining of DC 53 die steel.

Some researchers they have adopted more than one prediction techniques to predict WEDM responses are follows. Rao et al. (2017) predicted surface roughness by using artificial neural network and supporting vector machines (SVM). Material removal rate and surface roughness were predicted by adopted network-based fuzzy inference system and modified genetic algorithm (Sarkheyli et al. 2015). Box–Behnken design

and response surface methodology was used for prediction surface roughness by Das et al. (2017). Ugrasen et al. (2014) adopted ANN, Group Method Data Handling Technique (GMDH) and Multiple Regression Analysis (MRA) for the prediction of WEDM performances and found that the ANN was more accurate. Similarly Shandilya et al. (2013) compared ANN and RSM predicted with experimental values. Moreover they also found that ANN prediction technique gives more accurate than RSM prediction technique.

It is observed from the above literature that ANN prediction technique is more suitable than other prediction techniques because it predicts more accurately. Therefore, in the present study ANN prediction technique will be considered to predict the WEDM responses.

2.11 SUMMARY

Based on the above literature survey it can be inferred that during the conventional machining of SMA materials, higher tool wear and lower surface quality are commonly observed phenomenon, due to their high stain hardening effect, pseudo elastic behaviour and high toughness. Thus, SMA's can be effectively machined by non- conventional machining processes. Hence, there is scope for exploring the possibilities of applying WEDM process on TiNi based materials. Based on the literature survey research gaps has been found which are follows-

- From the literature it is understood that addition of third element to TiNi result in improvement of specific properties. The addition of cobalt as alloying element to TiNi binary shape memory alloy results in changes in transformation energy and mechanical strength (stiffness and yield strength). Hence there is scope for understanding the machining characteristics of TiNiCo systems with different percent addition of cobalt. In this regards, the proposed study shall be extended to explore the machinability aspect of ternary TiNiCo shape memory alloys.

- Machining performance such as material removal rate and surface roughness found the most significant performances of WEDM process. Hence there is scope to measure these responses after the machining of TiNiCo alloy.

- Also the machining performance evaluation depends on the microstructures, surface topography, recast layer thickness, microhardness and residual stresses. Therefore there is scope to study of these characterizations on machined surface.

- Various optimizations techniques are adopted by researchers to optimize the best combination of process parameters such as GRA and RSM. But the combinations of optimizations techniques are rarely used. Hence there is lot of scope of combination of multi-objective optimization techniques for getting optimal setting of WEDM process parameters.

- Analysis has been carried out rarely after the machining to examine the error between experimental and predicted WEDM responses. Therefore scope is there to find the error in between experimental and predicted WEDM responses.

2.12 OBJECTIVES OF CURRENT RESEARCH WORK

The following specific objectives have been derived from literature survey.

1. Development of $Ti_{50}Ni_{49}Co_1$, $Ti_{50}Ni_{45}Co_5$, and $Ti_{50}Ni_{40}Co_{10}$, shape memory alloys through vacuum arc melting.

2. Wire electro discharge machining of developed alloys by using L-33 orthogonal array which is created by response surface design method. To find the optimal setting of process parameters for better MRR and SR a combination of multi-objective optimization techniques will be used.

3. Machined surface characterization with respect to machined surface morphology, machined surface topography, recast layer thickness, micro hardness and residual stresses.

4. For further study two process parameters will be considered for machining of selected alloys. Detailed characterization of machined surface obtained at higher and lower values of MRR and SR.

5. ANN will be used as a prediction technique for the error analysis WEDM responses such as material removal rate and surface roughness.

CHAPTER 3

EXPERIMENTAL PROCEDURE

This chapter contains description of experimental equipment's and procedures adopted for development of $Ti_{50} Ni_{50-x}Co_x$ (x=1, 5 and 10 at. %) shape memory alloy, WEDM machining at optimized process parameters and characterization of machined surface.

3.1 DEVELOPMENT OF SHAPE MEMORY ALLOYS

Commercially available Titanium (99.3% purity), Nickel (99.90%) and cobalt (99.5%) were charged in to copper crucible in vacuum arc melting furnace to melt SMA of composition $Ti_{50}Ni_{50-x}Co_x$ (1, 5 and 10 at. %). Tungsten electrode was used for sparking and melting in an inert argon atmosphere. Fig. 3.1 depicts the setup of vacuum arc melting furnace. TiNi based alloys are very reactive to oxygen, nitrogen and carbon to form oxides and nitrides. Slight variation in the composition affects the transformation properties as these alloys are extreme sensitivity to impurities. In order to avoid these contaminations from the atmosphere and to ensure high purity of the ingot, melting was carried out in vacuum atmosphere. Fig. 3.2 shows the Vacuum arc melting chamber (a) raw material placed in the copper crucible, (b) Melted buttons and (c) Rectangular block of as-cast alloy.

Figure 3.1 Setup of vacuum arc melting furnace
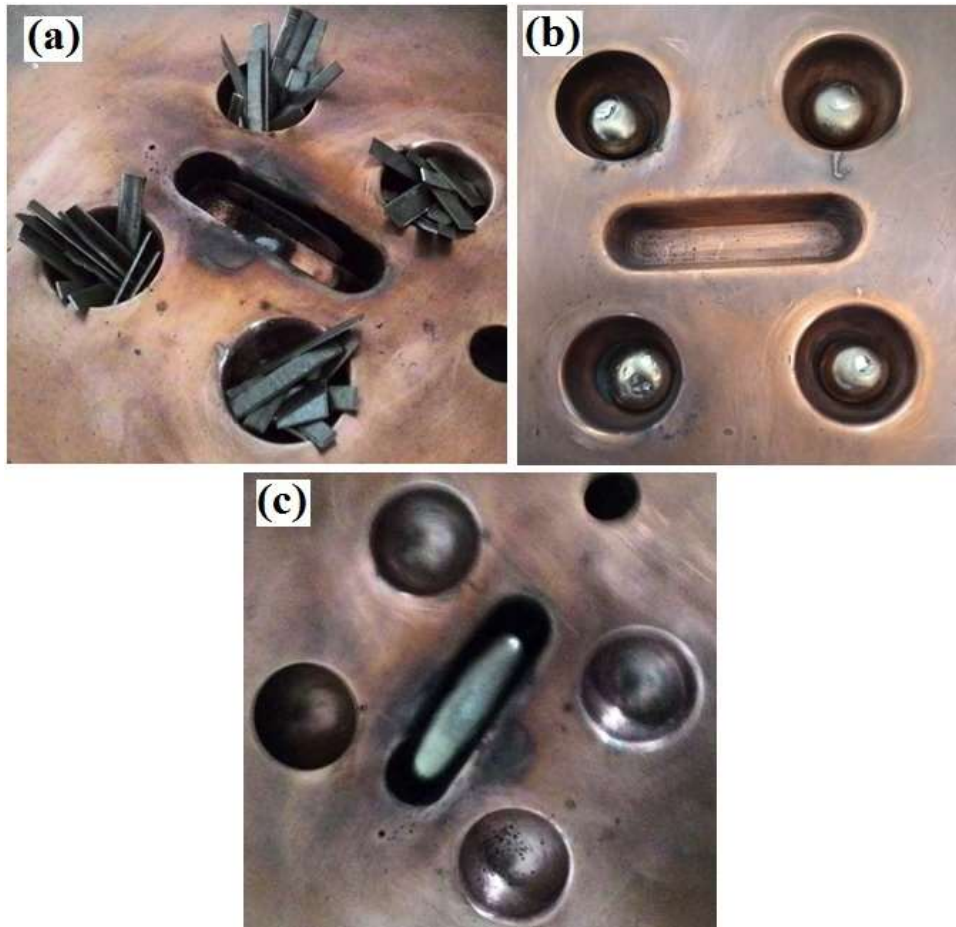
Figure 3.2 Vacuum arc melting chamber (a) raw material placed in the copper crucible, (b) Melted buttons and (c) Rectangular block of as-cast alloy.

Vacuum is created using the standard procedure, later the air present inside the chamber is flushed out of the system by rough pumping and the vacuum of 10^{-5} mbar was maintained and followed by backfilling of the argon gas. This is required in order to remove impurities present in the chamber and easy movement for TIG melting rod. The arc melting is carried out in argon purged environment to melt the material in the form of buttons. The melting and re-melting of buttons is six times in order to achieve homogeneity of the alloy. The materials were melted into button shape followed by further melting into rectangular blocks of size 50mm x 12mm x 10mm.The similar procedure is followed for different composition, and composition of the developed alloys is shown in Table 3.1.

Table 3.1 Composition (at. %) of TiNiCo alloys.

Alloys	Ti (at. %)	Ni (at. %)	Co (at. %)
1	50	49	1
2	50	45	5
3	50	40	10

3.2 EDX AND PHASE ANALYSIS OF AS-CAST TiNiCo ALLOYS

Energy dispersive X-ray (EDX) analysis was performed for as-cast materials using "ZEISS, SEMV018 EDX spectrometer" shown in Fig. 3.3 for the confirmation of the presence of alloying elements in developed alloys. Fig. 3.4 a, Fig. 3.4 b and Fig. 3.4 c clearly indicate the percentage of alloying elements of Ti, Ni, and Co alloy for each developed alloy. The phase analysis was carried out of as-cast alloy by using Bruker D8 advance using CuKα radiation and 2θ scanning rate was 2°/min. B2 austenite phase is present in the as cast alloy with the weak appearance of peaks belongs to B 19' martensite, which can be seen in Fig. 3.5 for $Ti_{50}Ni_{49}Co_1$ alloy, Fig.3.6 for $Ti_{50}Ni_{45}Co_5$ alloy and Fig. 3.7 for $Ti_{50}Ni_{40}Co_{10}$ alloy. Similar kind of phases has been observed in TiNiCo alloy by Mohammad et al. (2014).

Figure 3.3 Scanning electron microscope with EDAX attachment.
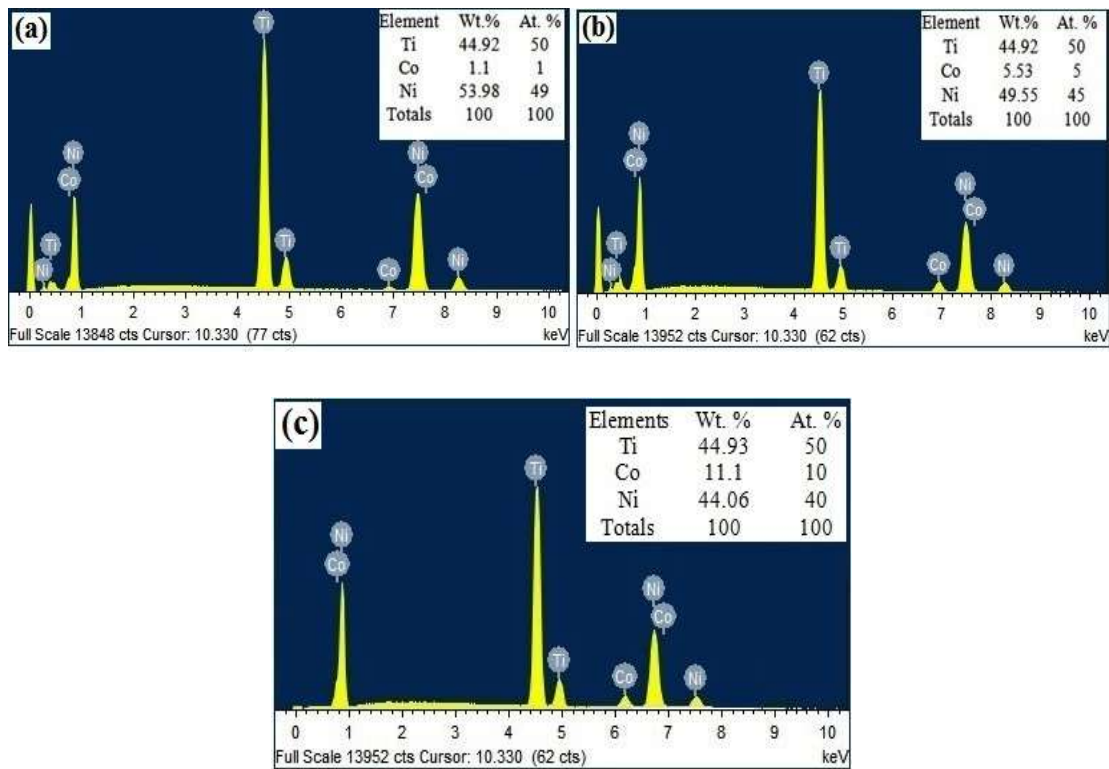
Figure 3.4 EDAX analysis of as cast alloys (a) for $Ti_{50}Ni_{49}Co_1$ alloy (b) $Ti_{50}Ni_{45}Co_5$ alloy and (c) $Ti_{50}Ni_{40}Co_{10}$ alloy.
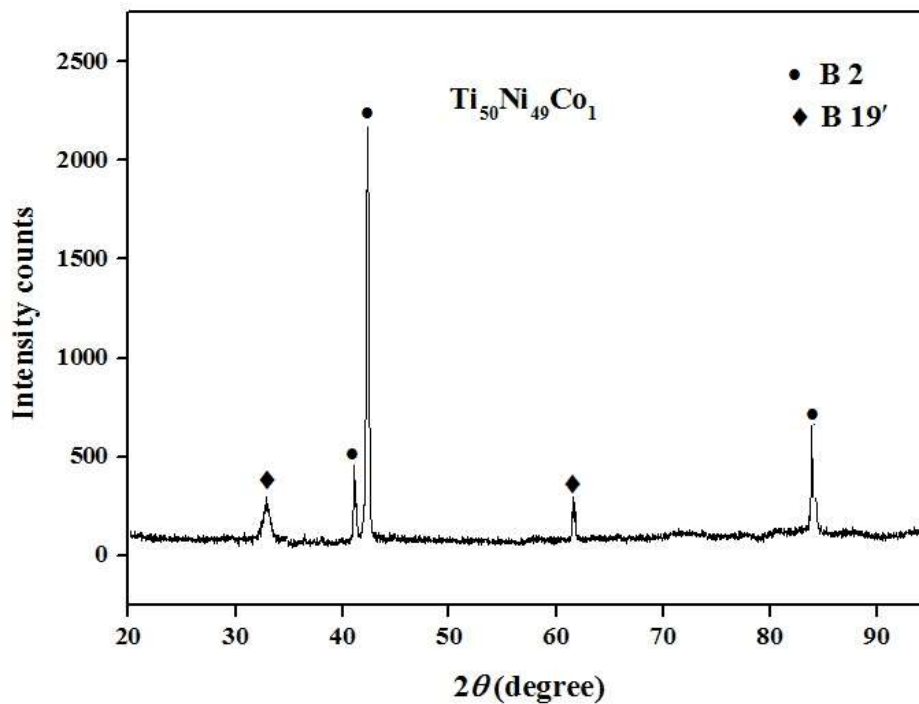
Figure 3.5 XRD analysis of as cast $Ti_{50}Ni_{49}Co_1$ alloy.
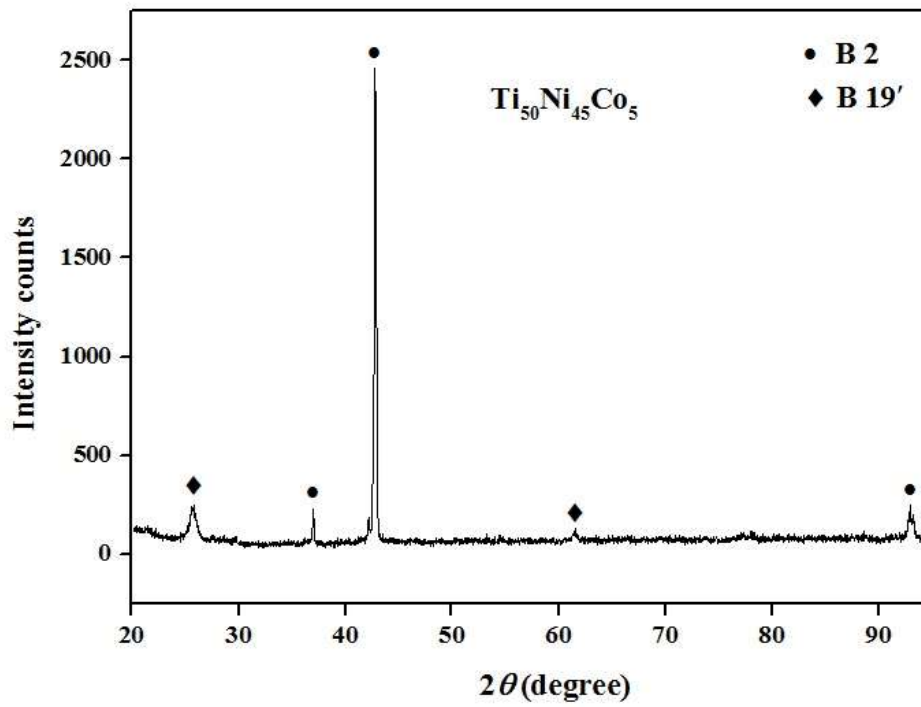
Figure 3.6 XRD analysis of as cast $Ti_{50}Ni_{45}Co_5$ alloy.
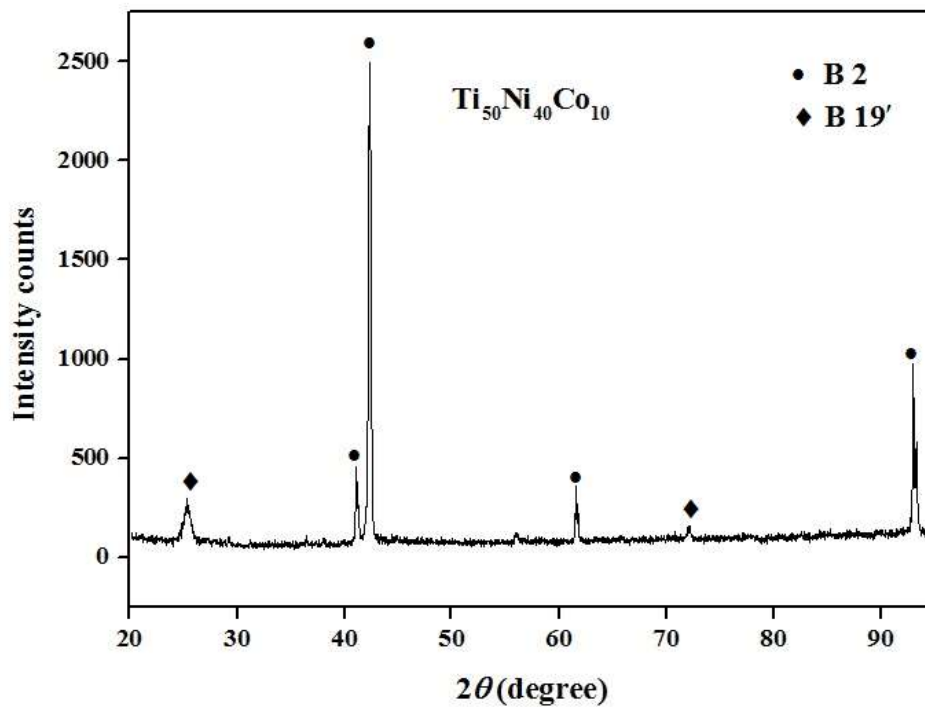
Figure 3.7 XRD analysis of as cast $Ti_{50}Ni_{40}Co_{10}$ alloy (Soni et al. 2017).

3.3 WIRE ELECTRO DISCHARGE MACHINING

WED machine (Model Electronica ELPULS15 CNC) was used for machining of shape memory alloys and is shown in Fig. 3.8. Pulse on time (T_{on}), Pulse off time (T_{off}), Servo voltage (SV), Servo feed (SF) and Wire speed (WS) were selected as input process parameters. Based on the trial experiments, parameters were selected at different levels and are shown in Table 3.2. Brass wire of diameter 0.25mm was used as the tool electrode (cathode) and workpiece as anode for electrical discharge and distilled water was used as dielectric fluid in the machining process. WEDM machining of TiNiCo shape memory alloys were carried out with respect to L-33 orthogonal array shown in Table 3.3 which is created by response surface design (DOE) by using Minitab 17 Software. Material removal rate and surface roughness were considered as output responses of wire electro discharge machining process.

Table 3.2 Input process parameters and their levels.

Input parameters	Levels				
	1	2	3	4	5
Pulse on time (μs)	105	110	115	120	125
Pulse off time (μs)	28	35	42	49	56
Servo voltage (V)	20	30	40	50	60
Servo feed (mu)	2160	2170	2180	2190	2200
Wire speed (m/min)	2	3	4	5	6

Table 3.3 L-33 Orthogonal array.

Run	Input process parameters				
	T_{on}	T_{off}	SV	SF	WS
1	120	35	50	2170	5
2	110	49	50	2190	3
3	115	42	40	2180	6
4	115	42	40	2160	2
5	110	35	50	2190	5

6	110	49	30	2170	3
7	110	35	50	2170	3
8	120	49	50	2170	3
9	120	49	30	2170	5
10	120	49	50	2190	5
11	115	42	40	2180	4
12	110	49	50	2170	5
13	110	49	30	2190	5
14	120	35	30	2190	5
15	125	42	40	2180	6
16	120	35	30	2170	3
17	120	42	40	2180	4
18	115	42	40	2180	4
19	110	35	30	2170	5
20	120	49	30	2190	3
21	110	35	30	2190	3
22	120	35	50	2190	3
23	115	42	40	2180	2
24	115	42	60	2180	4
25	105	42	40	2180	4
26	115	42	30	2180	4
27	115	42	20	2180	4
28	120	42	40	2180	6
29	115	56	40	2180	4
30	115	42	40	2180	3
31	115	42	40	2200	4
32	115	28	40	2180	4
33	125	42	40	2180	4

3.4 MEASUREMENT OF OUTPUT RESPONSES

From the literature survey it has been observed that material removal rate and surface roughness are most important output responses of WEDM process. Therefore these two responses were considered for the present study. Measurement of WEDM responses such as material removal rate and surface roughness was carried out. Further the process parameters are optimized to obtain low surface roughness with high material removal rate.
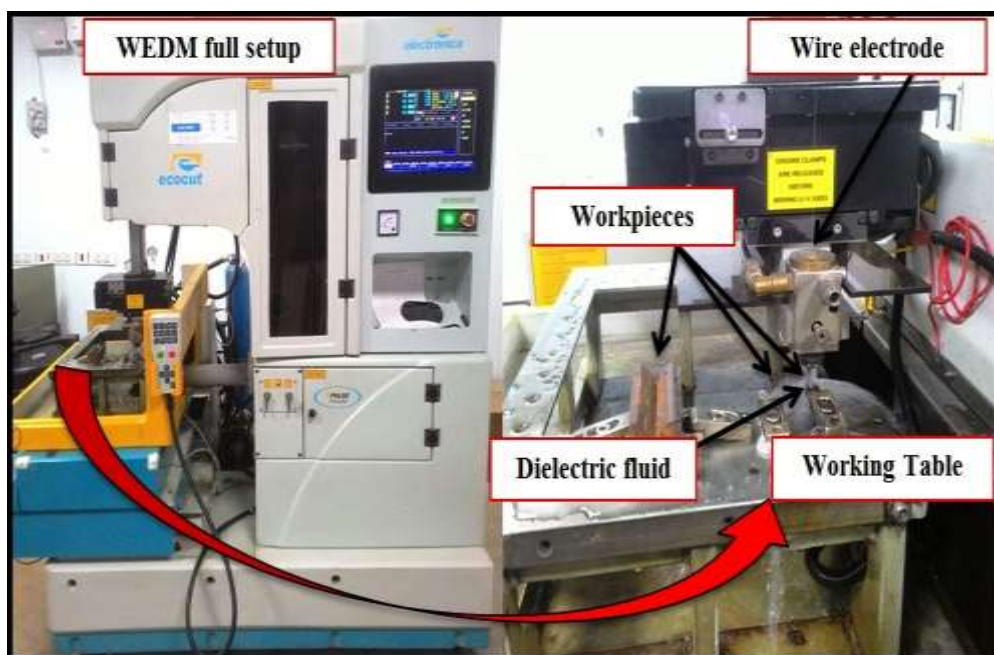
Figure 3.8 Wire EDM

3.4.1 Material removal rate

Material removal rate is a significant response for production of any product in the manufacturing industries. In the current investigation MRR was calculated using equation 1 (Manjaiah et al. 2015).

MRR (mm^3/min) = Cutting speed x Kerf width x height of work piece ---------- (1)

Where average cutting speed (mm/min) of each experimental run was considered for measurement of material removal rate.

Kerf width (mm) = 2 x spark gap (0.125mm) + diameter of wire (0.250 mm)

Workpiece height was 10mm during the machining.

3.4.2 Surface roughness (Ra)

The "surface roughness tester SJ-301 (Mitutoyo) was used to record the surface roughness of the machined surface. The roughness of each machined surface was measured at three different locations and the average surface roughness (R_a) was reported in the present study. The cut off length of 0.8 mm, evaluation length of 3 mm, and the stylus speed of 0.25 mm/s was used to record the surface roughness.

3.5 OPTIMIZATION TECHNIQUES

The best combinations of process parameters are obtained through hybrid combination of optimization techniques namely grey relational analysis, entropy measurement method and response surface design methodology. Fig.3.9 indicates the relation between combinations of these optimization techniques.
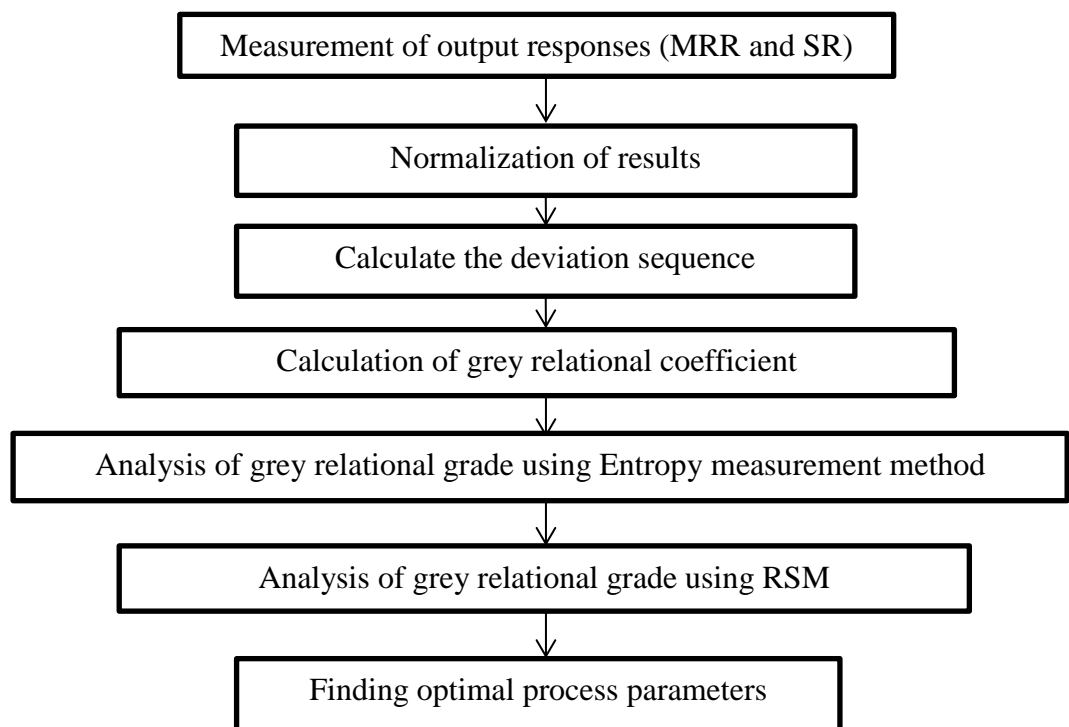
Figure 3.9 Flowchart showing hybrid combinations of optimization techniques.

3.5.1 Grey relational analysis (GRA)

GRA is one of the most practical analytical optimization methods. GRA provides suitable tools for examining a rank of order of multiple objects with resemblance from an objective (Majhi et al. 2013). GRA requires limited information to estimate the behavior of an uncertain system and discrete data problem. If the sequence range is large, the factors are effaceable therefore data pre-processing is an important steps to manage the factors of GRA (Pandey et al. 2014). The range of data pre-processing is from zero to one (Raju et al. 2016). For the data pre-processing, there are two conditions of normalization in the present study namely higher the better which will be used in the normalization of MRR and another one is lower the better for normalization of SR values. Table 3.4 indicates the two conditions of normalization.

Table 3.4 Conditions of normalization.

S. No.	Conditions	Equations
1	Lower is better	$X_i^*(k) = \dfrac{X_i(k) - \min X_i(k)}{\max X_i(k) - \min X_i(k)}$ ....(2)
2	Higher is better	$X_i^*(k) = \dfrac{\max X_i(k) - X_i(k)}{\max X_i(k) - \min X_i(k)}$ ....(3)

where i = 1, 2n, k = 1, 2, y, p; X_i^* (k) is the normalized value of the kth element in the ith sequence, max X_i (k) is the largest value of X_i (k), and min X_i (k) is the smallest value of $X_i(k)$, n is the number of experiments and p is the number quality characteristics.

After the normalization, grey relational co-efficient (γ) are calculated, this shows the interaction between optimal and actual normalized experimental results.

$$\gamma_i(k) = \gamma(x_0(k)) = \frac{\Delta\min + \zeta\Delta\max}{\Delta_{0,i}(k) + \zeta\Delta\max} \quad .... \text{(4)}$$

i=1; . . . ; n; k= 1; . . . ; p

Where $\Delta_{0,i}$ (k) = |x_0(k)−x_i(k)| is the difference of the absolute value called deviation sequence of the reference sequence x_0(k) and comparability x_i(k). The ξ is distinguishing coefficient or identification coefficient. In general, it is set to 0.5. The Grey relational grade (GRG) is a weighting-sum of the grey relational coefficients and it is defined as

$$\gamma(x_0, x_i) = \sum_n^{k=1} \beta_k(x_0, x_i) \ \dots\dots (5)$$

Where β_k represents the weighting value of the kth.

Performance characteristic, and $\sum_n^{k=1} \beta_k = 1$.

3.5.2 Entropy measurement method

Entropy measurement method is an objective weighting method. Discrete type of entropy is used in grey entropy measurement for properly conduct weighting analysis. Table 3.5 exhibits basic steps of entropy measurement method which is used for calculating grey relational grade. There are six stages for calculating weights of each characteristic (Mineta, et al. 2011). Grey relational grades are calculated by multiplying grey relational co-efficient with corresponding weight of each characteristic, and the values are given in Table 3.5 for each alloy.

Table 3.5 Basic steps for calculating grey relational grade (GRG).

S. No.	Stages	Formulas
1	Summation of each attribute's value for all sequences (D_k)	$D_k = \sum_{i=1}^{n} x_i(k)$ .....(6)
2	Calculate the normalization coefficient (K) Where m is the number of attributes.	$K = \dfrac{1}{(e^{0.5}-1)m}$ .....(7)
3	Find the entropy for the specific attribute (e_k)	$e_k = \dfrac{1}{K}\sum_{i=1}^{n} f(\dfrac{x_i(k)}{D_k})$ .....(8)
4	Calculate the total entropy value (E)	$E = \sum_{k=1}^{n} e_k$ .....(9)
5	Determine the relative weighting factor (λ_k)	$\lambda_k = \dfrac{(1-e_k)}{n-E}$ ......(10)
6	Normalized weight of each attribute is calculated (β_k)	$\beta_k = \dfrac{\lambda_k}{\sum_{k=1}^{n} \lambda_i}$ ....(11)

3.5.3 Response surface method (RSM)

Response surface methodology investigates the communication between many illustrative variables and one or more response variables (Hewidy et al. 2005). The most essential application of this approach is to utilize a series of designed experiments to get best response. Commonly a second-degree polynomial model is used in this approach. Even though these models are just a prediction, such a model is easy to estimate and apply, even when little is known about the process. In order to study the effect of WEDM process parameters of TiNiCo alloys on the volumetric surface roughness and metal removal rate, a second-order polynomial response can be fitted into the equation 12 (Layard et al. 2009).

$$Y = \beta_0 + \sum_{i=1}^{k} \beta_i X_i + \sum_{i=1}^{k} \beta_{ii} X_i^2 + \sum_{i,j=1,\ i\neq j}^{k} \beta_{ij} X_i X_j + \varepsilon \ \dots\dots\ (12)$$

Where ε is the noise or error observed in the response Y. X_i is the linear input variables and X_i^2 and X_i, X_j are the squares and interaction terms respectively, of these input variables. The unknown second order regression coefficients are β_o, β_i, β_{ij} and β_{ii}, which should be determined in the second-order model are obtained by the least square method.

Response surface methodology used in the present study includes designing of a series of experiments for sufficient and reliable measurement of the output responses and development of mathematical model of second order response surface with the best fittings. The optimal set of experimental parameters, thus produce a maximum or minimum value of the response (Helth et al. 2013).

3.6 CHARACTERIZATION OF MACHINED SURFACE OF TiNiCo ALLOYS

Machined surface characterization has been carried out for optimized process parameters with respect to recast layer thickness, surface topography, microhardness, XRD analysis and residual stresses.

3.6.1 Recast layer thickness (RLT)

Machined Surface morphology has been carried out through scanning electron microscopy (JEOL JSM-638OLA) and can be seen in Fig. 3.10. However During wire electro discharge machining rapid heating and quenching of the molten material by the dielectric fluid causes the formation of a solidified layer and gets deposited on the machined surface called recast layer (Soni et al. 2017). The thickness of recast layer was determine by the polishing the cross section of the machined surface by using SiC paper, diamond polishing with an etchant HNO_3+HF+H_2O. Similar measurement has been carried out by Manjaiah et al.(2015) and can be seen in Fig. 3.11.

Figure 3.10 Scanning electron microscopy for machines surface morphology.
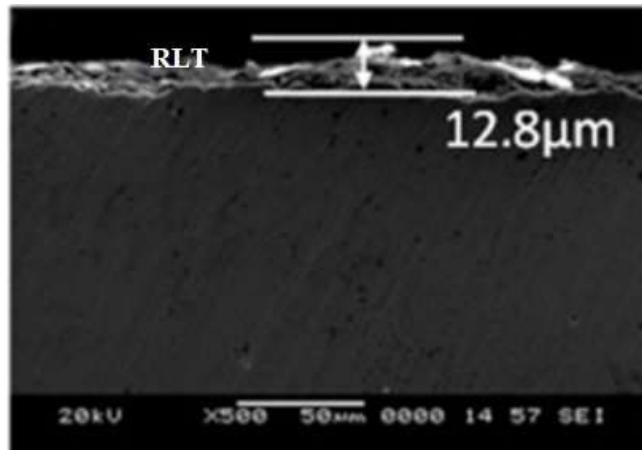
Figure 3.11 Cross-sectioned SEI micrographs of WED-machined $Ti_{50}Ni_{40}Cu_{10}$ SMA.

(Manjaiah et al. 2015)

3.6.2 Machined surface topography

The machined surface 3D topography has been measured through Confocal microscope LEST OLS4100' 3D. During the topographical analysis 1067 μm x 1067 μm area was selected to evaluation of machined surface and Cutoff (λc) =80μm was considered during the measurement. Figure 3.12 shows the captured image during the surface topographical analysis.
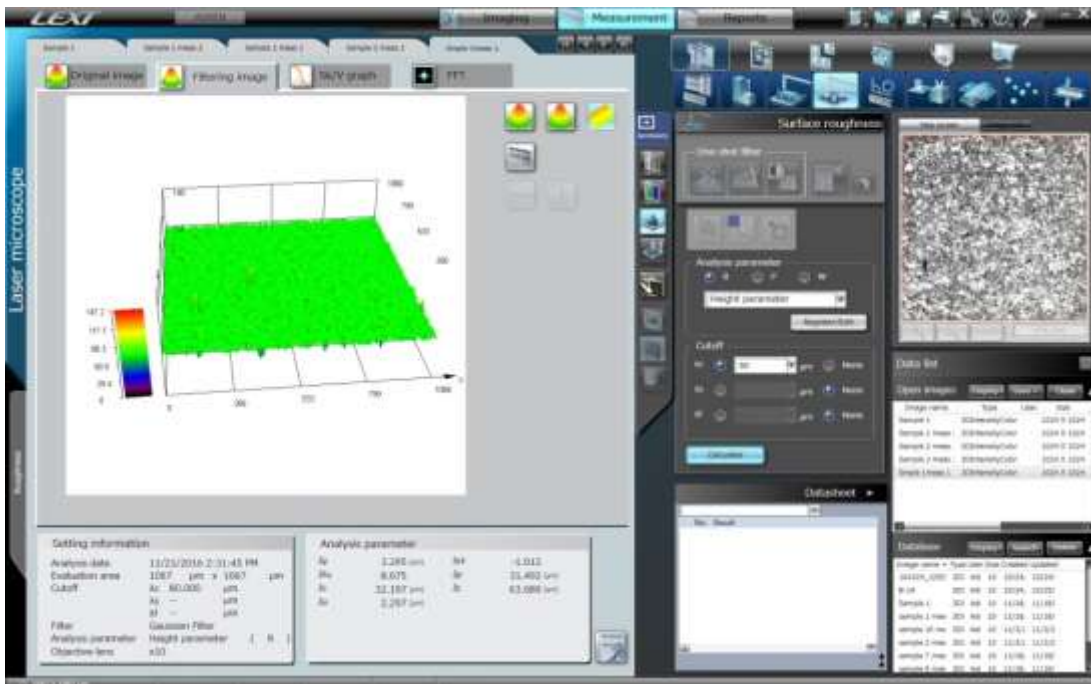
Figure 3.12 Captured image during the surface topographical analysis.

3.6.3 Micro hardness

The formation of layers from the machined surface toward the base material is presented in the Fig 3.13. Near the cutting edge was considered as a starting point (0μm) and measure the microhardness towards the base material till depth of 150μm. Where five times measured the hardness values for particular place of specimen and average microhardness values were considered for present study. Omni Tech Model: MVH-S-AUTO, microhardness tester was used for measurement of hardness values along the cross section, from machined surface to inner depth surface using 300 gram load and 15Sec. dwell time. Figure 3.14 shows the setup of Microhardness tester.
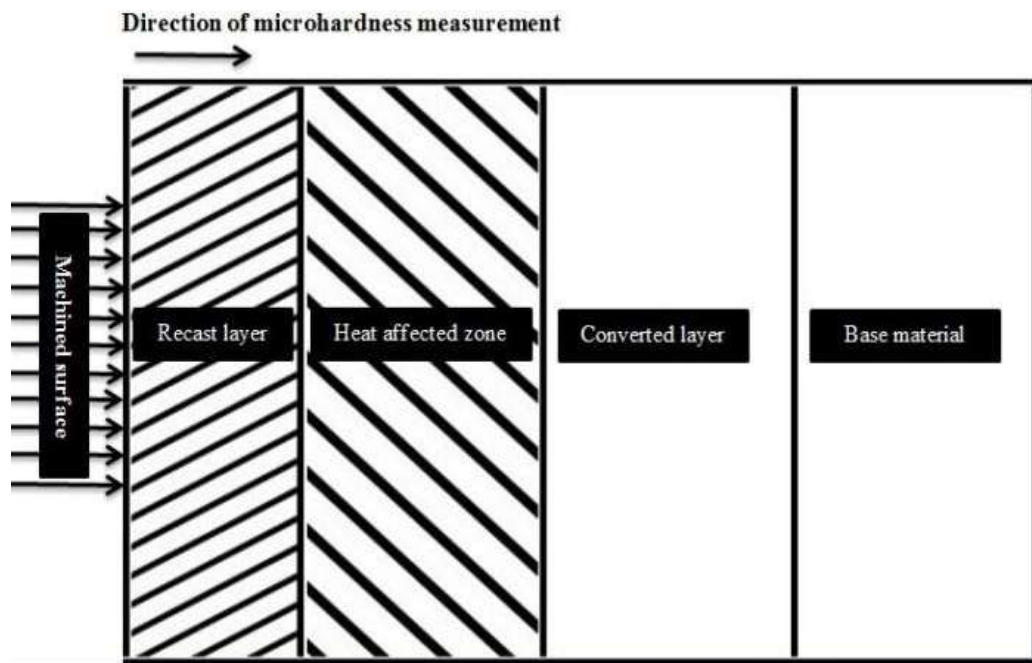
Figure 3.13 Schematic diagram of three kinds of layers on machined component (Soni et al. 2017).

Figure 3.14 Setup of Microhardness testers.

3.6.4 XRD analysis

XRD analysis is carried out to understand the formation of oxides and other phase changes on the machined surface. Diffraction patterns were obtained by Bruker AXS D-8 Advance Diffractometer (Germany) with CuKα radiation and nickel filter at 20 mA under a voltage of 35 kV. The specimens were scanned with a scanning speed of 1 Kcps in 2θ range of 20 to 95° and the intensities were recorded at a chart speed of 1 cm/min with 1°/min as Goniometer speed. The setup of XRD analysis is given in Figure 3.15. The relative intensities of all the peaks have been observed by assuming height of the most prominent peak as 100%. The diffractometer being interfaced with Bruker DIFFRAC plus X-Ray diffraction software provides'd' values directly on the diffraction pattern. These'd' values were then used for identification of various phases with the help of inorganic ASTM X-Ray diffraction data cards.
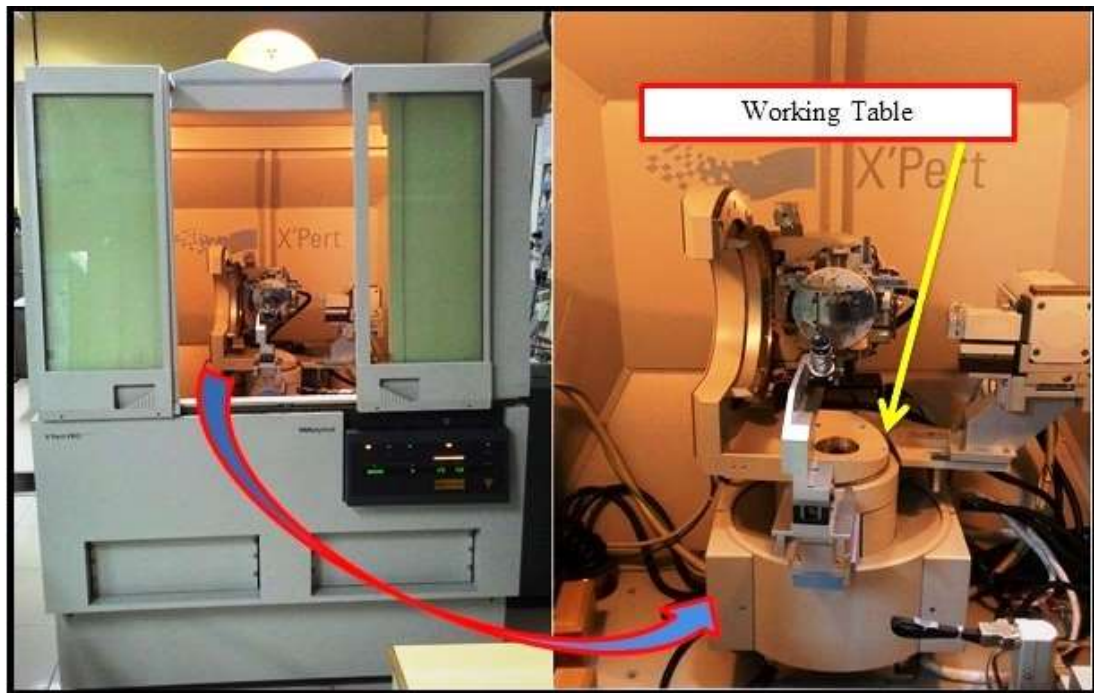
Figure 3.15 Setup for residual stress analysis.

3.6.5 Residual analysis

During machining, residual stresses will be generating on nonhomogeneous, plastically deformed machined surface causing metallurgical transformation. The degree of residual stress induced in the machined surface during Wire Electro discharge machining will be evaluating using X-ray diffraction technique. Before the residual stress measurement samples were prepared as per the equipment requirement (size of 3 x 3 x 5 mm) through WEDM process at optimized process parameters and polished through electro chemical polishing. Through electro chemical polishing of machined surface can be remove the recast layer on the machined component (Navas et al. 2008). And also, residual stresses have been measured without electro chemical polishing on machined surface i e. with recast layer for two process parameter approach.

During the optimization of WEDM process parameters it has been found that pulse on time and servo voltage were varying at optimized process parameters while rest of the process parameters were found constant in the best combination of process parameters for machining of $Ti_{50}Co_{49}Co_1$, $Ti_{50}Co_{45}Co_5$ and $Ti_{50}Co_{40}Co_{10}$ alloy. Therefore, further

study has been carried out at based on these two process parameters to see the detailed effects during the machining of $Ti_{50}Co_{49}Co_1$, $Ti_{50}Co_{45}Co_5$ and $Ti_{50}Co_{40}Co_{10}$ alloys.

3.7 TWO PROCESS PARAMETER APPROACH

During the two process parameters approach pulse on time and servo voltage were considered as process parameters with their five levels. L-25 orthogonal array (Table 3.6) has been created by using Taguchi DOE through Minitab 17 Software. The responses of MRR and SR have been measured. Further characterization has been carried out for machined surface at the lower and higher values of outputs with respect to microstructure, surface topography, recast layer thickness, micro hardness and residual stresses.

Table 3.6 L-25 orthogonal array for two process parameters approach.

Run	Pulse on time	Servo voltage
1	105	20
2	105	30
3	105	40
4	105	50
5	105	60
6	110	20
7	110	30
8	110	40
9	110	50
10	110	60
11	115	20
12	115	30
13	115	40
14	115	50
15	115	60
16	120	20
17	120	30

18	120	40
19	120	50
20	120	60
21	125	20
22	125	30
23	125	40
24	125	50
25	125	60

3.8 ARTIFICIAL NEURAL NETWORK FOR RESPONSES

ANN is an artificial illustration of human brain that tries to simulate its learning approach which is an interconnected pairs of artificial neurons that uses a mathematical model for information processing based on a connectionist method to computation. Neural networks are non-linear mapping systems that consist of simple processors which are called neurons, linked by weighed connections. Each neuron has inputs and generates an output that can be seen as the reflection of local information that is stored in connections. Among ANN models, the feed forward neural network based on back-propagation is the best general-purpose model. The ANN network had two inputs such as pulse on time and servo voltage because these two process parameters were found as most influential process parameters for machining of $Ti_{50}Co_{49}Co_1$, $Ti_{50}Co_{45}Co_5$ and $Ti_{50}Co_{40}Co_{10}$ alloys with respect to two outputs material removal rate and surface roughness. Matlab software was used for predicting the responses. As per the literature survey for the perfection of WEDM responses through ANN, experimental results has been divided in two kinds of data namely test data and training data. To getting best prediction values of responses training data should be consider 70% of experimental results and rest of the data should be test data (Ugrasen et al. 2014)**.** For present study 70% data was kept in training and rest of the data was test data during the prediction. To get the best regression plots which give accurate prediction 15 hidden layers were adopted during the training of the data. Developed ANN model can be seen in Fig. 3.16 and Fig. 3.17 is presented regression

plots. Same procedure implemented for prediction of WEDM responses for $Ti_{50}Co_{49}Co_1$, $Ti_{50}Co_{45}Co_5$ and $Ti_{50}Co_{40}Co_{10}$ alloy. Further study has been carried out for error analysis to find the error between of experimental and predicted values. Table 3.7 shows training parameters during the ANN.
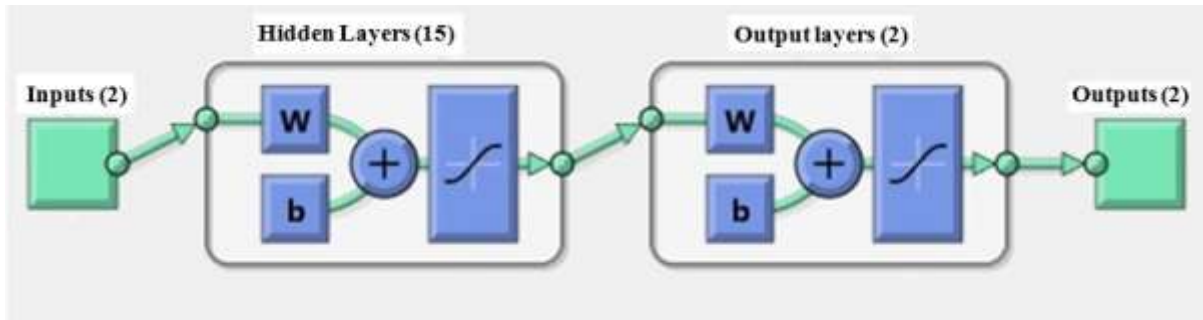
Figure 3.16 Developed ANN Model.

Table 3.7 Training parameters.

Input	Weight (W) Biases (b)	Output
(1) Pulse on time (2) Servo voltage	Randomly between -1 and +1	(1) Material removal rate (2) Surface roughness

3.9 ERROR ANALYSIS

Error analysis has been carried out through the comparison between experimental and predicted values. Artificial neural network (ANN) is used as predictor for the prediction of wire electro discharge machining (WEDM) responses such as the material removal rate (MRR) and surface roughness (SR) during the machining of $Ti_{50}Ni_{49}Co_1$, $Ti_{50}Ni_{45}Co_5$ and $Ti_{50}Ni_{40}Co_{10}$ shape memory alloy. L-25 orthogonal array has been created by using Taguchi design of experiment (DOE) for experimental plan.

3.9 SUMMARY

In this chapter machining of developed $Ti_{50}Ni_{50-x}Co_x$ (x=1, 5 and 10 at. %) shape memory alloys by using wire electro discharge machining have been discussed. For further study MRR and SR measured as per L-33 orthogonal array and optimized

process parameters. However machined surface characterization has been carried out at optimized parameters conditions for all three alloys. Moreover two process parameters approach was adopted for further machining and measured the machining responses. Detailed characterization of machined surface obtained at higher and lower values of MRR and SR. ANN was used for prediction of WEDM responses and compared with the experimental values of responses to found the error .The adopted methodology and details of used equipment for current research work were also discussed. The experimental plan of present work is shown in the flow chart (Figure 3.18).
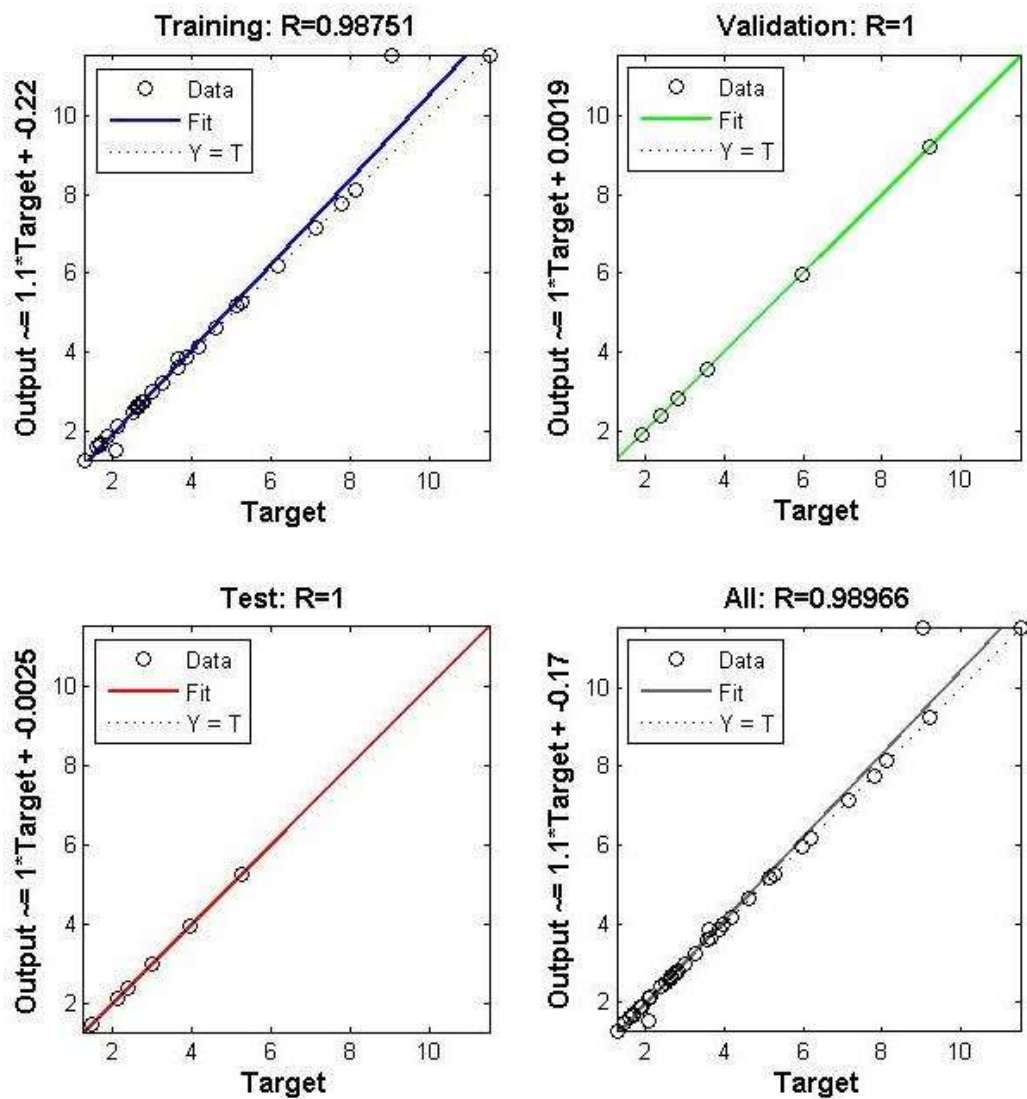
Figure 3.17 Regression plots of ANN model.
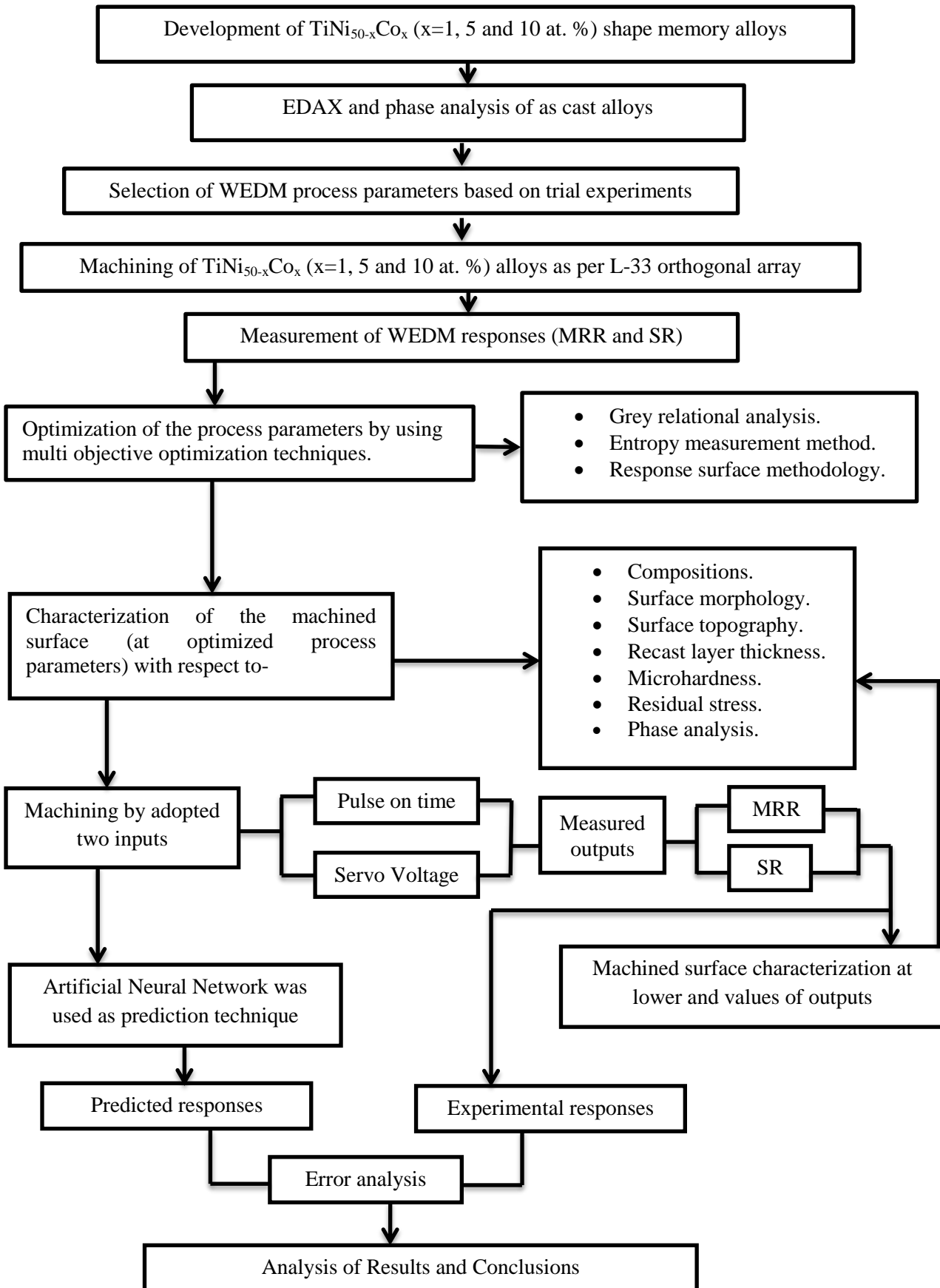
Figure 3.18 Flow Chart of Experimental Plan.

CHAPTER 4

WIRE ELECTRO DISCHARGE MACHINING CHARACTERISTICS

4.1 INTRODUCTION

This chapter describes the WEDM machining characteristics of developed TiNiCo alloys. Machining has been carried out as per L-33 orthogonal array and effect of process parameters on responses of material removal rate and surface roughness for the shape memory alloys $Ti_{50}Ni_{49}Co_1$, $Ti_{50}Ni_{45}Co_5$, and $Ti_{50}Ni_{40}Co_{10}$ are studied. Grey relational analysis was adopted for optimization of process parameters. The machined surfaces are characterised with respect to microstructure, surface topography, hardness and residual stress and phases present in the machined surface.

4.2 MACHINING OF SHAPE MEMORY ALLOYS

The machining of $Ti_{50}Ni_{49}Co_1$, $Ti_{50}Ni_{45}Co_5$ and $Ti_{50}Ni_{40}Co_{10}$ shape memory alloys is carried out through wire electro discharge machining as per L-33 orthogonal array created by response surface design. L-33 orthogonal array has been used for initially experiments and to see the effect of all selected process parameters on Wire EDM output responses. Material removal rate and surface roughness are measured as output responses. Details about the machining and machining process parameters have been presented in the section of 3.3 and Table 3.3. Table 4.1 indicates the machining responses for each alloy.

Table 4.1 Measured output responses of MRR and surface roughness.

Run Number	$Ti_{50}Ni_{49}Co_1$		$Ti_{50}Ni_{45}Co_5$		$Ti_{50}Ni_{40}Co_{10}$	
	MRR (mm^3/min)	SR (R_a)	MRR (mm^3/min)	SR (R_a)	MRR (mm^3/min)	SR (R_a)
1	1.26	3.36	1.720	3.47	4.556	3.09
2	1.97	3.29	0.720	2.65	1.472	2.27
3	3.25	2.74	2.221	3.45	4.08	2.89
4	3.68	3.5	2.074	2.95	3.948	2.58
5	2.07	2.29	1.457	2.72	2.04	2.69

6	2.53	2.56	1.228	2.44	2.366	2.62
7	2.13	2.52	1.212	2.58	2.866	2.96
8	2.56	2.58	1.462	2.63	3.65	2.51
9	5.37	3.45	3.719	2.93	5.837	4.38
10	2.73	2.7	1.643	2.71	2.954	3.5
11	3.29	3.33	2.253	3.65	3.453	2.84
12	1.11	3.01	0.622	2.27	1.56	1.85
13	1.88	2.51	1.237	2.78	2.048	3.08
14	5.42	3.98	3.798	4.11	5.616	4.08
15	3.25	2.62	1.231	3.24	3.918	3.5
16	5.25	3.75	1.869	3.74	6.084	3.89
17	3.15	2.59	2.680	2.86	3.881	2.86
18	4.57	2.71	8.538	3.48	5.437	2.87
19	3.13	2.62	2.485	2.59	4.417	2.96
20	5.53	2.38	1.659	2.7	5.812	3.76
21	3.26	2.55	2.828	2.59	3.258	2.41
22	4.11	2.79	2.760	3.44	5.022	4.33
23	2.24	3.11	2.730	2.92	3.63	2.91
24	2.32	2.96	0.792	3.24	1.664	2.49
25	2.01	2.29	1.107	2.34	2.157	2.53
26	4.23	0.96	2.010	2.98	3.49	3.21
27	5.32	3.57	2.539	3.55	5.058	3.7
28	3.38	2.44	1.778	2.89	3.916	2.74
29	2.31	2.75	1.305	2.65	3.142	2.66
30	3.52	2.89	1.761	2.75	4.616	2.75
31	3.58	3.31	2.251	3.17	4.417	2.94
32	5.44	2.87	3.014	3.89	5.612	3.51
33	6.52	2.89	1.720	3.47	6.864	2.74

4.3 EFFECTS OF PROCESS PARAMETERS ON OUTPUT RESPONSES

Effect of process parameters on outputs such as material removal rate and surface

roughness are given in Fig. 4.1 a to e, Fig. 4.2 a to e, Fig. 4.3 a to e, Fig. 4.4 a to e, Fig. 4.5 a to e and Fig. 4.6 a to e. A best combination of input process parameters are obtained through optimisation.

4.3.1 Effects of process parameters on material removal rate

MRR increases with increased pulse on time (T_{on}) as can be seen in Fig 4.1a for $Ti_{50}Ni_{49}Co_1$, Fig. 4.2a for $Ti_{50}Ni_{45}Co_5$, and Fig. 4.3a for $Ti_{50}Ni_{40}Co_{10}$ alloys. Further small reduction was noticed in MRR with increased pulse on time, for $Ti_{50}Ni_{45}Co_5$ alloy which can be attributed to poor flushing in the machining zone. MRR increases with increased pulse on time because at high pulse on time, spark intensity is high; due to this more thermal energy is available to remove the material from the work surface which results in less time required for removal of material from the work piece surface, hence leading to high MRR. Similar work presented by Roy et al. (2017) during the machining of TiNiCu shape memory alloy. From the Fig 4.1b for $Ti_{50}Ni_{49}Co_1$, Fig. 4.2b for $Ti_{50}Ni_{45}Co_5$, and Fig. 4.3b for $Ti_{50}Ni_{40}Co_{10}$ alloys it is observed that MRR decreases with increase in pulse off time. The decrease in MRR with high pulse off time is due to decrease in spark intensity as more time is required for flowing dielectric fluid leading to low MRR. But MRR increase at 42 μs pulse off time in Fig. 4.2b and Fig. 4.3b, which is may be due to the wire vibration in the machining zone. Same as reported by kumar et al. (2017) during the WEDM of pure titanium. It is noticed from Fig. 4.1c, Fig. 4.2c and Fig. 4.3c that MRR decrease with increase servo voltage because increase in servo voltage results in larger spark gap thereby reducing the spark intensity and eventually lesser amount of material is removed from the surface of the workpiece. Similar trend has been seen in Fig. 4.2c, but in this case MRR increase with initial increment in servo voltage till 30V. Fig. 4.3c shows that MRR decreases with increased servo voltage (SV) up to 50 V, further it is observed as constant, because sometime improper clamping during holding the workpiece on the working table affect the machining responses. Similar observation reported by Goswami et al. (2014) during the machining of Nimonic 80A (77.05% Ni, 18.39% Cr, 1.92% Ti, 1.05% Al, 0.63% Fe, 0.2% Mn, and 0.19% Si). Servo feed is not an effective process parameter with respect to MRR and the effect of servo feed was not unique for any alloy which can be seen in the Fig 4.1d for $Ti_{50}Ni_{49}Co_1$, Fig. 4.2d for $Ti_{50}Ni_{45}Co_5$, and Fig. 4.3d for $Ti_{50}Ni_{40}Co_{10}$ alloys. Similar results are

reported by other researchers in their study on machining of nanostructured hard facing materials using WEDM (Saha et al. 2016). From Fig. 4.1e and Fig. 4.3e it is noticed that MRR increases with increased wire speed (WS) up to 4 m/min, but further increase in wire speed up to 5 m/min resulting in decreased MRR. Small improvement is noticed in MRR with increased wire speed from 5 m/min to 6 m/min for $Ti_{50}Ni_{49}Co_1$ alloy and $Ti_{50}Ni_{40}Co_{10}$ alloy. It is seen from Fig 4.2e that MRR increases with increase in wire speed up to 4 m/min because more melted material splashed through the machining zone and hence leads to high MRR. If the wire speed is more than 4 m/min, wire vibration reduces the dynamic stability of the wire and causes unfavourable sparking condition and hence leads to lower MRR. Similar results have been noticed for Inconel 706 by using WEDM (Sharma et al. 2015).
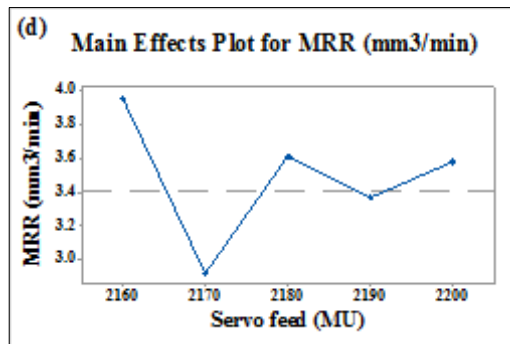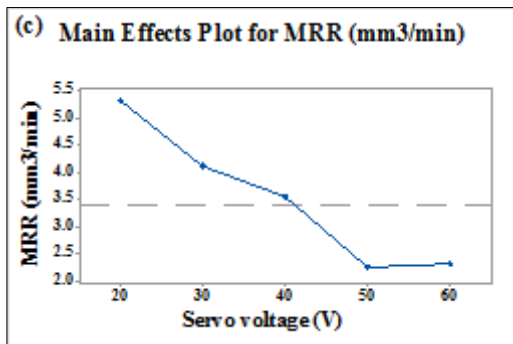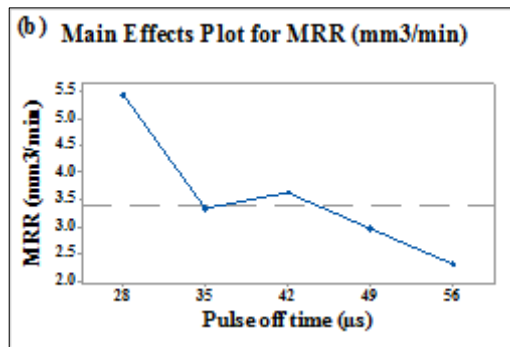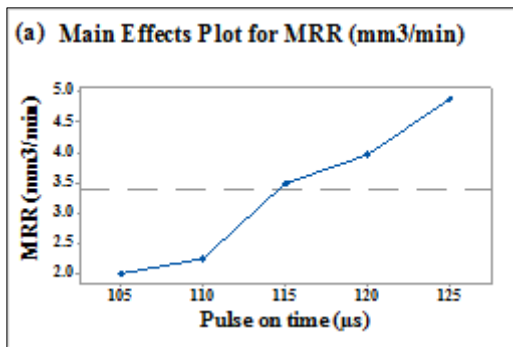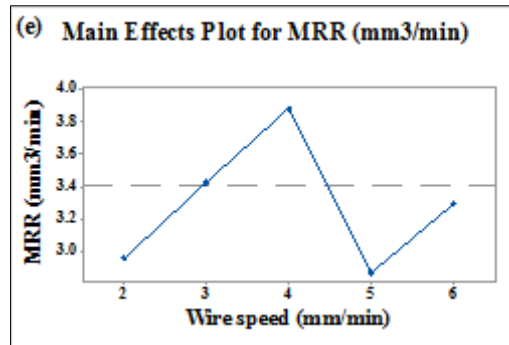
Figure 4.1 Effects of process parameters on MRR for $Ti_{50}Ni_{49}Co_1$ alloy.
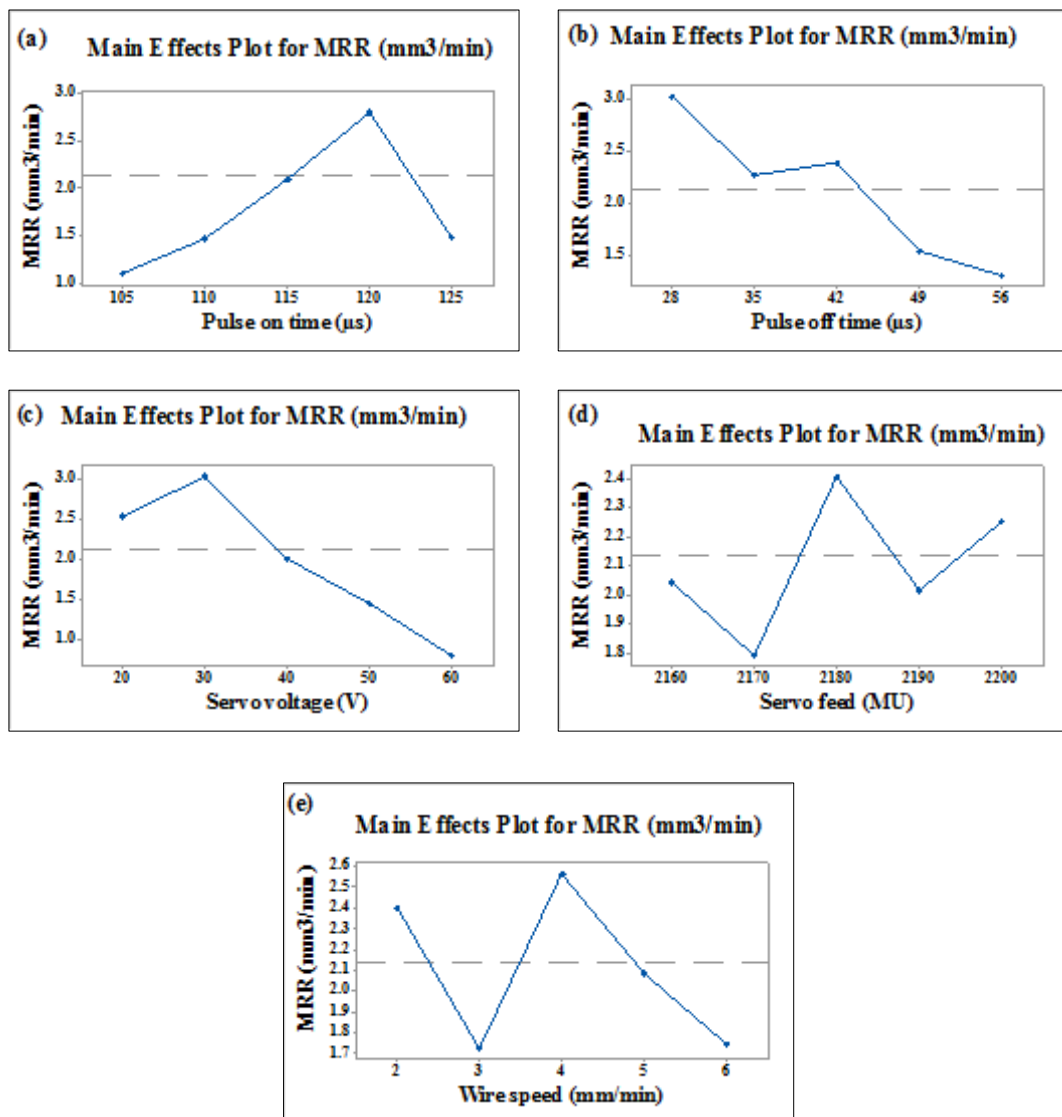
Figure 4.2 Effects of process parameters on MRR for $Ti_{50}Ni_{45}Co_5$ alloy.
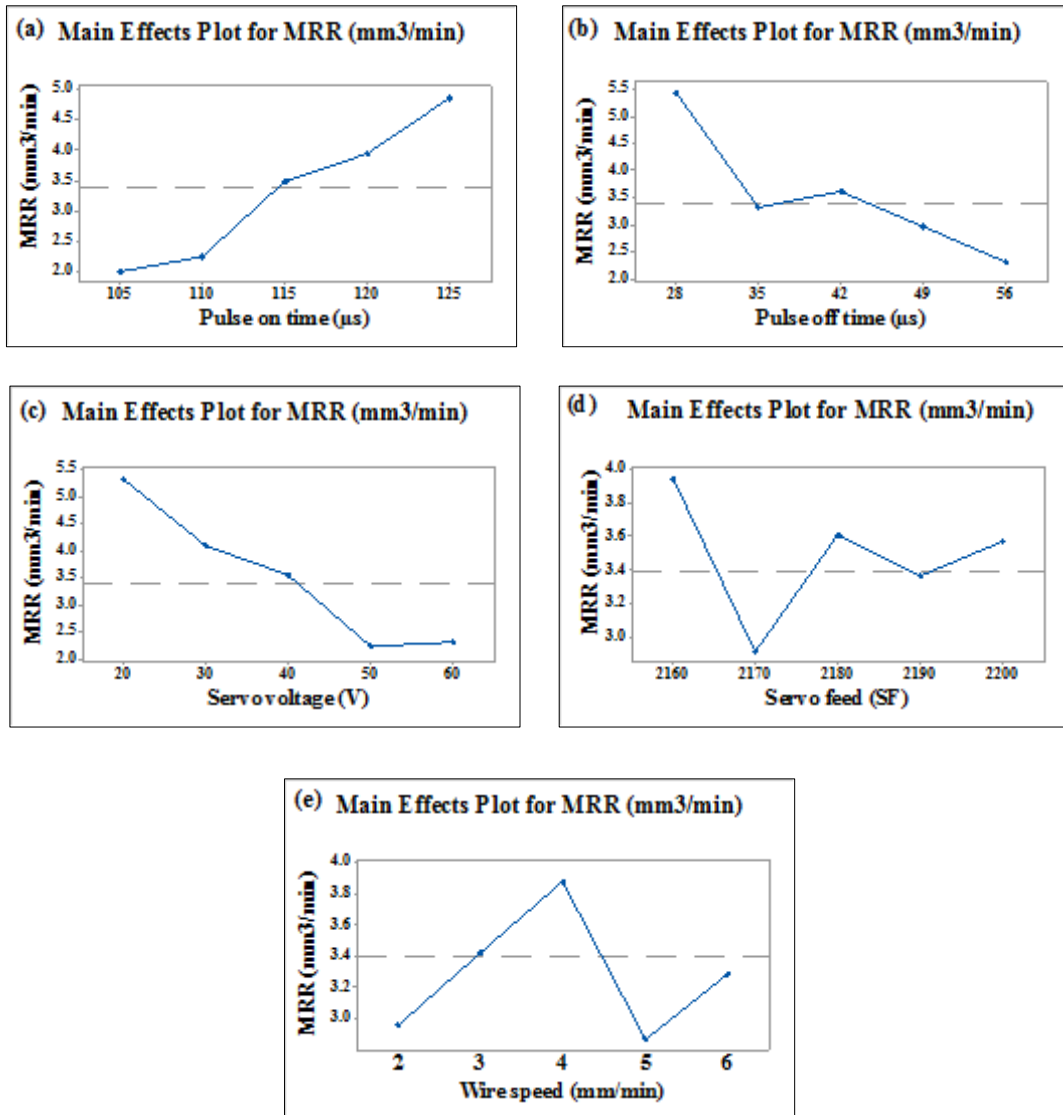
Figure 4.3 Effects of process parameters on MRR for $Ti_{50}Ni_{40}Co_{10}$ alloy.

4.3.2 Effects of process parameters on surface roughness

During surface roughness analysis (Fig 4.4, Fig. 4.5 and Fig. 4.6), it is observed that surface roughness increase with pulse one time. Fig. 4.4a and Fig. 4.6a exhibit that surface roughness increases with increased pulse on time up to 115 (μs) and further it slightly reduces for $Ti_{50}Ni_{49}Co_1$ alloy and $Ti_{50}Ni_{40}Co_{10}$ alloy. This may be due to the poor sparking during the machining process. Surface roughness increases with increased pulse on time because when it removes more amount of material, some of the molten material are flushed off by dielectric fluid and remaining molten metal

solidify on machined surface and it forms craters and micro globules leading to higher surface roughness. Similar work presented by other researcher after the machining of low-carbon steel $G_{21}Mn_5$ (Mordyuk et al. 2017). It is clearly seen form Fig. 4.4b and Fig 4.5b that surface roughness decreases with increase pulse off time for $Ti_{50}Ni_{49}Co_1$ alloy and $Ti_{50}Ni_{45}Co_{05}$ alloy while Fig.4.6b indicates that surface roughness slightly increased with increase in pulse off time (T_{off}) up to 35 (μs) which is negligible and further surface roughness decreases with all specific levels of servo voltage for $Ti_{50}Ni_{40}Co_{10}$ alloy. Surface roughness decreases with increase pulse off time (T_{off}), this may be ascribed to, at high pulse off time most of the molten metal is flushed away from the machined surface and reduce the formation of craters and micro globules hence leading to low surface roughness. Same as reported by Azhiri et al. (2013) during the WEDM of Al/SiC metal matrix composite. It is noticed from Fig. 4.4c.for $Ti_{50}Ni_{49}Co_1$ alloy that surface roughness decrease with increase in servo voltage, whereas Fig. 4.5c and Fig. 4.6c shows that surface roughness (SR) decreases with increased servo voltage (SV) up to 50 V, further surface roughness slightly increases up to 60 V for both for $Ti_{50}Ni_{45}Co_5$ alloy and $Ti_{50}Ni_{40}Co_{10}$ alloy. Reduction in surface roughness with improvement in servo voltage is due to, at high servo voltage less amount of material are melted on machined surface; this can be easily flushed away from the machined surface through dielectric fluid leading to low surface roughness. Same as observed by Pramanik (2016) during the machining of 6061 aluminum alloy by using lector discharge machining. Fig. 4.4d depicts that surface roughness decrease with increase in servo feed up to 2180mu further it increase up to 2190 mu then again it decrease for $Ti_{50}Ni_{49}Co_1$ alloy. Similar trend in variation of SF with respect to servo feed is observed in Fig. 4.6d for $Ti_{50}Ni_{40}Co_{10}$ alloy. Usually, the spark rate will be in the range of 10-100 kHz which is very high, hence servo feed control is limited for proper control of WEDM because it may result in loss of stability. This may cause server instabilities in the controlled feed rate leading to high surface roughness for $Ti_{50}Ni_{49}Co_1$ alloy and $Ti_{50}Ni_{40}Co_{10}$ alloys. On the other hand it can be seen in Fig. 4.5d that there is not much effects of surface roughness on servo feed for the machining of $Ti_{50}Ni_{45}Co_5$ alloy. Similar results of servo feed variation while WED machining of $Ti_{50}Ni_{40}Cu_{10}$ alloy has been reported by Manjaiah et al. (2015). Fig. 4.4e indicates that surface roughness was low at 2 m/min

wire speed (WS) but latter it increases with the increased wire speed up to 3 m/min further it decrease up to 4 m/min then again increase up to 5 m/min and again it decrease up to 6 m/min for Ti$_{50}$Ni$_{49}$Co$_1$ alloy. But in the Fig.4.5e it is seen that surface roughness decreases with wire speed up to 3 m/min, and when wire speed raised to 4 m/min, reduction is noted in surface roughness for the machining of Ti$_{50}$Ni$_{45}$Co$_5$ alloy. Fig.4.6e indicates that initially surface roughness was low at 2 m/min wire speed but latter it decreases with the increased wire speed up to 6 m/min for the machining of Ti$_{50}$Ni$_{40}$Co$_{10}$ alloy. At higher wire speed up to 6 m/min, surface roughness reduces due to enhanced splashing of molten material. However due to wire instability irregular craters and also uneven spark generation occurs on the work surface. Similar work presented by Wang et al. (2017) during the wire electro discharge machining of Inconel 718.
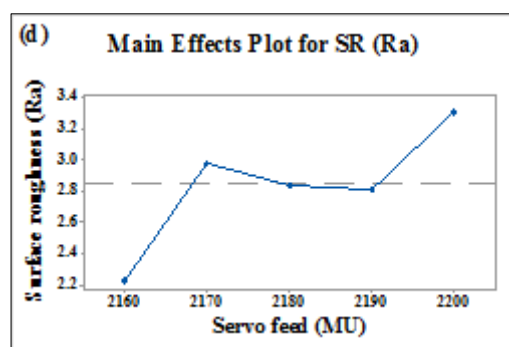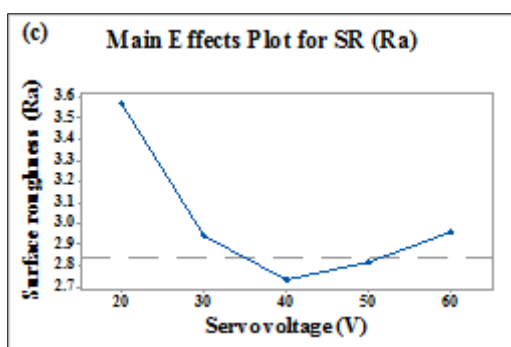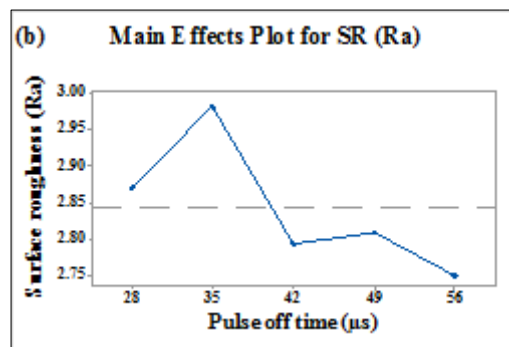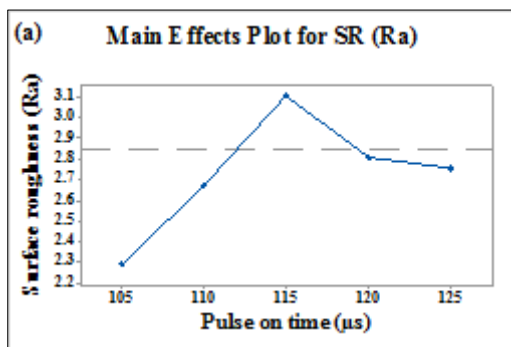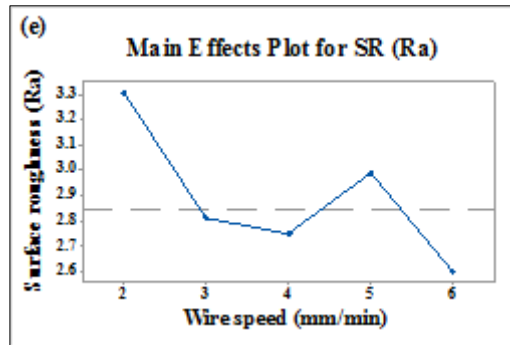
Figure 4.4 Effects of process parameters on SR for $Ti_{50}Ni_{49}Co_1$ alloy.
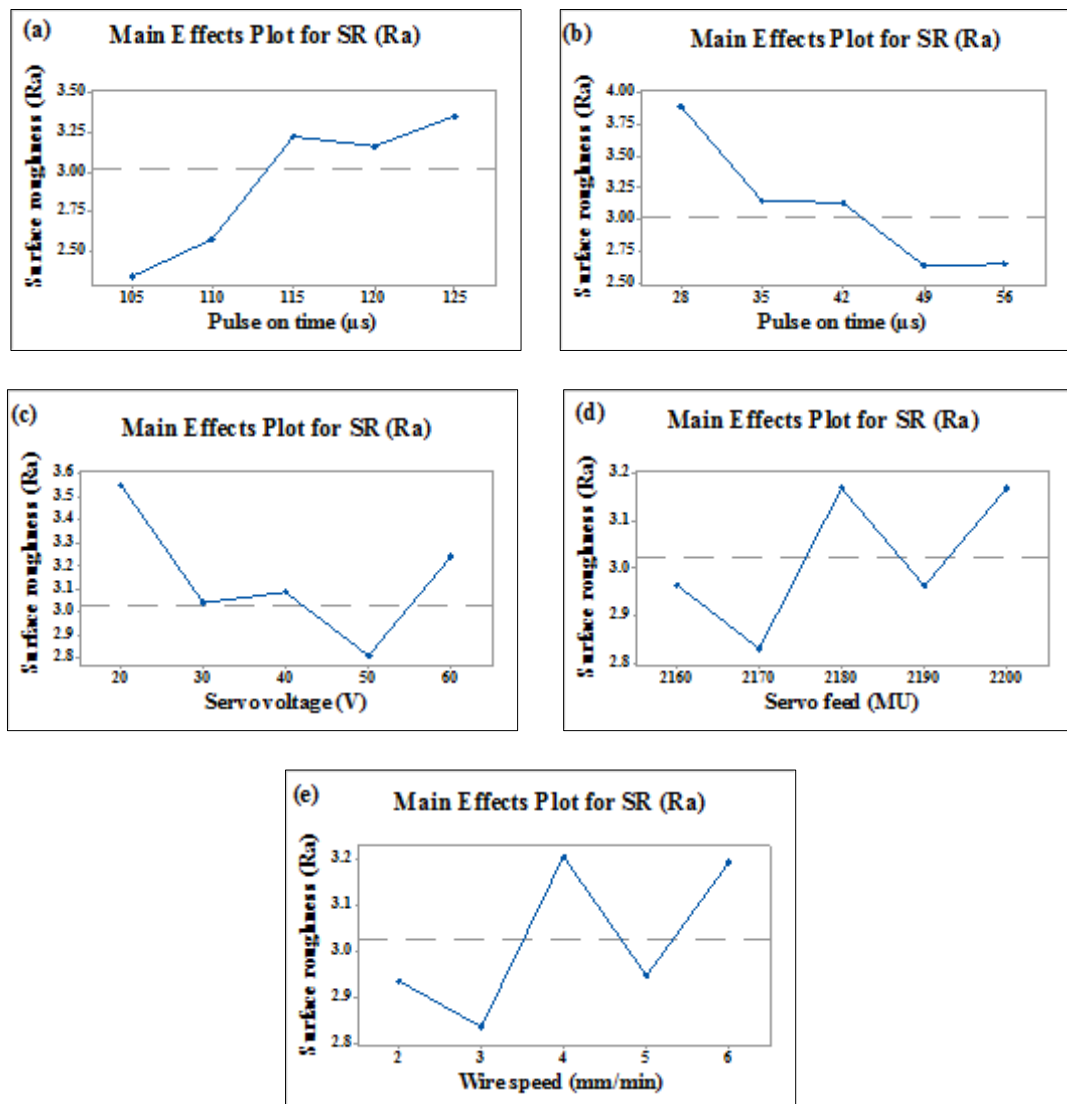
Figure 4.5 Effects of process parameters on SR for $Ti_{50}Ni_{45}Co_5$ alloy.

84
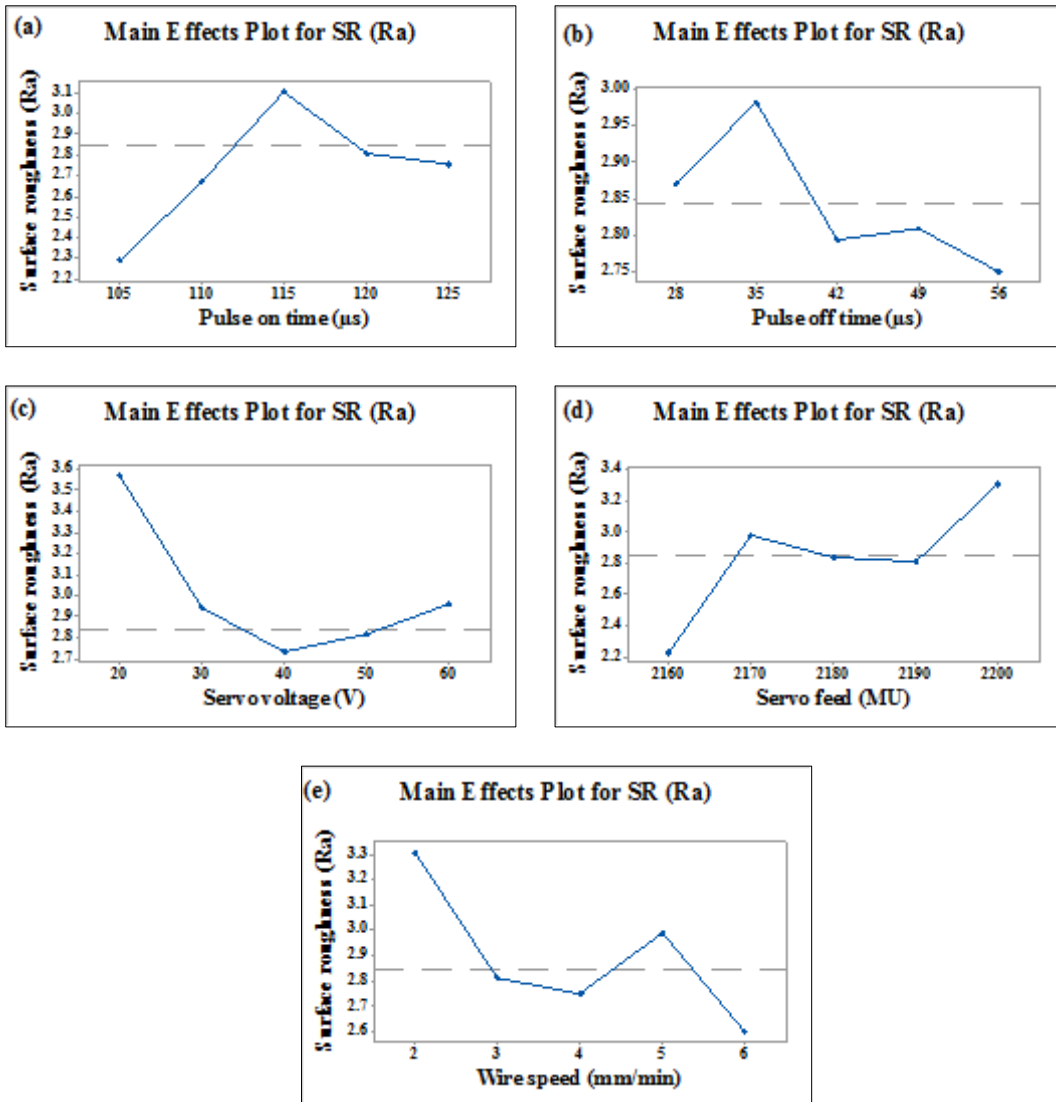
Figure 4.6 Effects of process parameters on SR for $Ti_{50}Ni_{40}Co_{10}$ alloy.

Effects of WEDM process parameters such as pulse on time, pulse off time, servo voltage, servo feed and wire speed on WEDM output responses such as material removal rate and surface roughness were discussed in the above sections. From the observations that pulse on time increasing material removal rate as well as surface roughness with increased the value of pulse on time at the same time pulse off time and servo voltage were decreased both output responses with increased values of these two process parameters. However effects of servo feed and wire speed on MRR and SR were noticed with a small variations, which means these two process parameters do not much influence on MRR and SR. From the above studies the trend of process parameters on outputs can be seen but best combination of process

parameters to get higher MRR with better surface roughness is difficult; therefore to find the best combination of process parameters for machining of each alloy multi objective optimization techniques were adopted. The detailed about the adopted optimization techniques have been presented in section of 3.5. Calculation of optimization techniques for each alloy further discussed in section of 4.5.

4.4 OPTIMIZATION OF MACHINING PROCESS PARAMETERS

The combinations of grey relational analysis, entropy measurement method and response surface methodology were implemented to obtain the best combination of process parameters for each alloy. If the sequence range is large, the factors are effaceable therefore data pre-processing is an important steps to manage the factors of GRA. For the data pre-processing, there are two conditions of normalization in the present study namely higher the better which were used in the normalization of MRR and another one is lower the better for normalization of SR values. Values of normalizations and further steps of optimization techniques are provided in Table 4.2, Table 4.3 and Table 4.4 for alloys $Ti_{50}Ni_{49}Co_1$, $Ti_{50}Ni_{45}Co_5$ and $Ti_{50}Ni_{40}Co_{10}$ respectively. From the Table 4.2, Table 4.3 and Table 4.4 the GRG values calculated for each alloy and presented Table 4.5. Table 4.5 exhibits the output responses MRR and surface roughness with GRG for each alloy where maximum value of GRG shows the best combination of process parameters. Based on the maximum value of GRG Run no. 26 found the best combination of process parameters for $Ti_{50}Ni_{49}Co_1$ alloy. Similarly Run no. 18 for $Ti_{50}Ni_{45}Co_5$ alloy and Run no. 33 for $Ti_{50}Ni_{40}Co_{10}$ alloy were optimized the as the best combination of process parameters. The values of optimized process parameters has presented in the Table 4.6. From the Table 4.6 it has been found that pulse on time and servo voltage were varying for each alloy at the same time rest of the process parameters were found constant for each alloy. Machined surface characterization has been carried out at these optimized process parameters for each $Ti_{50}Ni_{49}Co_1$, $Ti_{50}Ni_{45}Co_5$ and $Ti_{50}Ni_{40}Co_{10}$ alloys. However, machined surface marphology, recast layer thickness and microhardness analyis of $Ti_{50}Ni_{40}Co_{10}$ alloy adoting one process parameters approcah was first discussed. Thereafter analyis of all machined surface chracterizations of $Ti_{50}Ni_{49}Co_1$,

Ti$_{50}$Ni$_{45}$Co$_5$ and Ti$_{50}$Ni$_{40}$Co$_{10}$ alloys machined under optimized process parameters has been carried out.

Table 4.2 Calculation of GRG for $Ti_{50}Ni_{49}Co_1$ alloy.

Ru o.	MRR (mm^3/min)	SR	Nor.MRR	Nor.SR	Dev.MRR	Dev.Sr	GRC MRR	GRC SR	MRR x/d	SR x/d	MRR f(x/d)	SR f(x/d)	GRG	order
1	1.26	3.36	0.027	0.205	0.973	0.795	0.340	0.386	0.021	0.025	0.070	0.086	0.363	33
2	1.97	3.29	0.158	0.228	0.842	0.772	0.373	0.393	0.023	0.026	0.077	0.088	0.383	31
3	3.25	2.74	0.396	0.411	0.604	0.589	0.453	0.459	0.028	0.030	0.094	0.103	0.456	17
4	3.68	3.5	0.475	0.159	0.525	0.841	0.488	0.373	0.030	0.025	0.101	0.083	0.430	26
5	2.07	2.29	0.177	0.560	0.823	0.440	0.378	0.532	0.023	0.035	0.078	0.119	0.455	18
6	2.53	2.56	0.262	0.470	0.738	0.530	0.404	0.486	0.025	0.032	0.084	0.109	0.445	20
7	2.13	2.52	0.188	0.483	0.812	0.517	0.381	0.492	0.023	0.032	0.079	0.110	0.436	23
8	2.56	2.58	0.268	0.464	0.732	0.536	0.406	0.482	0.025	0.032	0.084	0.108	0.444	21
9	5.37	3.45	0.787	0.175	0.213	0.825	0.701	0.378	0.043	0.025	0.145	0.085	0.539	5
10	2.73	2.7	0.300	0.424	0.700	0.576	0.417	0.465	0.025	0.031	0.086	0.104	0.441	22
11	3.29	3.33	0.402	0.215	0.598	0.785	0.456	0.389	0.028	0.026	0.094	0.087	0.422	28
12	1.11	3.01	-0.001	0.321	1.001	0.679	0.333	0.424	0.020	0.028	0.069	0.095	0.379	32
13	1.88	2.51	0.142	0.487	0.858	0.513	0.368	0.493	0.022	0.032	0.076	0.110	0.431	25
14	5.42	3.98	0.796	0.000	0.204	1.000	0.710	0.333	0.043	0.022	0.147	0.075	0.522	8
15	3.25	2.62	0.395	0.450	0.605	0.550	0.453	0.476	0.028	0.031	0.094	0.107	0.465	13
16	5.25	3.75	0.766	0.076	0.234	0.924	0.681	0.351	0.041	0.023	0.141	0.079	0.516	9
17	3.15	2.59	0.378	0.460	0.622	0.540	0.446	0.481	0.027	0.032	0.092	0.108	0.463	14
18	4.57	2.71	0.639	0.421	0.361	0.579	0.581	0.463	0.035	0.030	0.120	0.104	0.522	7
19	3.13	2.62	0.374	0.450	0.626	0.550	0.444	0.476	0.027	0.031	0.092	0.107	0.460	15
20	5.53	2.38	0.818	0.530	0.182	0.470	0.733	0.515	0.045	0.034	0.152	0.115	0.624	3
21	3.26	2.55	0.398	0.474	0.602	0.526	0.454	0.487	0.028	0.032	0.094	0.109	0.470	12
22	4.11	2.79	0.554	0.394	0.446	0.606	0.529	0.452	0.032	0.030	0.109	0.101	0.490	10
23	2.24	3.11	0.209	0.288	0.791	0.712	0.387	0.413	0.024	0.027	0.080	0.092	0.400	30
24	2.32	2.96	0.224	0.338	0.776	0.662	0.392	0.430	0.024	0.028	0.081	0.096	0.411	29
25	2.01	2.29	0.166	0.560	0.834	0.440	0.375	0.532	0.023	0.035	0.078	0.119	0.453	19
26	**4.23**	**0.96**	**0.576**	**1.000**	**0.424**	**0.000**	**0.541**	**1.000**	**0.033**	**0.066**	**0.112**	**0.224**	**0.771**	**1**
27	5.32	3.57	0.779	0.136	0.221	0.864	0.693	0.367	0.042	0.024	0.144	0.082	0.530	6
28	3.38	2.44	0.419	0.510	0.581	0.490	0.463	0.505	0.028	0.033	0.096	0.113	0.484	11
29	2.31	2.75	0.222	0.407	0.778	0.593	0.391	0.458	0.024	0.030	0.081	0.102	0.424	27
30	3.52	2.89	0.445	0.361	0.555	0.639	0.474	0.439	0.029	0.029	0.098	0.098	0.456	16
31	3.58	3.31	0.456	0.222	0.544	0.778	0.479	0.391	0.029	0.026	0.099	0.088	0.435	24
32	5.44	2.87	0.801	0.368	0.199	0.632	0.715	0.442	0.043	0.029	0.148	0.099	0.578	4
33	6.52	2.89	1.000	0.361	0.000	0.639	1.000	0.439	0.061	0.029	0.207	0.098	0.719	2
Min	**1.11**	**0.96**				D_k	**16.435**	**15.202**		SUM	**3.403**	**3.403**		
Max	**6.52**	**3.98**				K	**50.869**	**50.869**						
						e_k	**0.067**	**0.067**	**0.134**					
						λ_k	**0.028**	**0.028**	**0.057**					
						β_k	**0.5**	**0.5**						

88

Table 4.3 Calculation of GRG for $Ti_{50}Ni_{45}Co_5$ alloy.

Run	MRR (mm³/min)	SR (Ra)	Nor.MRR	Nor.SR	Dev.MRR	Dev.Sr	GRC MRR	GRC SR	MRR x/d	SR x/d	MRR f(x/d)	SR f(x/d)	GRG	order
1	1.72	3.47	0.139	0.491	0.861	0.509	0.367	0.496	0.028	0.024	0.095	0.080	0.431	28
2	0.72	2.65	0.013	0.835	0.987	0.165	0.336	0.752	0.026	0.036	0.087	0.122	0.544	13
3	2.22	3.45	0.202	0.499	0.798	0.501	0.385	0.500	0.029	0.024	0.100	0.081	0.442	26
4	2.07	2.95	0.184	0.709	0.816	0.291	0.380	0.632	0.029	0.030	0.098	0.102	0.506	20
5	1.46	2.72	0.106	0.806	0.894	0.194	0.359	0.720	0.027	0.034	0.093	0.117	0.539	14
6	1.23	2.44	0.077	0.923	0.923	0.077	0.351	0.867	0.027	0.041	0.091	0.140	0.609	4
7	1.21	2.58	0.075	0.864	0.925	0.136	0.351	0.787	0.027	0.037	0.091	0.127	0.569	7
8	1.46	2.63	0.106	0.843	0.894	0.157	0.359	0.762	0.027	0.036	0.093	0.123	0.560	8
9	3.72	2.93	0.391	0.718	0.609	0.282	0.451	0.639	0.034	0.030	0.117	0.103	0.545	11
10	1.64	2.71	0.129	0.810	0.871	0.190	0.365	0.725	0.028	0.034	0.095	0.117	0.545	12
11	2.25	3.65	0.206	0.415	0.794	0.585	0.386	0.461	0.029	0.022	0.100	0.075	0.424	29
12	0.62	2.27	0.000	0.995	1.000	0.005	0.333	0.989	0.025	0.047	0.086	0.160	0.661	2
13	1.24	2.78	0.078	0.781	0.922	0.219	0.352	0.695	0.027	0.033	0.091	0.113	0.523	18
14	3.80	4.11	0.401	0.222	0.599	0.778	0.455	0.391	0.035	0.019	0.118	0.063	0.423	30
15	1.23	3.24	0.077	0.587	0.923	0.413	0.351	0.548	0.027	0.026	0.091	0.089	0.450	24
16	1.87	3.74	0.158	0.378	0.842	0.622	0.373	0.446	0.028	0.021	0.097	0.072	0.409	32
17	2.68	2.86	0.260	0.747	0.740	0.253	0.403	0.664	0.031	0.032	0.105	0.107	0.534	16
18	**8.54**	**3.48**	**1.000**	**0.487**	**0.000**	**0.513**	**0.999**	**0.493**	**0.076**	**0.023**	**0.259**	**0.080**	**0.746**	**1**
19	2.48	2.59	0.235	0.860	0.765	0.140	0.395	0.782	0.030	0.037	0.103	0.127	0.588	6
20	1.66	2.7	0.131	0.814	0.869	0.186	0.365	0.729	0.028	0.035	0.095	0.118	0.547	10
21	2.83	2.59	0.279	0.860	0.721	0.140	0.409	0.782	0.031	0.037	0.106	0.127	0.596	5
22	2.76	3.44	0.270	0.504	0.730	0.496	0.407	0.502	0.031	0.024	0.105	0.081	0.454	23
23	2.73	2.92	0.266	0.722	0.734	0.278	0.405	0.642	0.031	0.031	0.105	0.104	0.524	17
24	0.79	3.24	0.022	0.587	0.978	0.413	0.338	0.548	0.026	0.026	0.088	0.089	0.443	25
25	1.11	2.34	0.062	0.965	0.938	0.035	0.348	0.935	0.026	0.044	0.090	0.151	0.641	3
26	2.01	2.98	0.175	0.697	0.825	0.303	0.377	0.622	0.029	0.030	0.098	0.101	0.500	21
27	2.54	3.55	0.242	0.457	0.758	0.543	0.398	0.480	0.030	0.023	0.103	0.078	0.439	27
28	1.78	2.89	0.146	0.734	0.854	0.266	0.369	0.653	0.028	0.031	0.096	0.106	0.511	19
29	1.31	2.65	0.087	0.835	0.913	0.165	0.354	0.752	0.027	0.036	0.092	0.122	0.553	9
30	1.76	2.75	0.144	0.793	0.856	0.207	0.369	0.707	0.028	0.034	0.096	0.115	0.538	15
31	2.25	3.17	0.206	0.617	0.794	0.383	0.386	0.566	0.029	0.027	0.100	0.092	0.476	22
32	3.01	3.89	0.302	0.315	0.698	0.685	0.417	0.422	0.032	0.020	0.108	0.068	0.420	31
33	3.24	4.64	0.331	0.000	0.669	1.000	0.428	0.333	0.033	0.016	0.111	0.054	0.381	33
Min	**0.62**	**2.27**				D_k	13.123	21.021		SUM	3.402	3.403		
Max	**8.54**	**4.64**				K	50.869	50.869						
						e_k	0.0669	0.0669	0.1338					
						λ_k	0.0284	0.0284	0.0568					
						β_k	0.5000	0.5000						

Table 4.4 Calculation of GRG for Ti$_{50}$Ni$_{40}$Co$_{10}$ alloy.

Run	MRR (mm³/min)	SR (Ra)	Nor.MRR	Nor.SR	Dev.MRR	Dev.Sr	GRC MRR	GRC SR	MRR x/d	SR x/d	MRR f(x/d)	SR f(x/d)	GRG	order
1	4.556	3.09	0.572	0.510	0.428	0.490	0.539	0.505	0.032	0.028	0.109	0.095	0.522	17
2	1.472	2.27	0.000	0.834	1.000	0.166	0.333	0.751	0.020	0.042	0.067	0.142	0.542	11
3	4.08	2.89	0.484	0.589	0.516	0.411	0.492	0.549	0.029	0.030	0.099	0.104	0.520	18
4	3.948	2.58	0.459	0.711	0.541	0.289	0.480	0.634	0.028	0.035	0.097	0.120	0.557	9
5	2.04	2.69	0.105	0.668	0.895	0.332	0.359	0.601	0.021	0.033	0.072	0.113	0.480	27
6	2.366	2.62	0.166	0.696	0.834	0.304	0.375	0.622	0.022	0.034	0.076	0.117	0.498	26
7	2.866	2.96	0.259	0.561	0.741	0.439	0.403	0.533	0.024	0.030	0.081	0.101	0.468	28
8	3.65	2.51	0.404	0.739	0.596	0.261	0.456	0.657	0.027	0.036	0.092	0.124	0.557	10
9	5.837	4.38	0.810	0.000	0.190	1.000	0.724	0.333	0.043	0.018	0.146	0.063	0.529	14
10	2.954	3.5	0.275	0.348	0.725	0.652	0.408	0.434	0.024	0.024	0.082	0.082	0.421	33
11	3.453	2.84	0.367	0.609	0.633	0.391	0.441	0.561	0.026	0.031	0.089	0.106	0.501	24
12	1.56	1.85	0.016	1.000	0.984	0.000	0.337	1.000	0.020	0.055	0.068	0.189	0.669	2
13	2.048	3.08	0.107	0.514	0.893	0.486	0.359	0.507	0.021	0.028	0.072	0.096	0.433	32
14	5.616	4.08	0.769	0.119	0.231	0.881	0.684	0.362	0.040	0.020	0.138	0.068	0.523	16
15	3.918	3.5	0.454	0.348	0.546	0.652	0.478	0.434	0.028	0.024	0.096	0.082	0.456	31
16	6.084	3.89	0.855	0.194	0.145	0.806	0.776	0.383	0.046	0.021	0.156	0.072	0.579	4
17	3.881	2.86	0.447	0.601	0.553	0.399	0.475	0.556	0.028	0.031	0.096	0.105	0.515	19
18	5.437	2.87	0.735	0.597	0.265	0.403	0.654	0.554	0.039	0.031	0.132	0.105	0.604	3
19	4.417	2.96	0.546	0.561	0.454	0.439	0.524	0.533	0.031	0.030	0.106	0.101	0.528	15
20	5.812	3.76	0.805	0.245	0.195	0.755	0.719	0.398	0.043	0.022	0.145	0.075	0.559	7
21	3.258	2.41	0.331	0.779	0.669	0.221	0.428	0.693	0.025	0.038	0.086	0.131	0.560	6
22	5.022	4.33	0.658	0.020	0.342	0.980	0.594	0.338	0.035	0.019	0.120	0.064	0.466	29
23	3.63	2.91	0.400	0.581	0.600	0.419	0.455	0.544	0.027	0.030	0.092	0.103	0.499	25
24	1.664	2.49	0.036	0.747	0.964	0.253	0.341	0.664	0.020	0.037	0.069	0.125	0.503	22
25	2.157	2.53	0.127	0.731	0.873	0.269	0.364	0.650	0.022	0.036	0.073	0.123	0.507	21
26	3.49	3.21	0.374	0.462	0.626	0.538	0.444	0.482	0.026	0.027	0.089	0.091	0.463	30
27	5.058	3.7	0.665	0.269	0.335	0.731	0.599	0.406	0.035	0.023	0.121	0.077	0.502	23
28	3.916	2.74	0.453	0.648	0.547	0.352	0.478	0.587	0.028	0.033	0.096	0.111	0.532	12
29	3.142	2.66	0.310	0.680	0.690	0.320	0.420	0.610	0.025	0.034	0.085	0.115	0.515	20
30	4.616	2.75	0.583	0.644	0.417	0.356	0.545	0.584	0.032	0.032	0.110	0.110	0.565	5
31	4.417	2.94	0.546	0.569	0.454	0.431	0.524	0.537	0.031	0.030	0.106	0.101	0.531	13
32	5.612	3.51	0.768	0.344	0.232	0.656	0.683	0.432	0.040	0.024	0.138	0.082	0.558	8
33	**6.864**	**2.74**	**1**	**0.648**	**0.000**	**0.352**	**1.000**	**0.587**	**0.059**	**0.033**	**0.201**	**0.111**	**0.794**	**1**
Min	1.472	1.85				D$_k$	16.891	18.021		SUM	3.403	3.403		
Max	6.864	4.38				K	50.869	50.869						
						e$_k$	0.0669	0.067	0.1338					
						λ$_k$	**0.028**	**0.028**	0.0568					
						β$_k$	**0.500**	**0.500**						

Table 4.5 Output response of surface roughness and MRR with GRG.

Run No.	Ti$_{50}$Ni$_{49}$Co$_1$			Ti$_{50}$Ni$_{45}$Co$_5$			Ti$_{50}$Ni$_{40}$Co$_{10}$		
	MRR (mm^3/min)	SR (R$_a$)	GRG	MRR (mm^3/min)	SR (R$_a$)	GRG	MRR (mm^3/min)	SR (R$_a$)	GRG
1	1.26	3.36	0.363	1.720	3.47	0.431	4.556	3.09	0.522
2	1.97	3.29	0.383	0.720	2.65	0.544	1.472	2.27	0.542
3	3.25	2.74	0.456	2.221	3.45	0.442	4.08	2.89	0.520
4	3.68	3.5	0.430	2.074	2.95	0.506	3.948	2.58	0.557
5	2.07	2.29	0.455	1.457	2.72	0.539	2.04	2.69	0.480
6	2.53	2.56	0.445	1.228	2.44	0.609	2.366	2.62	0.498
7	2.13	2.52	0.436	1.212	2.58	0.569	2.866	2.96	0.468
8	2.56	2.58	0.444	1.462	2.63	0.560	3.65	2.51	0.557
9	5.37	3.45	0.539	3.719	2.93	0.545	5.837	4.38	0.529
10	2.73	2.7	0.441	1.643	2.71	0.545	2.954	3.5	0.421
11	3.29	3.33	0.422	2.253	3.65	0.424	3.453	2.84	0.501
12	1.11	3.01	0.379	0.622	2.27	0.661	1.56	1.85	0.669
13	1.88	2.51	0.431	1.237	2.78	0.523	2.048	3.08	0.433
14	5.42	3.98	0.522	3.798	4.11	0.423	5.616	4.08	0.523
15	3.25	2.62	0.465	1.231	3.24	0.450	3.918	3.5	0.456
16	5.25	3.75	0.516	1.869	3.74	0.409	6.084	3.89	0.579
17	3.15	2.59	0.463	2.680	2.86	0.534	3.881	2.86	0.515
18	4.57	2.71	0.522	8.538	3.48	0.746	5.437	2.87	0.604
19	3.13	2.62	0.460	2.485	2.59	0.588	4.417	2.96	0.528
20	5.53	2.38	0.624	1.659	2.7	0.547	5.812	3.76	0.559
21	3.26	2.55	0.470	2.828	2.59	0.596	3.258	2.41	0.560
22	4.11	2.79	0.490	2.760	3.44	0.454	5.022	4.33	0.466
23	2.24	3.11	0.400	2.730	2.92	0.524	3.63	2.91	0.499
24	2.32	2.96	0.411	0.792	3.24	0.443	1.664	2.49	0.503
25	2.01	2.29	0.453	1.107	2.34	0.641	2.157	2.53	0.507
26	4.23	0.96	0.771	2.010	2.98	0.500	3.49	3.21	0.463
27	5.32	3.57	0.530	2.539	3.55	0.439	5.058	3.7	0.502

28	3.38	2.44	0.484	1.778	2.89	0.511	3.916	2.74	0.532
29	2.31	2.75	0.424	1.305	2.65	0.553	3.142	2.66	0.515
30	3.52	2.89	0.456	1.761	2.75	0.538	4.616	2.75	0.565
31	3.58	3.31	0.435	2.251	3.17	0.476	4.417	2.94	0.531
32	5.44	2.87	0.578	3.014	3.89	0.420	5.612	3.51	0.558
33	6.52	2.89	0.719	1.720	3.47	0.381	6.864	2.74	0.794

Table 4.6 Optimized process parameters for each alloy.

S. No.	Alloys	T_{on}	T_{off}	SV	SF	WS
1	$Ti_{50}Ni_{49}Co_1$	115	42	30	2180	4
2	$Ti_{50}Ni_{45}Co_5$	115	42	40	2180	4
3	$Ti_{50}Ni_{40}Co_{10}$	125	42	40	2180	4

4.5 CHARACTERIZATION OF MACHINED SURFACE

Characterization of machined surface of each shape memory alloy is carried out with respect to microsructure, surface topography, recast layer thickness, microhardness, residual stress, composition and phase constituents. All these alloys were machined at optimized process paramters mentioned Table 4.6.

4.5.1 EDX analysis of machined surface

Fig. 4.7 a to c exhibit the EDX analysis of machined surface of $Ti_{50}Ni_{49}Co_1$, $Ti_{50}Ni_{45}Co_5$ and $Ti_{50}Ni_{40}Co_{10}$ alloys. The results indicate the presence of Ti, Ni and Co on the machined surface of all three alloys. The residuals of copper (Cu) and Zinc (Zn) were recognized in all three alloys. This might be because of the melting and re-solidification of the wire material during spark erosion in WEDM process. The presence of oxygen in these alloys was observed because of oxidation as a result of high temperature involved in the WEDM process. Although EDX results showed that carbon (C) and oxygen (O) exists in all three alloys; these elements were observed due to the fact that dielectric fluid normally contains carbon (C) from minute minerals present and oxygen (O) from water molecules. Similar finding were presented by Sharma et al. (2017) during WEDM of nickel based aerospace alloy.
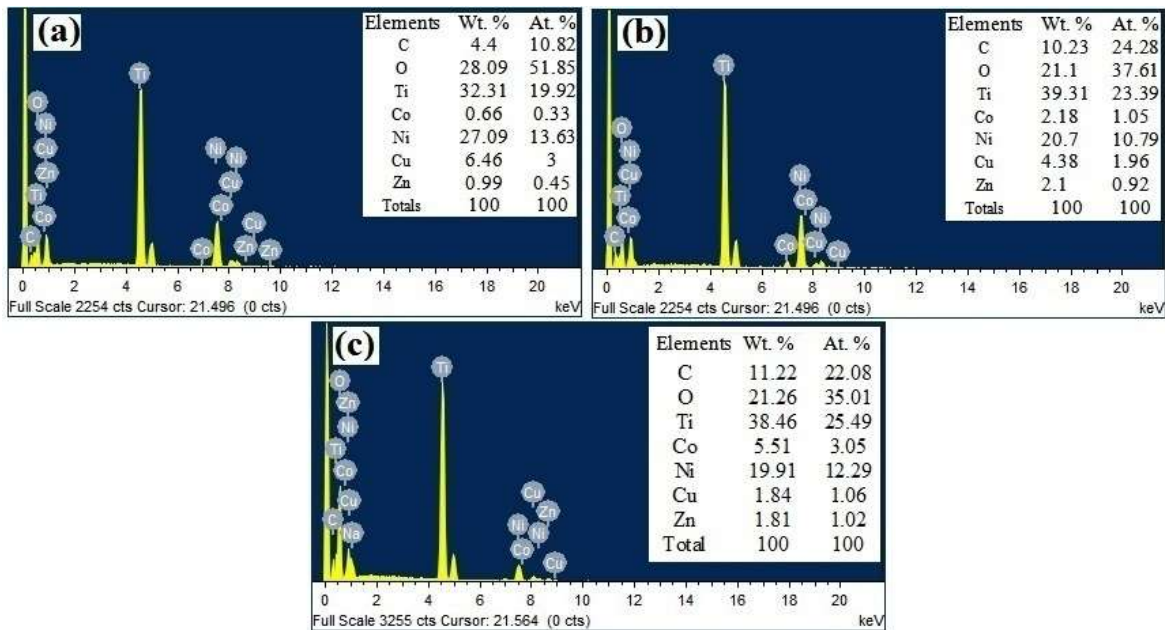
Figure 4.7 EDX analyses of machined surface (a) $Ti_{50}Ni_{49}Co_1$, (b) $Ti_{50}Ni_{45}Co_5$ and (c) $Ti_{50}Ni_{40}Co_{10}$.

4.5.2 Machined surface morphology

4.5.2.1 Machined surface morphology at one parameter approach

The machined surface morphology of $Ti_{50}Ni_{40}Co_{10}$ alloy adopting one process parameters approach was first discussed. Thereafter analysis of the machined surface morphology $Ti_{50}Ni_{49}Co_1$, $Ti_{50}Ni_{45}Co_5$ and $Ti_{50}Ni_{40}Co_{10}$ alloys machined under optimized process parameters has been carried out. As above discussed machined surface morphology has been presented in the Fig.4.8 a to f for $Ti_{50}Ni_{40}Co_{10}$ alloy. Melted drops, crater, cracks and micro globules are observed on the machined surface, and which are shown in Fig. 4.8a to 4.8f. It is noticed that pulse on time, pulse off time and servo voltage are major process parameters during WEDM machining. Therefore effects of these parameters on microstructure have been analysed on machined surface of $Ti_{50}Ni_{40}Co_{10}$ alloy at lower and higher values of their effective process parameters. It can be seen from Fig. 4.8a and Fig. 4.8b that at high pulse on time more cracks, micro globules and large size craters are present on machined surface comparatively at low pulse on time. Due to at high pulse on time, more amount of thermal energy is transferred to the material which results in the

melting of more amount of material from the work piece. This, in turn, contributes to the increase in size of the craters formed on the machined surface and consequently produces a rough surface on the machined components, from Fig. 4.6a indicates clearly the rough surface on the machined surface at high pulse on time. Fig. 4.8c and 4.8d represented the microstructures at high and low servo voltage. It can be seen from Fig. 4.8c that at low servo voltage of 20 V, cracks appeared on the machined surface are more when compared to samples machined at higher servo voltage. At low servo voltage, surface roughness will be higher due to more intense spark discharge on the machining surface that leads to formation of larger and abrupt crater along with faster resolidification of molten material by dielectric quenching. The entire process is largely complicated during the electrical discharge, the dielectric barrier is broken due to formation of plasma channel which have a temperature of around 10,000°C that is more than enough to melt, vaporize and disintegrate the material from its bulk core (Soni et al. 2017). However this is not sufficient enough to produce the required localised pressure which can splash all the molten material from the machining zone which is to be washed away due to flushing pressure. But some of the molten materials remain attached with the machined surface which tend to entrap some air bubbles and thus produces micro voids and micro globules on the machined surface. The effects of pulse off time on microstructures of machined surface are given in Fig. 4.8e and 4.8f. It is evident from microstructures that at high pulse off time comparatively less surface cracks, micro globules, craters, micro void, melted drops and blow holes are observed. Because at higher pulse off time more time is allowed for flushing in the machining zone that results in more amount of material removal per unit time from the machined surface. Hence, less re-solidified molten material is found on the machined surface (Choudhary et al. 2010).
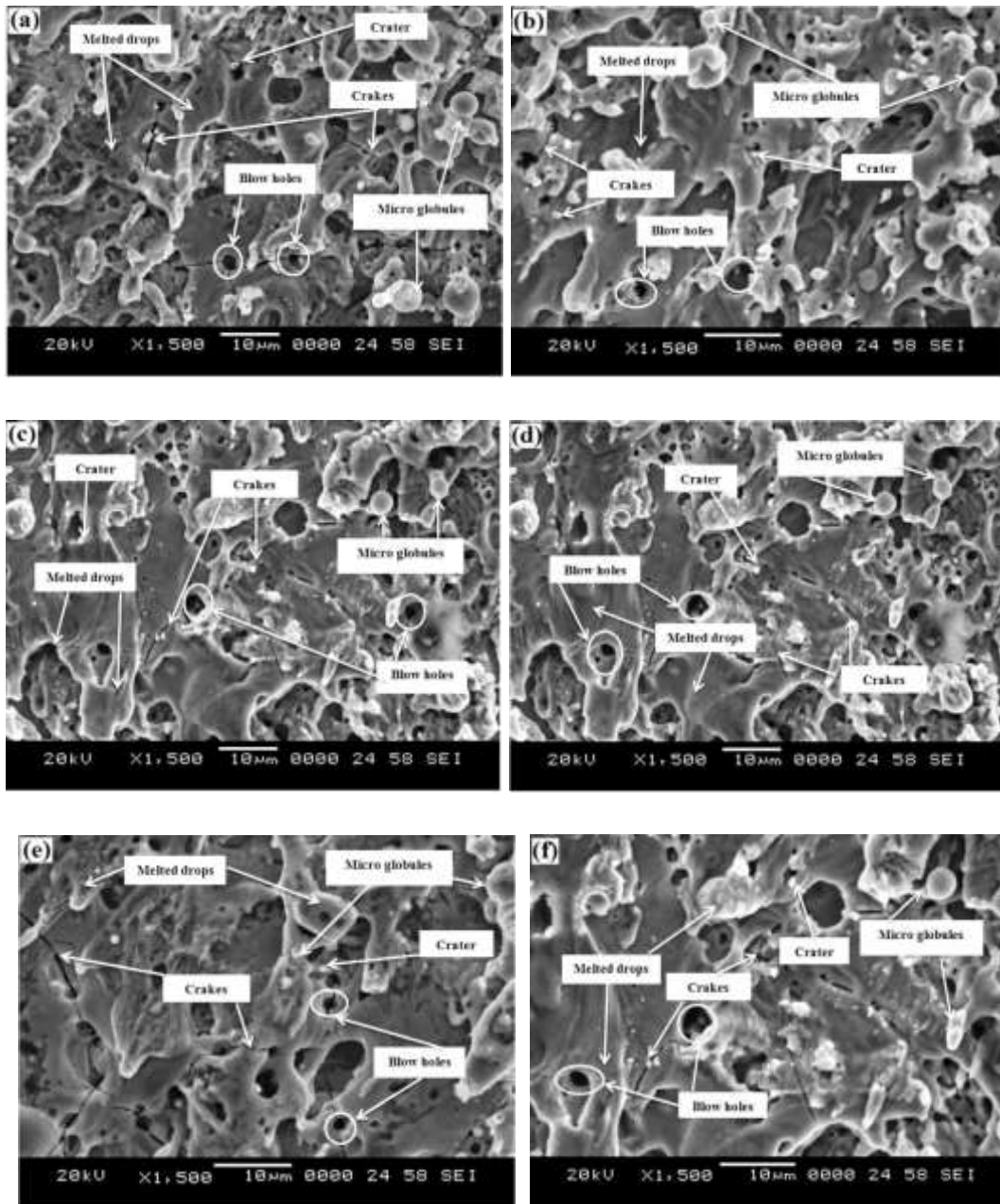
Figure 4.8 SEM microstructures of one process parameters approach machined surface: (a) At high pulse on time (125μs), (b) Low pulse on time (105μs), (c) Low servo voltage (20V), (d) High servo voltage, (e) Low pulse off time (28μs) and (f) High pulse off time (56μs).

4.5.2.2 Machined surface morphology at optimized process parameters

Surface morphology of shape memory alloys machined at optimized process parameters is shown in Figure 4.9. Melted drops, crater, cracks and micro globules are observed on the machined surface. Greater crater, more melting drops and micro

globules were observed on machined surface of $Ti_{50}Ni_{49}Co_1$ alloy (Fig. 4.9a). This may be due to the lower servo voltage where surface roughness will be higher due to more intense spark discharge on the machining surface that leads to formation of larger and abrupt crater along with faster resolidification of molten material by dielectric quenching. The machined surface quality is better for $Ti_{50}Ni_{45}Co_5$ as seen in Fig 4.9b where cracks size, crater, melted drops and micro globules are lower, because the adopted pulse on time and servo voltage are average which improve the surface quality. While machined surface of $Ti_{50}Ni_{40}Co_{10}$ alloy as observed in Fig. 4.9 c exhibit more melted drops and crater because high pulse on time of 125µs is adopted for machining which resulting in more amount of thermal energy is transferred to the material and the melting of more amount of material from the work piece occur. This, in turn, contributes to the increase in size of the craters and melted drops formed on the machined surface and consequently produce a rougher surface on the machined components. Similar kind of results is observed by Kumar et al. (2016) during WEDM of pure titanium.
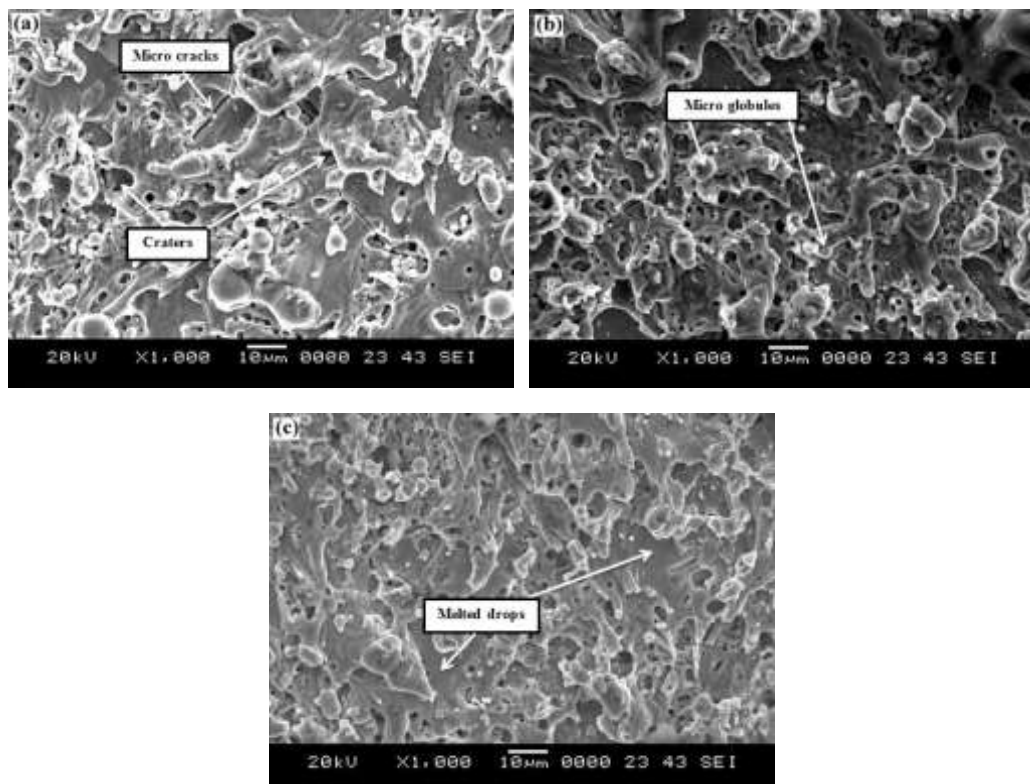
Figure 4.9 Machined surface morphology at optimized process parameters (a) $Ti_{50}Ni_{49}Co_1$, (b) $Ti_{50}Ni_{45}Co_5$ and (c) $Ti_{50}Ni_{40}Co_{10}$.

4.5.3 Machined surface topography

Fig. 4.10 exhibit surface topography of $Ti_{50}Ni_{49}C0_1$, $Ti_{50}Ni_{45}C0_5$ and $Ti_{50}Ni_{40}C0_{10}$ shape memory alloys machined at optimised parameters. The surface topography exposed that servo voltage and pulse on time are major effective parameters for the machining of these alloys. The machined surface of $Ti_{50}Ni_{49}C0_1$ alloy exhibit a surface roughness of 2.05µm (Ra) and topography is shown in Fig. 4.10 a. Roughness value was noticed higher comparatively for $Ti_{50}Ni_{49}C0_1$ alloy because lower servo voltage 30V was optimized for the machining of $Ti_{50}Ni_{49}C0_1$ alloy. However lower servo voltage increases spark intensity and less time is there for removing the molten material from the machined surface during the machining hence some of melted material is remove from the machined surface rest of the material get deposited in the form of recast layer and it creates rougher surface. Similar trend was noticed and presented by Wang et al. (2017) during the WEDM of Inconel 718 alloy. The surface roughness (Ra) of the machined surface was achieved for $Ti_{50}Ni_{45}C0_5$ and $Ti_{50}Ni_{40}C0_{10}$ alloys are 1.05µm and 2.01µm respectively which can be seen in Fig. 4.10a and Fig. 4.10c. The lower surface roughness of $Ti_{50}Ni_{45}C0_5$ alloy is because of machining at higher servo which increases the surface quality. Fig. 4.10c exhibits poor surface quality due to higher pulse on time of 125µs because more amount of thermal energy will be transferred to material at higher pulse on time which as discussed in the section of 4.6.2.1 and can be seen in Fig. 4.8a.
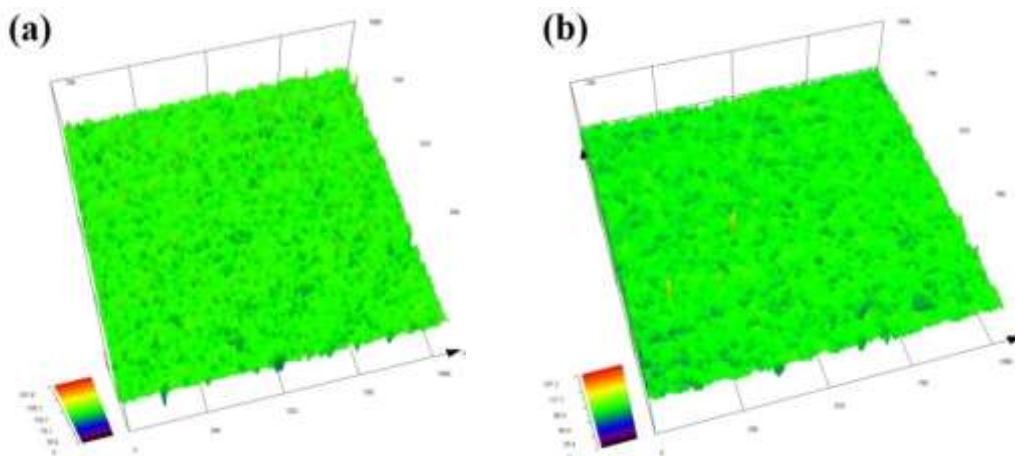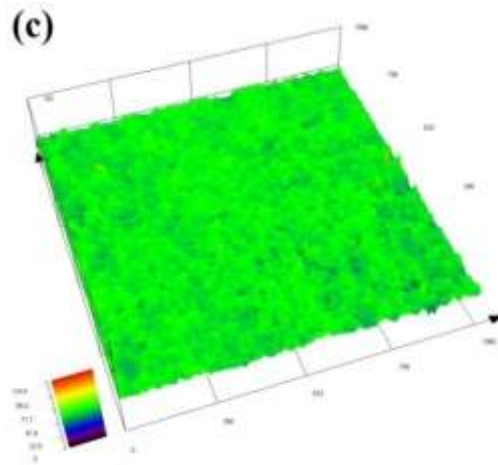
Figure 4.10 Surface topography of machined surface of (a) $Ti_{50}Ni_{49}Co_1$, (b) $Ti_{50}Ni_{45}Co_5$ and (c) $Ti_{50}Ni_{40}Co_{10}$.

4.5.4 Residual stress analysis

Residual stress that exists on the machined surface is either tensile or compressive in nature. The residual stresses exist on the WED machined surface, due to non-homogeneity of heat flow and metallurgical transformations in the machining surface and plastic deformation (Ekmekci et al. 2005; Newton et al. 2009). Plastic deformation induces the compressive residual stresses by mechanical load and tensile residual stress by thermal load (Rao et al. 2016). The phase transformations led to the change in volume of surface and subsurface layers, so the decrease or increase of its volume was hindered by bulk material resulting in generation of tensile or compressive residual stresses respectively. Generally, WEDM induced tensile residual stresses on the machined surface or in the recast layer zone further decreases from the heat affected zone because of high spark energy involved in the machining zone (Ekmekci et al. 2005). Fig. 4.11 indicates the compressive residual stress on machined surface at optimized process parameters which are given in Table 4.6. Compressive residual stress was noticed during wire electro discharge machining process for all three alloys. However, compressive residual stresses improve fatigue life of material, while tensile stresses are destructive in nature (Guu and Hocheng 2001). Due to compressive residual stress on machined surface harder surface has

been found near the cutting edge of machined component which can be seen in microhardness profiles shown in Fig. 4.15. Similar kind of results was noticed by other researcher during the observation of residual stress effect on hardness (Tosha 2002). Fig. 4.11 indicates the residual stresses for each alloy where -252.6 MPa for $Ti_{50}Ni_{49}Co_1$ alloy, -270.2 MPa for $Ti_{50}Ni_{45}Co_5$ and -265.9 for $Ti_{50}Ni_{40}Co_{10}$ alloy have been noticed, the variation in the residual stresses on the machined surface due to process parameters of WEDM. Greater residual stresses has been found for $Ti_{50}Ni_{45}Co_5$ alloy because during machining of this alloy pulse on time was lower 115µs and servo voltage was high 40 in the combination of process parameters compare to other alloys. Since at higher pulse on time and lower servo voltage, machined surface will be better it means lesser cracks on the machined surface (Rao et. al. 2009) which is leads to the greater compressive residual stresses. While in the case of $Ti_{50}Ni_{49}Co_1$ alloy servo voltage was 30V which is lower comparatively other alloys and $Ti_{50}Ni_{40}Co_{10}$ while pulse on time was high 125µs was optimized at this pulse on time cutting speed will be more which may create some micro cracks on the machined surface, hence it can be reduce the compressive residual stress.

Figure 4.11 Residual stress measurement of machined surface for each alloy.

4.5.5 Recast layer thickness

4.5.5.1 Recast layer thickness at one process parameter approach

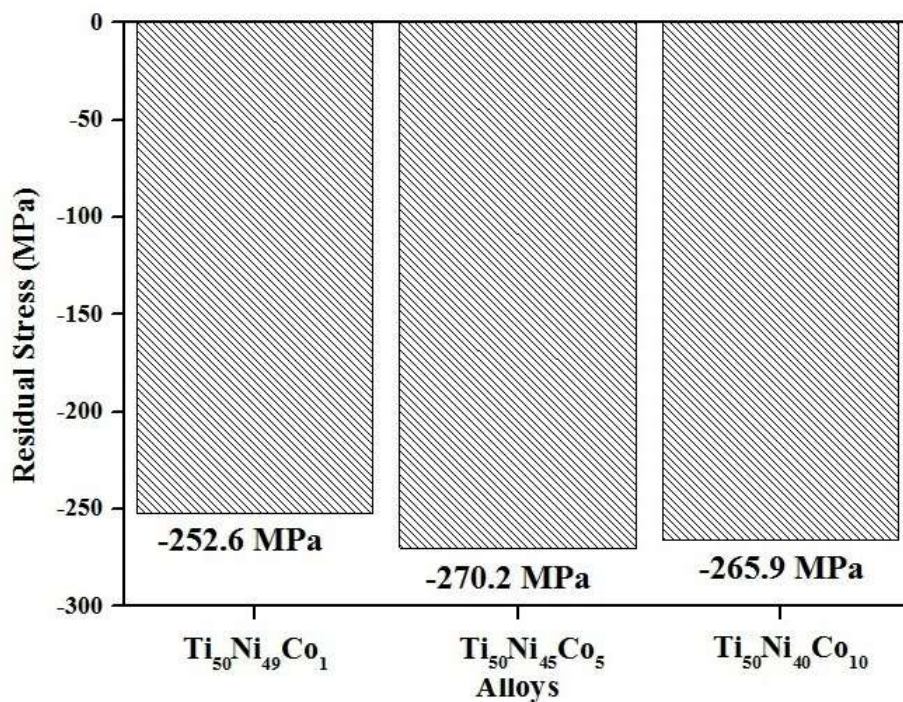Recast layer thickness measurement has been carried out of $Ti_{50}Ni_{40}Co_{10}$ alloy adopting one process parameters approach was first discussed. Thereafter analysis of the machined Recast layer thickness of $Ti_{50}Ni_{49}Co_1$, $Ti_{50}Ni_{45}Co_5$ and $Ti_{50}Ni_{40}Co_{10}$ alloys machined under optimized process parameters has been carried out. During wire electro discharge machining rapid heating and quenching of the molten material by the dielectric fluid causes the formation of a solidified layer and gets deposited on the machined surface. It is observed from Fig. 4.12 a-d that high pulse on time and low servo voltage are major affecting parameters, hence a thicker recast layer deposits has been observed and this can be seen in Fig. 4.12a and 4.12d. At higher pulse on time and low servo voltage, more thermal energy is transferred to the workpiece that results in more amount of molten material re-solidify on the surface of workpiece in the machining zone, leading to thicker recast layer on the machined surface. On the other hand, thin recast layer was noticed from the Fig. 4.12b and 4.12c and is influenced due to lower pulse on time 105 µs and higher servo voltage 60V. Similar results have been reported by Newton et al. (20009) during WED machining of Inconel 718. As observed from Fig. 4.12a recast layer thickness was in the range of 34µm to 44µm for machining with lower servo voltage 20V, whereas at high servo voltage as evident from Fig. 4.12b minimum and maximum recast layer thickness of 5µm and 10µm was observed respectively. Similarly at low pulse on time 105µs, average recast layer thickness of 4.21µm was noticed while at high pulse on time 125µs, average recast layer thickness of 35.4µm was observed. This is because at high pulse on time workpiece receives more spark discharge of higher intensity which leads to thicker recast layer formation. Longer pulse duration generally leads to higher discharge energy per unit cycle that melts more material and re-solidifies them as well due to rapid quenching by constantly flowing de-ionized water on the machined surface (Hsieh et al. 2013). During our observation thicker recast layer was found at high pulse on time 125µs and lower servo voltage 20V while it was thin comparatively at lower pulse on time 105µs and higher servo voltage 60V which can be seen in Fig. 4.12.
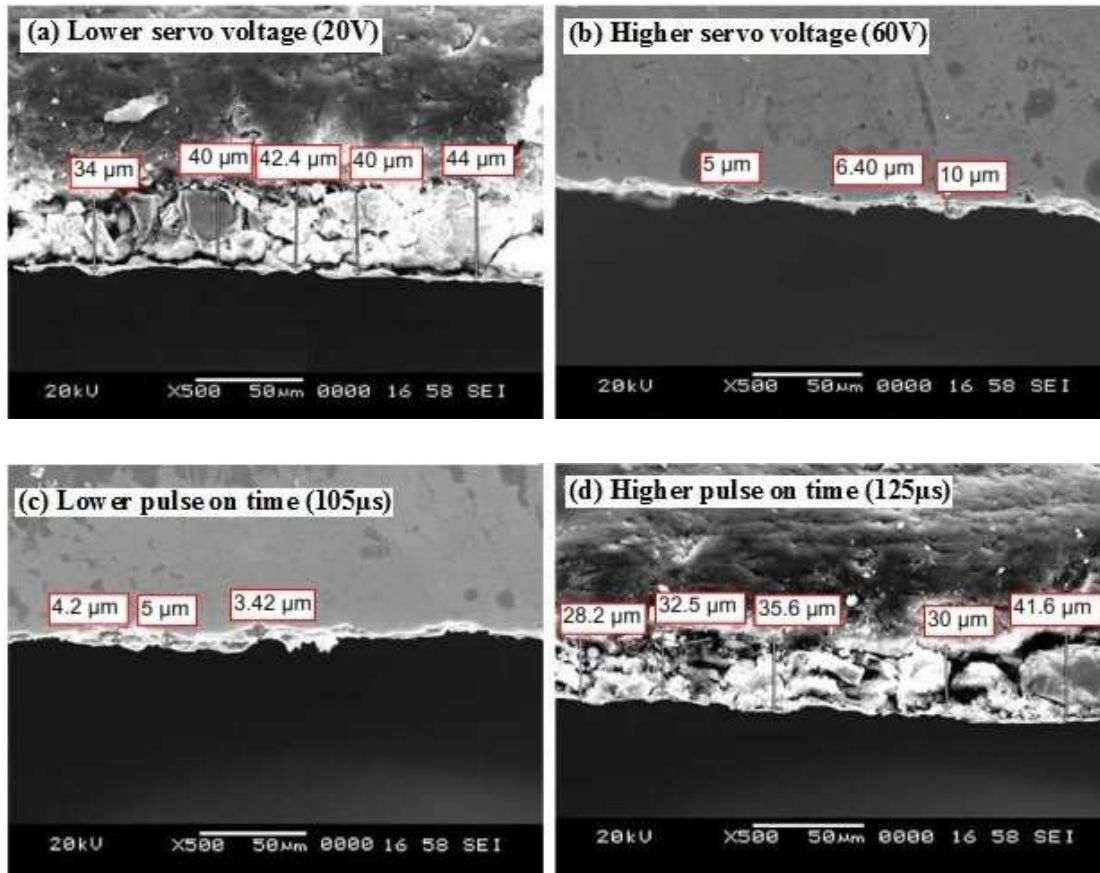
Figure 4.12 Cross section morphology showing recast layer at various process parameters (a) at low servo voltage (20V) (b) at high servo voltage (60V) (c) at lower pulse on time (105μs) and (d) at higher pulse on time (120μs).

4.5.5.2 Recast layer thickness at optimized process parameter

Recast layer thickness measurement has been carried out of machined surface at optimized process parameters for each alloy which can be seen in Fig. 4.13a – 4.13c. During wire electro discharge machining, rapid heating and quenching of the molten material by the dielectric fluid causes the formation of a solidified layer and gets deposited on the machined surface, which makes harder surface of machined component. During optimized process parameters minimum recast layer thickness has been observed. Hence it is best combination of process for each alloy. From Fig. 4.13c, maximum recast layer 7.16μm has been noticed on the machined surface of $Ti_{50}Ni_{40}Co_{10}$ alloy which due to higher pulse on time of 125μs because at higher pulse on time, more thermal energy is transferred to the workpiece that results in more

101

amount of molten material that re-solidify on the surface of workpiece in the machining zone, leading to thicker recast layer on the machined surface. While Fig. 4.13a and Fig. 4.13b exhibit recast layer 3.04 µm and 5.00 µm respectively on machined surface for $Ti_{50}Ni_{49}Co_1$ and $Ti_{50}Ni_{45}Co_5$ alloys due to lower pulse on time 115µs. Similar results has been reported by (Prakash et al. 2017) during WED machining of Inconel 706. During our observation average recast layer were 2 µm for $Ti_{50}Ni_{49}Co_1$ alloy, 2.8 µm for $Ti_{50}Ni_{45}Co_5$ alloy and 4 µm for $Ti_{50}Ni_{40}Co_{10}$ alloy were noticed. Average value of recast layer was noticed minimum on the machined surface for each alloy which is the negligible.
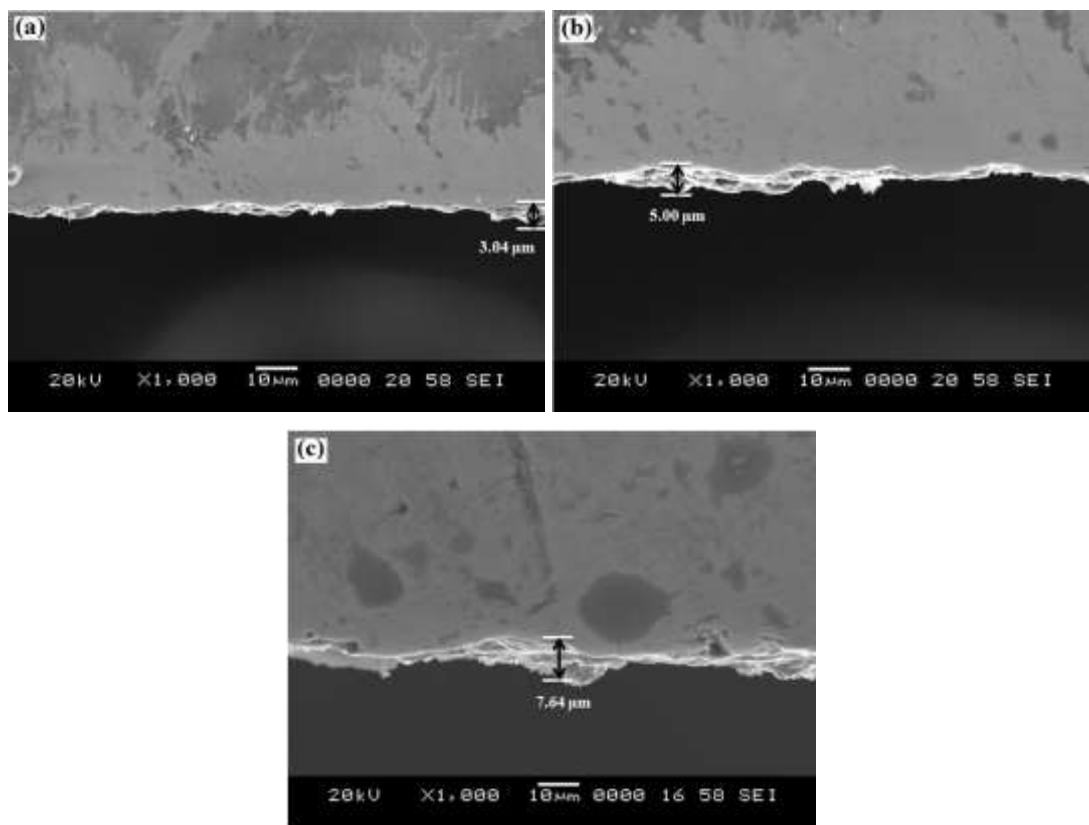
Figure 4.13 Recast layer thickness of machined surface at optimized process parameters of (a) $Ti_{50}Ni_{49}Co_1$, (b) $Ti_{50}Ni_{45}Co_5$ and (c) $Ti_{50}Ni_{40}Co_{10}$.

4.5.6 Machined surface microhardness

4.5.6.1 Machined surface microhardness at one process parameters approach

Machined surface microhardness measurement has been carried out of $Ti_{50}Ni_{40}Co_{10}$ alloy adopting one process parameters approach was first discussed. Thereafter analysis of the machined surface hardness of $Ti_{50}Ni_{49}Co_1$, $Ti_{50}Ni_{45}Co_5$ and $Ti_{50}Ni_{40}Co_{10}$ alloys machined under optimized process parameters has been carried out. Microhardness has been studied on the machined surface of $Ti_{50}Ni_{40}Co_{10}$ shape memory alloy at low servo voltage 20V, high servo voltage 60V, low pulse on time 105µs and higher pulse on time 125µs. During the machining process three kinds of layers are generated on the machined surface such as recast layer, heat affected zone and converted layer (Choudhary et al. 2010). Recast layer near the cutting edge was considered as a starting point 0µm and measure the microhardness towards the base material, microhardness results are shown in Fig. 4.14. Recast layer formed on the machined surface was about 3.5 - 45µm which was hard and 442 HV average microhardness is noticed in this zone. This high hardness on the machined surface is due to formation of surface oxides of TiO_2, $NiTiO_3$ and NiO. Below the recast layer heat affected zone gives 375 HV average hardness, this is may be due to phase transformation in the TiNiCo alloy which can be seen in Fig.4.16. Beneath the heat affected zone converted layer shows hardness of 343 HV. Converted layer is not much affected during WEDM process hence hardness was almost constant in this zone. Such kind of variation in hardness were noticed by Hsieh et al. (2009 and 2013) during the electro discharge machining of TiNiZr and TiAlfe alloys.
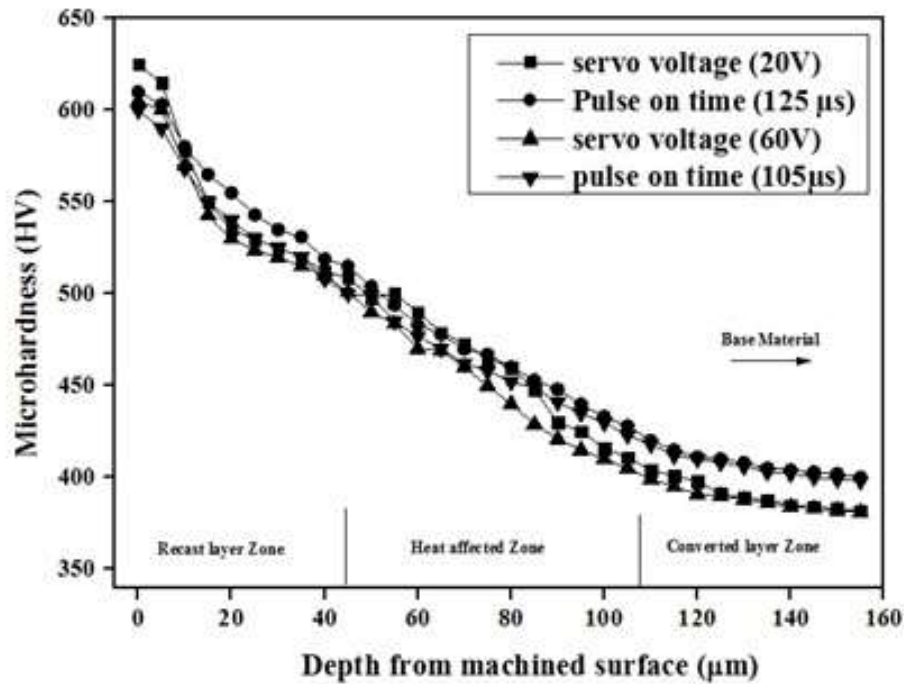
Figure 4.14 Micro hardness analyses of the $Ti_{50}Ni_{40}Co_{10}$ alloy after machining.

4.5.6.2 Machined surface microhardness at optimized process parameters

The variation in the microhardness along the cross section of the machined surface is studied. During the WEDM process three kinds of zones are generated on the machined surface Choudhary et al. (2010). For hardness measurement, cutting edge was considered as the starting point in the recast layer zone and continued until the base material where uniform hardness was observed. Microhardness results are shown in Fig. 4.15 and Table 4.7 which clearly indicates the average microhardness for all three alloys. The recast layer of $Ti_{50}Ni_{40}Co_{10}$ alloy is found harder comparatively because pulse on time adopted for machining is 125μs which is high in combination of process parameters. Moreover at the high pulse on time, spark intensity is high which creates the more discharge energy result in formation of oxides on the machined surface in the form of recast layer which makes harder surface of machined component. The average recast layer thickness is higher for $Ti_{50}Ni_{40}Co_{10}$ alloy compared to $Ti_{50}Ni_{45}Co_5$ and $Ti_{50}Ni_{45}Co_1$ alloys. Phase transformation is responsible for change in the microhardness of machined component toward the base material. Beneath the heat affected zone converted layer comes in the picture which has lower

microhardness than both recast layer and heat affected zone. This converted layer is not much affected during WEDM process; hence no change was noticed in this zone. Hardness of this zone is almost closer to hardness of base material. Such kind of variation in hardness was also noticed by Hsieh et al. (2013) during the electro discharge machining of TiNiZr and TiAlFe alloys. Moreover harder surface near cutting edge was observed due to lesser micro cracks on the machined surface noticed at optimized process parameters and can be seen in Fig. 4.9. Densities of surface cracks are negligible which imply compressive residual stress on the machined surface which can be seen in Fig. 4.10. Similar result has been reported by other researchers that microhardness is influenced by the residual stress, hardness decreases due to tensile stress while it increases due to compressive stress (Tosha 2002).

Table 4.7 Average microhardness in the different zones of the machined surface.

Material	Recast layer (HV)	Heat affected zone (HV)	Converted layer (HV)
$Ti_{50}Ni_{49}Co_1$	426	331	304
$Ti_{50}Ni_{45}Co_5$	473	413	391
$Ti_{50}Ni_{40}Co_{10}$	523	469	429
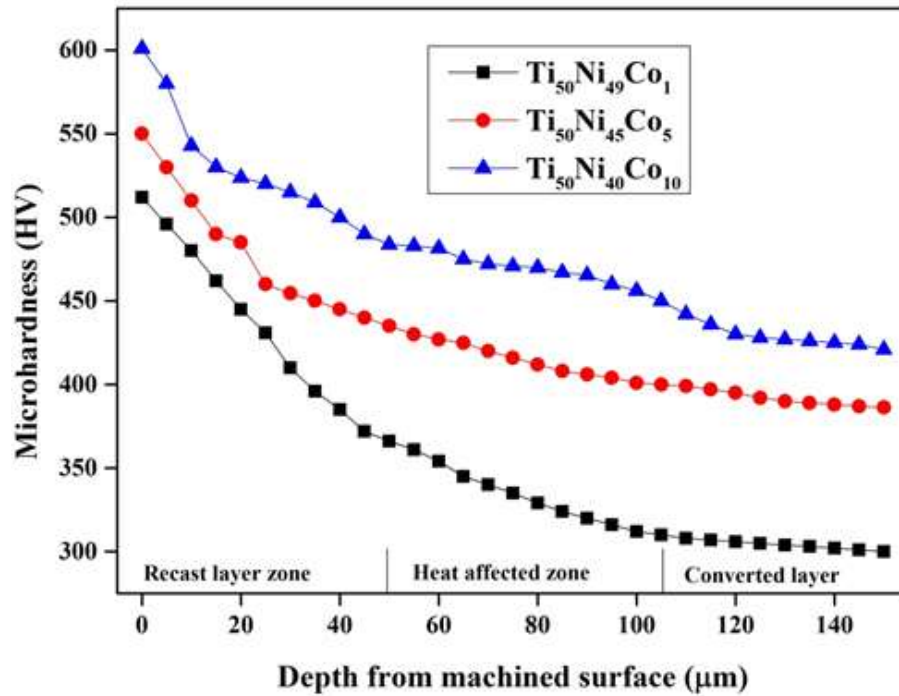
Figure 4.15 Microhardness profiles of machined surface of shape memory alloys.

4.5.7 Phase analysis of machined surface

The assessment of the XRD patterns to identify the phases which are present on the surface of machined component, phases were analysed by using X'Pert high score plus software. Generally XRD analyses are performed on specific surfaces that are subjected to high temperature which may lead to transformation to different phases. Since wire electro discharge machining involves melting of surface material caused due to electrical discharge, XRD analysis has been carried out for at optimized process parameters which can be seen in Fig. 4.16. XRD graph indicates the presence of B19' martensite phase, β' phase and TiNiCo peaks of the shape memory alloy. Other peaks of NiO_2, TiO_2, and TiNi were also noticed on the machined surface. However the formation of NiO_2, and TiO_2, oxides are credited to the high reactivity of Ti, and Ni with demineralised water used as the dielectric fluid during machining. The formation of oxides are responsible for recast layer on the machined surface that results in increment of net increase in hardness of the machined surface which is evident from Fig.4.15. Similar trend have been observed by Hsieh et al. 2013 during the wire electro discharge machining of TiNi based ternary alloys.
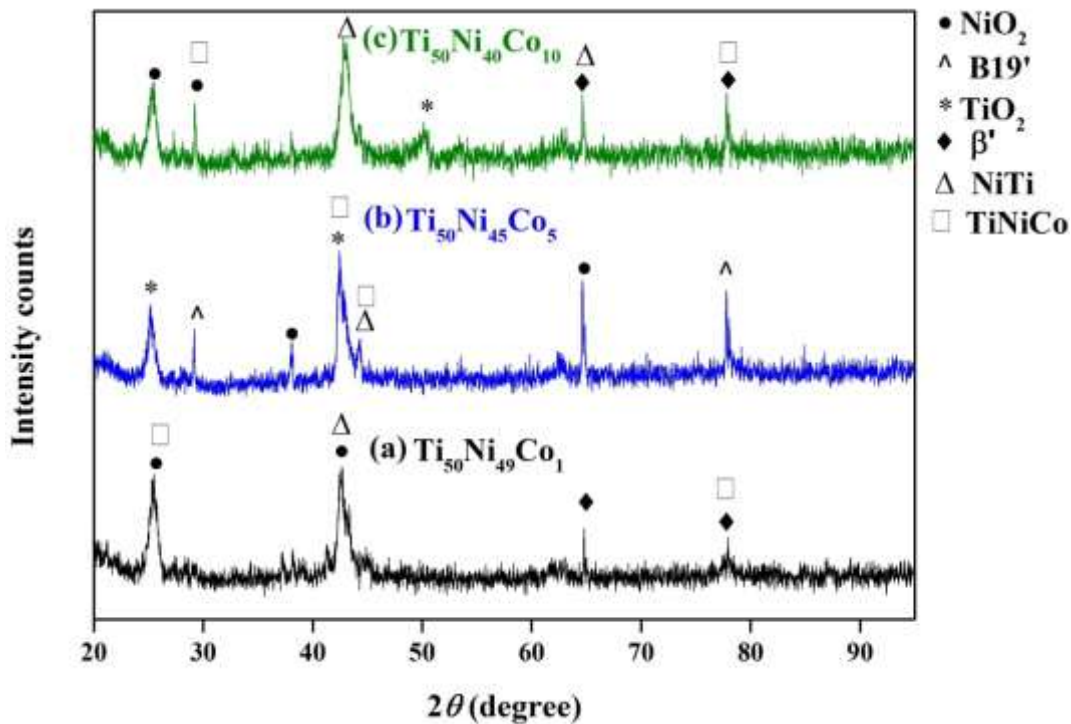
Figure 4.16 XRD analysis of machined surface at optimized process parameters for each alloy.

4.6 SUMMARY

Machininig of $Ti_{50}Ni_{49}Co_1$, $Ti_{50}Ni_{45}Co_5$, and $Ti_{50}Ni_{40}Co_{10}$ shape memory alloys has been carried out by using wire electro discharge machining as per L-33 orthogonal array and measured the WEDM responses (MRR and SR). To find the best combination of process parameters multi-objective optimization techniques were used. Further machined surface characterizations were studied at the optimized process parameters. Based on the above studies the following highlights are listed below-

- It was found that MRR and SR increases upto 5 mm^3/min and 3.46 µm respectively with increment in pulse on time. Similarly increase in pulse off time and servo voltage decreases MRR on an average upto 1 mm^3/min and SR 1.46 µm. Trend of servo feed and wire speed were not uniform on these output responses.

- Formation of micro cracks, micro globules, micro voids are more consistent at high pulse on time 125µs and at low servo voltage 20V and hence the machined surface offers poor surface quality.

- Compressive residual stress has been noticed at the optimized process parameters for all three alloys. Compressive residual stress of 252.6 Mpa for $Ti_{50}Ni_{49}Co_1$ alloy, 270.2 Mpa for $Ti_{50}Ni_{45}Co_5$ alloy and 265.9 Mpa for $Ti_{50}Ni_{40}Co_{10}$ alloy were found at optimized process parameters.

- The cross sectional microstructure of the machined surface revealed that recast layer surface is 35.4µm at pulse on time of 125 µs and low servo voltage of 20 V. Moreover, minimum RLT (4.21µm) was obtained at low pulse on time and high servo voltage.

- Harder surface was noticed near the machined surface due to NiO_2 and TiO_2 oxides formation which is confirmed by XRD analysis.

From the above observations it has been found that levels of pulse on time and servo voltage for each alloy were different and rest of the process parameters were constant for each alloys. Hence to understand deeply the effect of these two process parameters, further study of these two process parameters will be considered for machining and consequent WEDM responses will be measured. Detailed characterization will be carried out at lower and higher values of MRR and SR.

CHAPTER 5

PARAMETRIC STUDY OF PULSE ON TIME AND SERVO VOLTAGE DURING MACHINING OF TiNiCo SHAPE MEMORY ALLOYS

5.1 INTRODUCTION

It is observed from chapter-4 that pulse on time and servo voltage are most influential process parameters for machining of TiNiCo shape memory alloys. Therefore in the present chapter two parameter approach has been adopted to observe deeply the effect of pulse on time and servo voltage on the machining of different compositions of TiNiCo shape memory alloys. Moreover, error analysis has been carried out considering two parameter approach during the machining of all three alloys. Pulse on time and servo voltage is considered as two influential parameters. This chapter presents the comparison between experimental and predicted values. Artificial neural network (ANN) is used as a predictor for the prediction of wire electro-discharge machining (WEDM) responses such as the material removal rate (MRR) and surface roughness (SR) during the machining of $Ti_{50}Ni_{49}Co_1$, $Ti_{50}Ni_{45}Co_5$ and $Ti_{50}Ni_{40}Co_{10}$ shape memory alloy. Table 5.1 indicates input process parameters and their levels. Pulse on time and servo voltage were varied and the other machining parameters of Pulse off time, wire speed and servo feed are kept constant. To see the deeply effects of pulse on time and servo voltage on MRR and SR L-25 orthogonal array was adopted hence machining has been carried out as per L-25 orthogonal array created using Taguchi design of experiment method and is as given in Table 5.2. The machining performance MRR and SR are measured and the same is tabulated in Table 5.3.

Table 5.1 Input process parameters and their levels.

Input process parameters	Levels
Pulse on time (μs)	105, 110, 115, 120, 125
Servo voltage (V)	20, 30, 40, 50, 60
Pulse off time (μs)	42

Wire speed (m/min)	4
Servo feed (mu)	2180

Table 5.2 L-25 Orthogonal array adopted for machining.

Run No.	Pulse on time (μs)	Servo voltage (V)
1	105	20
2	105	30
3	105	40
4	105	50
5	105	60
6	110	20
7	110	30
8	110	40
9	110	50
10	110	60
11	115	20
12	115	30
13	115	40
14	115	50
15	115	60
16	120	20
17	120	30
18	120	40
19	120	50
20	120	60
21	125	20
22	125	30
23	125	40

	24	125	50
	25	125	60

Table 5.3 Machining performances measured for each alloy.

Run	$Ti_{50}Ni_{49}Co_1$		$Ti_{50}Ni_{45}Co_5$		$Ti_{50}Ni_{40}Co_{10}$	
	SR (μm)	MRR (mm^3/min)	SR (μm)	MRR (mm^3/min)	SR (μm)	MRR (mm^3/min)
1	1.68	4.62	1.51	3.71	1.44	3.51
2	1.61	3.64	1.46	3.12	1.22	3.06
3	1.48	2.99	1.33	2.28	1.18	2.11
4	1.37	2.6	1.19	1.89	1.06	1.69
5	1.29	1.8	1.11	1.5	1.04	1.36
6	2.49	5.27	2.29	4.42	1.98	3.17
7	2.07	5.14	2.2	3.19	1.84	3.06
8	1.89	3.58	2.03	2.21	1.67	2.28
9	1.65	2.73	1.76	2.19	1.59	2.01
10	1.71	2.01	1.67	1.84	1.2	1.51
11	115	3.1	7.8	2.72	6.18	2.45
12	2.51	6.18	2.26	5.01	2.31	4.81
13	2.43	4.16	2.25	3.71	2.16	3.51
14	2.5	2.99	2.41	2.86	2.15	2.41
15	2.01	2.94	2.15	2.51	1.98	2.15
16	3.9	9.23	3.85	8.32	3.41	8.08
17	2.76	7.15	2.57	6.31	2.41	6.17
18	2.51	5.97	2.43	5.58	2.2	5.14
19	2.65	3.97	2.35	3.58	2.2	3.84
20	2.57	2.9	2.32	2.81	2.17	2.47
21	4.51	11.51	4.01	9.43	3.63	9.06
22	3.63	9.04	3.2	8.65	3.01	6.55

23	3.25	8.13	3.07	8.06	2.45	5.6
24	2.98	5.27	2.41	5.2	2.26	4.9
25	2.81	3.85	2.39	3.38	2.2	2.99

5.2 VARIATION OF MRR WITH EXPERIMENTAL RUN FOR EACH ALLOY

Fig. 5.1 exhibits variation in material removal rate with respect to different experimental run for each alloy. From Fig. 5.1 observed that material removal rate decreases up to experiment no 5; this can be attributed to increase in servo voltage from experiment run 1 to 5 under constant pulse on time. When comes to the experiment no. 6 again material removal rate increases then further it decreases till experiment run 10 because of increase in servo voltage. Similar trend has been noticed after each five experiments. Material removal rate decrease with increase in servo voltage, because increase in servo voltage results in larger spark gap thereby reducing the spark intensity and eventually lesser amount of material is removed from the workpiece. Sharma et al. (2013) observed similar kind of result during wire electro discharge machining of High- strength low-alloy steel (HSLA).

5.3 VARIATION OF SR WITH EXPERIMENTAL RUN FOR EACH ALLOY

The variation of surface roughness with respect to experimental run is given in the Fig. 5.2. It has been found that surface roughness decreasing from experiment run 1 to 5. This can be attributed to increase in servo voltage from experiment run 1 to 5 under constant pulse on time. Similar trend in SR is observed for experimental run 6 to 10, 11 to 15, 16 to 20 and 21 to 25. Surface roughness decrease with increase in servo voltage because at the higher servo voltage less amount of material is melted on machined surface, this can be easily flushed away from the machined surface by dielectric fluid leading to low surface roughness. Khanna & Singh (2016) reported

similar variation of in SR with respect to servo voltage during wire electro discharge machining of high carbon high chromium cold alloy tool (D-3) steel.
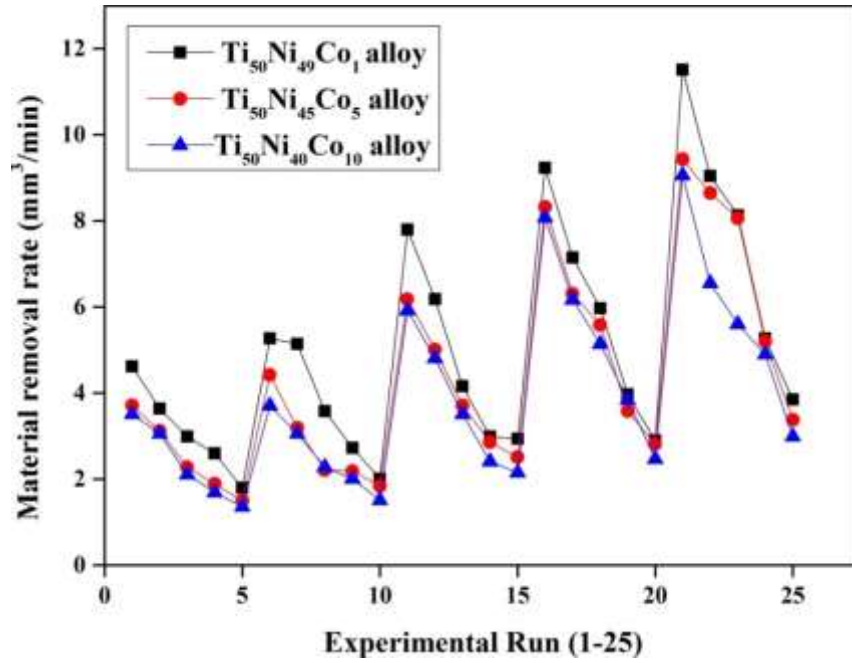
Figure 5.1 Material removal rate with respect to experimental run.
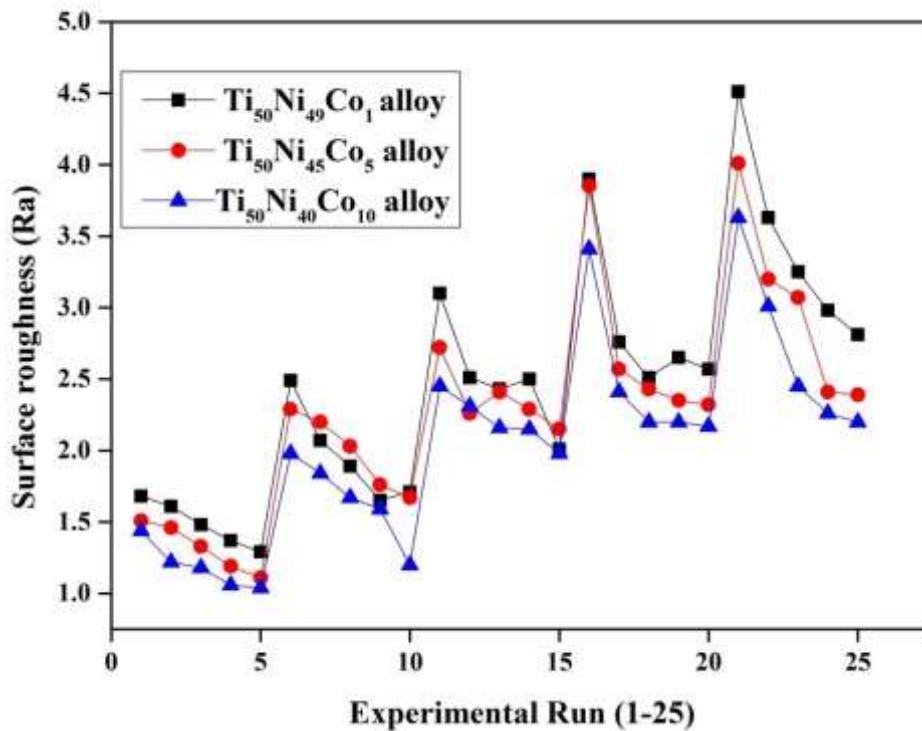
Figure 5.2 Surface roughness with respect to experimental run.

5.4 INDIVIDUAL EFFECTS OF INPUT PROCESS PARAMETERS ON MRR AND SR

The individual effects of process parameters of pulse on time and servo voltage on material removal rate and surface roughness is studied, by varying one parameter, keeping other parameter constant. The results are tabulated in the Table 5.4 and Table 5.5. The effects of individual parameter on output responses are given in Fig. 5.7, Fig. 5.8, Fig. 5.9 and Fig. 5.10.

Table 5.4 Effect of pulse on time under constant servo voltage.

Servo voltage (V)	Pulse on Time (μs)	$Ti_{50}Ni_{49}Co_1$		$Ti_{50}Ni_{45}Co_5$		$Ti_{50}Ni_{40}Co_{10}$	
		SR (μm)	MRR (mm³/min)	SR (μm)	MRR (mm³/min)	SR (μm)	MRR (mm³/min)
20	105	1.68	4.62	1.51	3.71	1.44	3.51
	110	2.49	5.27	2.29	4.42	1.98	3.71

114

		Ti$_{50}$Ni$_{49}$Co$_1$		Ti$_{50}$Ni$_{45}$Co$_5$		Ti$_{50}$Ni$_{40}$Co$_{10}$	
	115	3.1	7.8	2.72	6.18	2.45	5.92
	120	3.9	9.23	3.85	8.32	3.41	8.08
	125	4.51	11.51	4.01	9.43	3.63	9.06
30	105	1.61	3.64	1.46	3.12	1.22	3.06
	110	2.07	5.14	2.2	3.19	1.84	3.06
	115	2.51	6.18	2.26	5.01	2.31	4.81
	120	2.76	7.15	2.57	6.31	2.41	6.17
	125	3.63	9.04	3.2	8.65	3.01	6.55
40	105	1.48	2.99	1.33	2.28	1.18	2.11
	110	1.89	3.58	2.03	2.21	1.67	2.28
	115	2.43	4.16	2.25	3.71	2.16	3.51
	120	2.51	5.97	2.43	5.58	2.2	5.14
	125	3.25	8.13	3.07	8.06	2.45	5.6
50	105	1.37	2.6	1.19	1.89	1.06	1.69
	110	1.65	2.73	1.76	2.19	1.59	2.01
	115	2.5	2.99	2.41	2.86	2.15	2.41
	120	2.65	3.97	2.35	3.58	2.2	3.84
	125	2.98	5.27	2.41	5.2	2.26	4.9
60	105	1.29	1.8	1.11	1.5	1.04	1.36
	110	1.71	2.01	1.67	1.84	1.2	1.51
	115	2.01	2.94	2.15	2.51	1.98	2.15
	120	2.57	2.9	2.32	2.81	2.17	2.47
	125	2.81	3.85	2.39	3.38	2.2	2.99

Table 5.5 Effect of servo voltage under constant pulse on time.

Pulse on Time (µs)	Servo voltage (V)	Ti$_{50}$Ni$_{49}$Co$_1$		Ti$_{50}$Ni$_{45}$Co$_5$		Ti$_{50}$Ni$_{40}$Co$_{10}$	
		SR (µm)	MRR (mm^3/min)	SR (µm)	MRR (mm^3/min)	SR (µm)	MRR (mm^3/min)
105	20	1.68	4.62	1.51	3.71	1.44	3.51

	30	1.61	3.64	1.46	3.12	1.22	3.06
	40	1.48	2.99	1.33	2.28	1.18	2.11
	50	1.37	2.6	1.19	1.89	1.06	1.69
	60	1.29	1.8	1.11	1.5	1.04	1.36
	20	2.49	5.27	2.29	4.42	1.98	3.71
	30	2.07	5.14	2.2	3.19	1.84	3.06
110	40	1.89	3.58	2.03	2.21	1.67	2.28
	50	1.65	2.73	1.76	2.19	1.59	2.01
	60	1.71	2.01	1.67	1.84	1.2	1.51
	20	3.1	7.8	2.72	6.18	2.45	5.92
	30	2.51	6.18	2.26	5.01	2.31	4.81
115	40	2.43	4.16	2.41	3.71	2.16	3.51
	50	2.5	2.99	2.29	2.86	2.15	2.41
	60	2.01	2.94	2.15	2.51	1.98	2.15
	20	3.9	9.23	3.85	8.32	3.41	8.08
	30	2.76	7.15	2.57	6.31	2.41	6.17
120	40	2.51	5.97	2.43	5.58	2.2	5.14
	50	2.65	3.97	2.35	3.58	2.2	3.84
	60	2.57	2.9	2.32	2.81	2.17	2.47
	20	4.51	11.51	4.01	9.43	3.63	9.06
	30	3.63	9.04	3.2	8.65	3.01	6.55
125	40	3.25	8.13	3.07	8.06	2.45	5.6
	50	2.98	5.27	2.41	5.2	2.26	4.9
	60	2.81	3.85	2.39	3.38	2.2	2.99

5.4.1 Effects of pulse on time on material removal rate under constant servo voltage

Fig. 5.3 (a-e) shows the effects of pulse on time under constant servo voltage on material removal rate. It is observed that material removal rate increase with increase in pulse on time. Also the increase in servo voltage results in lower material removal

rate. At higher pulse on time more amount of spark create in the machining zone which are responsible for removal of more amount of material from the surface of work piece. At the same time if servo voltage is increased during machining, the average spark gap increases, consecutively decreasing the spark intensity and leading to lower material removal rate. Similar results have been reported by Timur et al. (2016) during the wire electro discharge machining of titanium alloy (BT5). When all the three alloys are machined at the same process parameters, material removal rate is decreasing with increase in the percentage of cobalt in TiNi shape memory alloy. This is due to increasing in the hardness with increase in percent of Co in TiNi alloy. Similarly Bagoury (2014) observed that hardness is affected by addition of Co in TiNi.
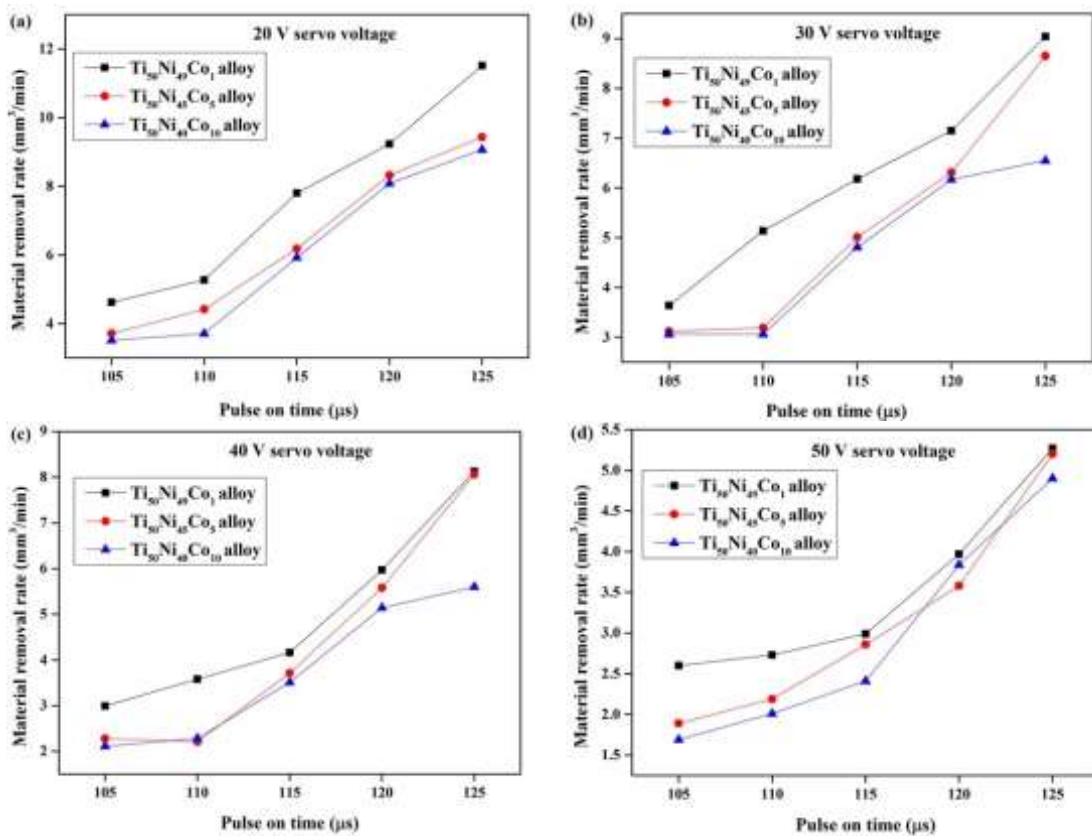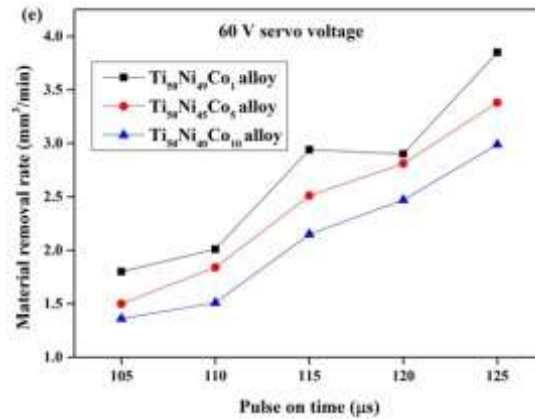
Figure 5.3 Effects of pulse on time on material removal rate under constant servo voltage of (a) 20V, (b)30 V, (c) 40V, (d) 50V and (e) 60V.

5.4.2 Effects of pulse on time on surface roughness under constant servo voltage

Effects of pulse on time on surface roughness with constant servo voltage have been presented in the Fig. 5.4 (a-e). It is observed that surface roughness is increasing with increase in pulse on time with constant servo voltage. Also increase in servo voltage resulting in decrease of surface roughness at the same values of pulse on time. At higher pulse on time less time is available for flushing to remove the molten material from the machined surface which is resolidify on the surface of machined components in the form of melted drops and micro globules as seen in the Fig. 5.7. Hence higher surface roughness observed at higher values of pulse on time. When servo voltage is increased, surface roughness is decreased this is due to increase in servo voltage results in larger spark gap thereby reducing the spark intensity and eventually lesser amount of material is removed from the surface of the workpiece. Comparatively higher surface roughness is observed for $Ti_{50}Ni_{49}Co_1$ alloy, while lower surface roughness is noticed during the machining of $Ti_{50}Ni_{40}Co_{10}$ alloy at the same levels of process parameters.
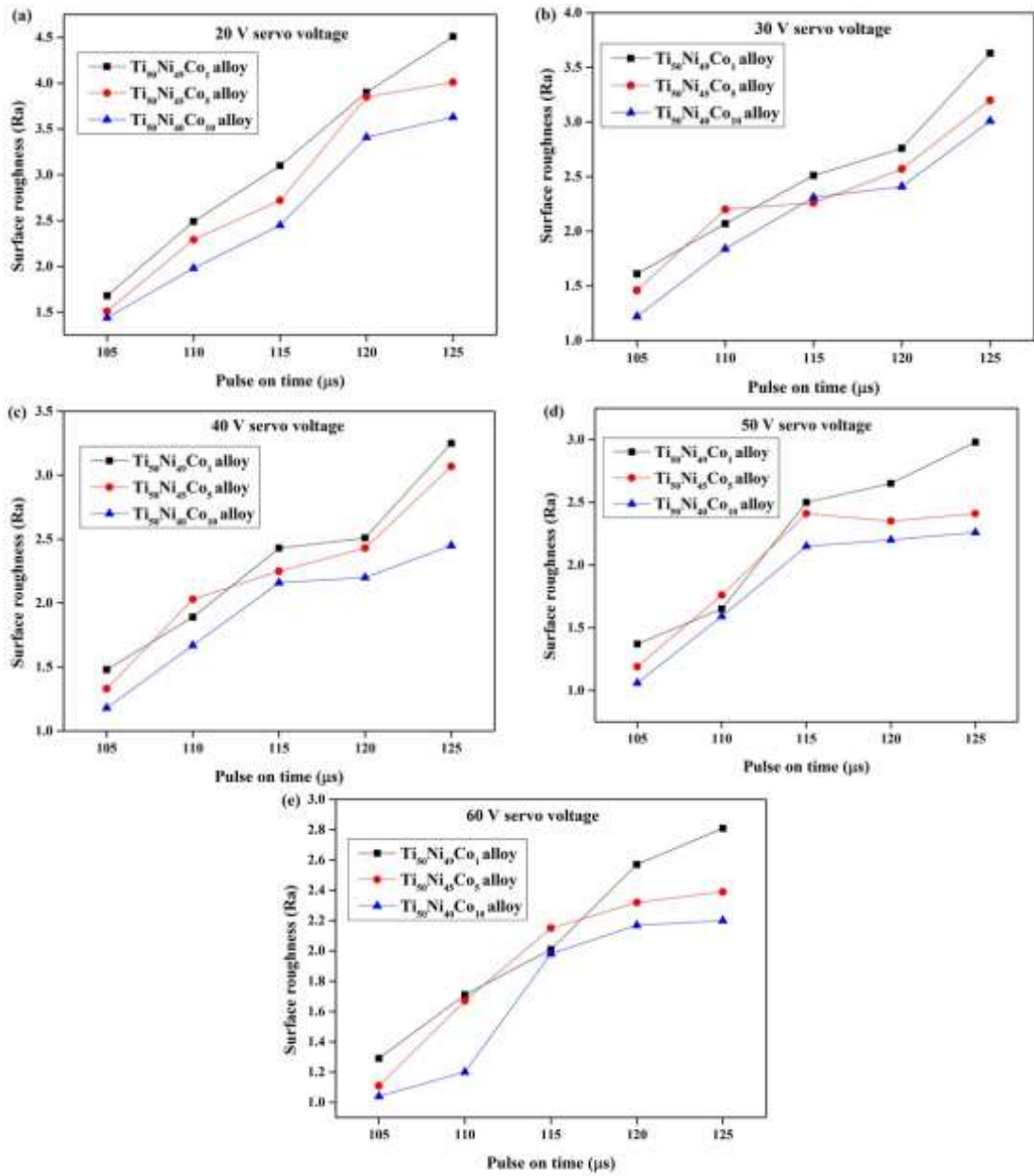
Figure 5.4 Effects of pulse on time on surface roughness under constant servo voltage (a) 20V, (b)30 V, (c) 40V, (d) 50V and (e) 60V.

5.4.3 Effects of servo voltage on material removal rate under constant pulse on time

Fig. 5.5 (a-e) indicates effect of servo voltage with constant pulse on time. It is observed that material removal rate decrease with the increase in servo voltage and at

the same time material removal rate is increased with increase in values of pulse on time. Because at high pulse on time 125µs and lower servo voltage 20V spark intensity will be high at the same time lesser spark gap, hence more amount of material melted from machined surface which leads to higher material removal rate. However detailed explanation about the same trend has been discussed in the section 4.3.1.
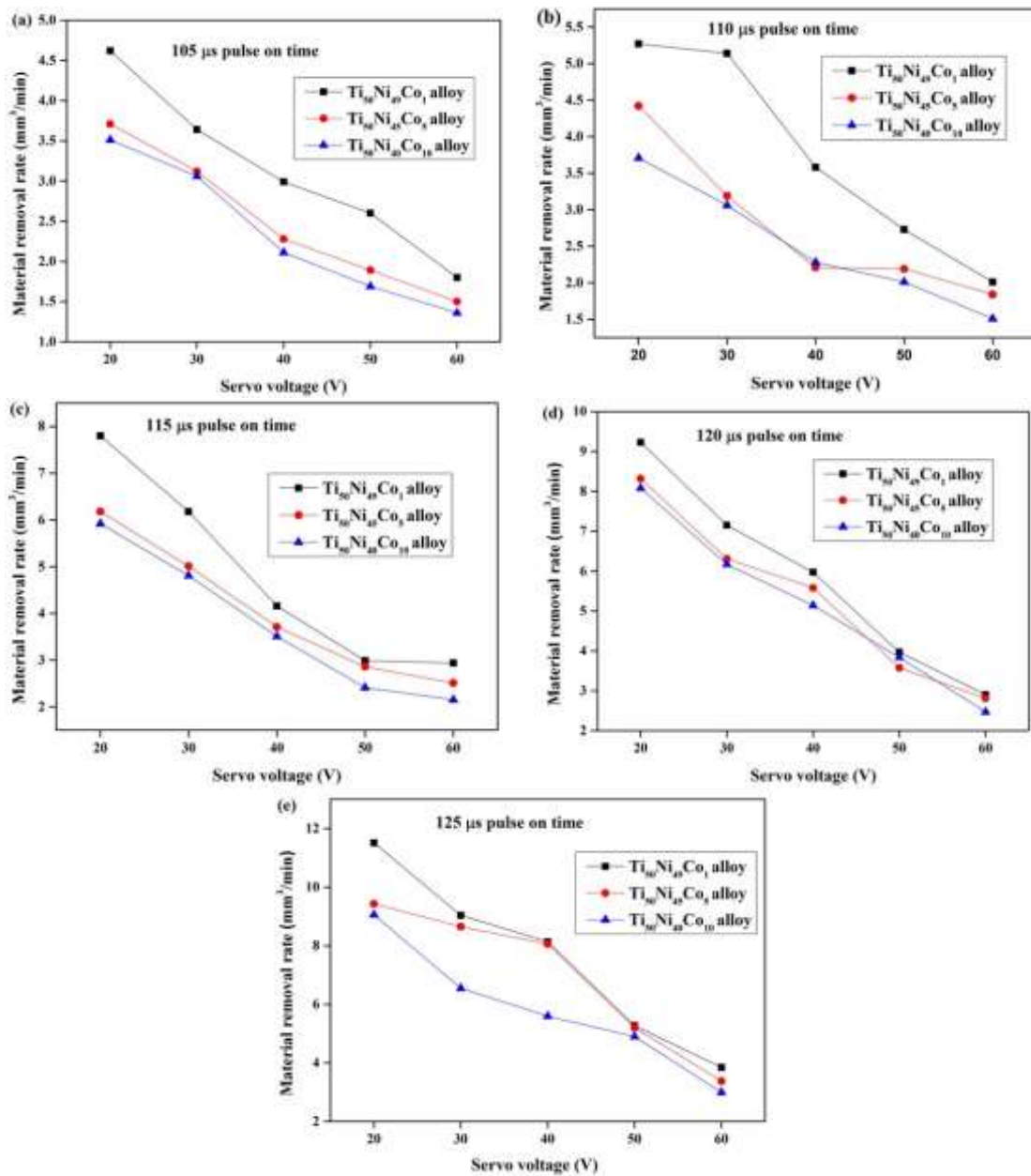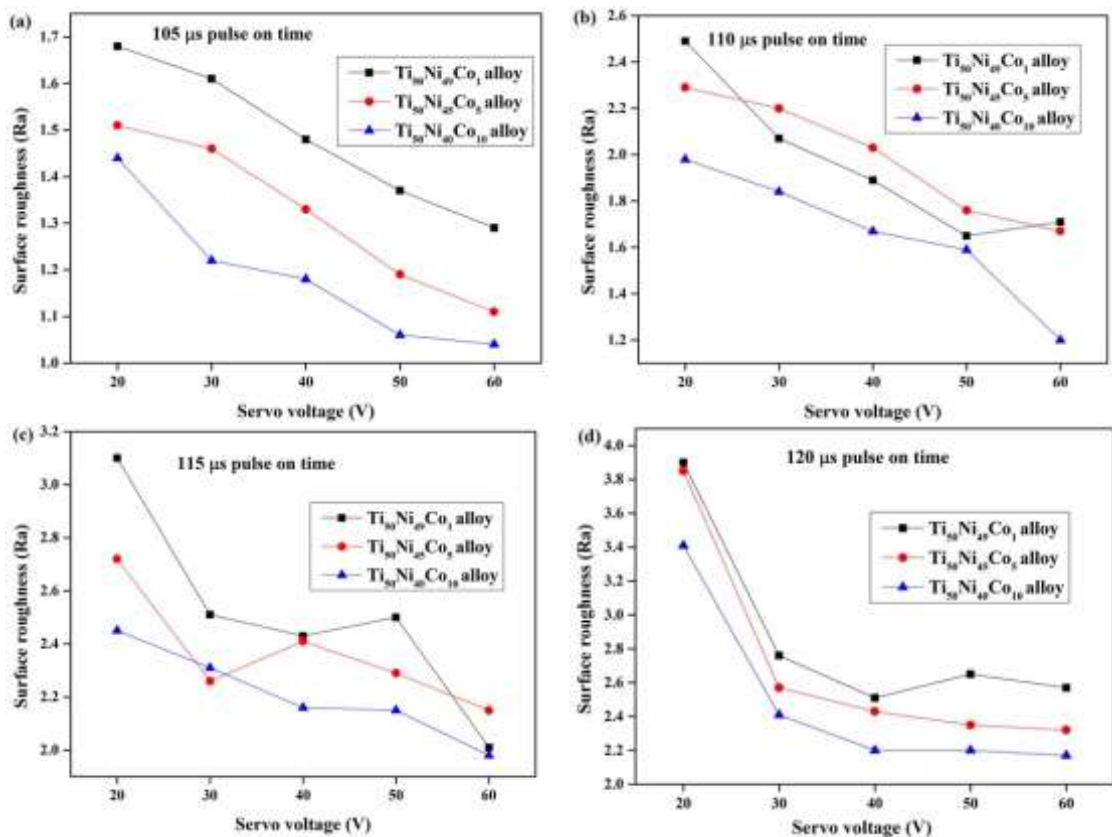

Figure 5.5 Effects of servo voltage and constant pulse on time on material removal rate (a) 105 µs, (b) 110 µs, (c) 115 µs, (d) 120 µs and (e) 125 µs.

5.4.4 Effects of servo voltage on surface roughness under constant pulse on time

Fig. 5.6 (a-e) represents the effect of servo voltage on surface roughness with constant pulse on time. Reduction in the surface roughness is noticed with the increase in servo voltage. When pulse on time is increased at the same values of servo voltage, increment in surface roughness is noticed. More sparks produce at higher pulse on time which is responsible to melt more amount of material from the surface of workpiece, some of melted material is taken away by dielectric fluid, leftover molten material deposited on the surface of workpiece in the form of melted drops and micro globules and leads to higher surface roughness. Same as explained with detail in the section of 4.3.2. Lower values of surface roughness have been observed for machining under pulse on time of 105μs and higher surface roughness was measured at 125 μs pulse on time.
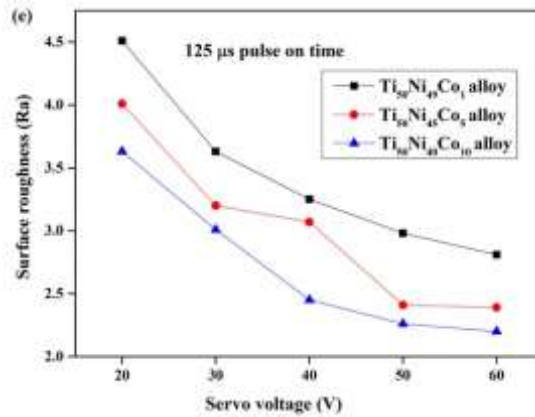
Figure 5.6 Effects of servo voltage and constant pulse on time on surface roughness
(a) 105 µs, (b) 110 µs, (c) 115 µs, (d) 120 µs and (e) 125 µs.

5.5 MORPHOLOGY OF MACHINED SURFACE

Microstructural analysis has been carried out at the lower and higher values of materials removal rate and surface roughness which is shown in the Fig. 5.7 (a-f). Lower values of outputs found the at run number 5 (pulse on time 105µs and servo voltage 60V) and higher values of outputs are found at the run number 21 (pulse on time 125µs and servo voltage 20V) for all three alloys.1.8 mm^3/min MRR for $Ti_{50}Ni_{49}Co_1$, 1.5 mm^3/min MRR for $Ti_{50}Ni_{45}Co_5$ and 1.36 mm^3/min MRR for $Ti_{50}Ni_{40}Co_{10}$ have been noticed as lower values of material removal rate. 1.29 µm SR for $Ti_{50}Ni_{49}Co_1$, 1.11 µm SR for $Ti_{50}Ni_{45}Co_5$ and 1.04 µm SR for $Ti_{50}Ni_{40}Co_{10}$ have been noticed as lower values of surface roughness. 11.51 mm^3/min MRR for $Ti_{50}Ni_{49}Co_1$, 9.43 mm^3/min MRR for $Ti_{50}Ni_{45}Co_5$ and 9.06 mm^3/min MRR for $Ti_{50}Ni_{40}Co_{10}$ have been noticed as higher values of material removal rate. 4.51 µm SR for $Ti_{50}Ni_{49}Co_1$, 4.01 µm SR for $Ti_{50}Ni_{45}Co_5$ and 3.63 µm SR for $Ti_{50}Ni_{40}Co_{10}$ have been noticed as higher values of surface roughness. The trend of variation in material removal rate and surface roughness are similar with the same process parameters for all three alloys, but the values of these outputs are reduced with increase in the percentage of Co in TiNi shape memory alloy. Comparatively $Ti_{50}Ni_{40}Co_{10}$ alloy exhibit better surface roughness at higher material removal rate, whereas rougher surface was observed for $Ti_{50}Ni_{49}Co_1$ alloy as can be seen in the Fig. 5.4. The microstructure exhibit the presence of few micro globules, melted drops and micro

cracks due to lower pulse on time (105μs) and higher servo voltage (60V) during the machining, because at the lower pulse on time spark intensity is low and this results in lower amount of spark created in the machining zone and lesser amount of material is removed from the surface of workpiece which can be easily removed through flushing with help of dielectric fluid from the machined surface. This reduces the formation of machining defects on the machined surface such as micro cracks, micro globules and melted drops. At the same time, when the servo voltage is high, the spark gap is increased; hence more time is available for flushing the melted material from the machined surface therefore most of the melted material is remove from the machined surface results in only few micro cracks, micro globules and melted drops. The microstructures 5.7b for $Ti_{50}Ni_{49}Co_1$ alloy, Fig. 5.7d for $Ti_{50}Ni_{45}Co_5$ alloy, and Fig. 5.7f for $Ti_{50}Ni_{40}Co_{10}$ alloy exhibit higher values of material removal rate and surface roughness. The microstructures, shows the presence of higher amount of microcracks, melted drops, microglobules on the machined surface during machining under higher pulse on time 125μs and lower servo voltage 20V. At high pulse on time, spark intensity is high and hence less time is available to remove the melted material form the machined surface. Hence less amount of melted material are removed, rest of the melted material are resolidify on the machined surface in the form of microcracks, melted drops, microglobules on the machined surface, this leads to the higher surface roughness (Fig. 5.5e). Moreover, high temperature experienced by the material due to continuous sparking in the machining zone along with dielectric breakdown results in formation of microglobules as seen from the micrographs depicted in Fig. 5.7. On the other hand more cracks appeared on the machined surface at the lower servo voltage when compared to samples machined at higher servo voltage. At low servo voltage, surface roughness will be higher due to more intense spark discharge on the machining surface that leads to formation of larger and abrupt crater along with faster resolidification of molten material by dielectric quenching. Similar results have been reported by Chen et al. (2007) during the electro discharge machining of TiNiCr and TiNiZr shape memory alloys.
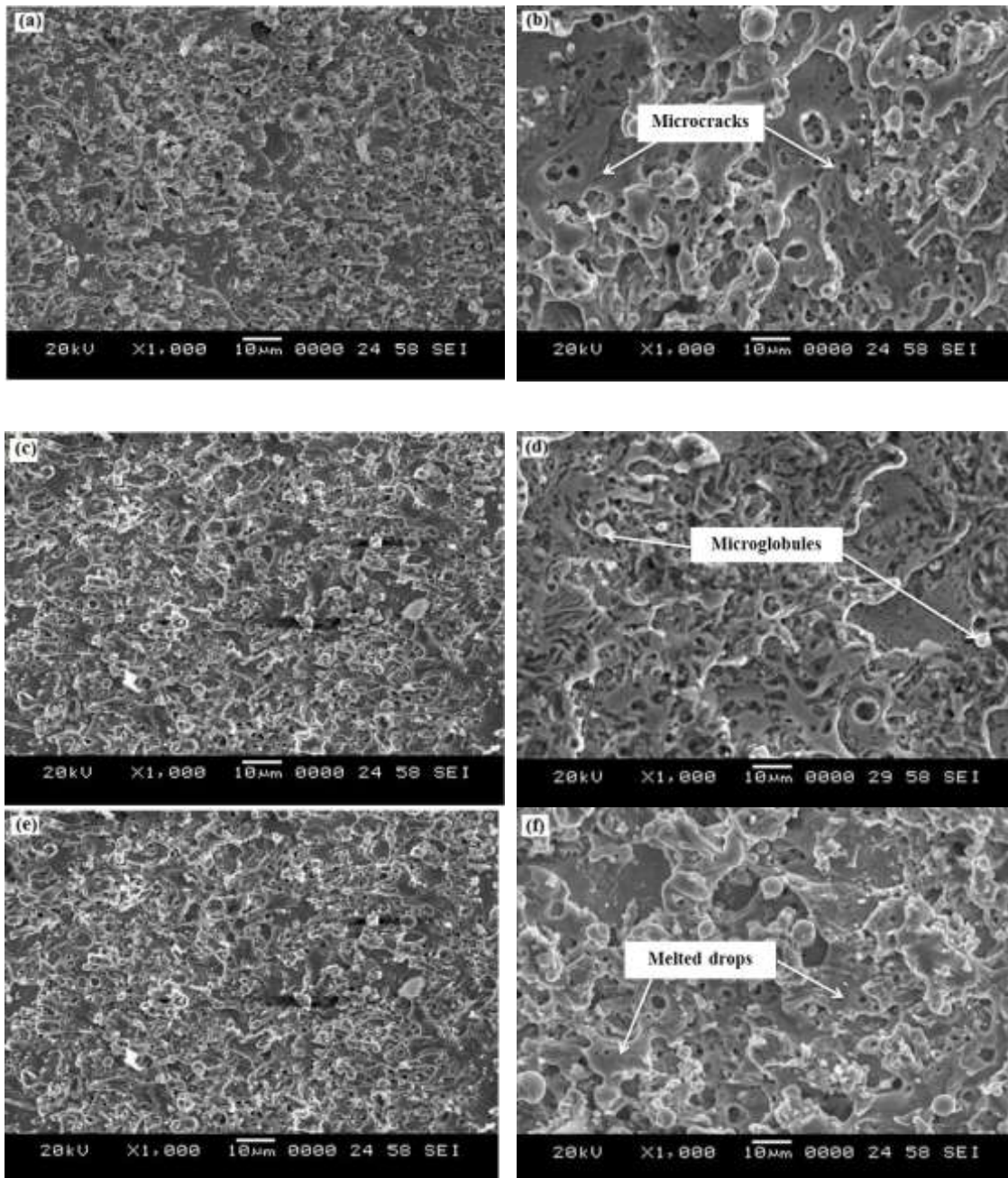
Figure 5.7 Machined surface morphology at higher value of outputs (a) $Ti_{50}Ni_{49}Co_1$ alloy, (c) $Ti_{50}Ni_{45}Co_5$ alloy, and (e) $Ti_{50}Ni_{40}Co_{10}$ alloy) and lower values of outputs (b) $Ti_{50}Ni_{49}Co_1$ alloy, (d) $Ti_{50}Ni_{45}Co_5$ alloy, and (f) $Ti_{50}Ni_{40}Co_{10}$ alloy).

5.6 SURFACE TOPOGRAPHY

Surface topography analysis has been carried out at lower and higher values of MRR and SR for all the three alloys. 1.8 mm^3/min MRR for $Ti_{50}Ni_{49}Co_1$, 1.5 mm^3/min

MRR for $Ti_{50}Ni_{45}Co_5$ and 1.36 mm^3/min MRR for $Ti_{50}Ni_{40}Co_{10}$ have been noticed as lower values of material removal rate. 1.29 μm SR for $Ti_{50}Ni_{49}Co_1$, 1.11 μm SR for $Ti_{50}Ni_{45}Co_5$ and 1.04 μm SR for $Ti_{50}Ni_{40}Co_{10}$ have been noticed as lower values of surface roughness. Fig. 5.8a, c and e for $Ti_{50}Ni_{49}Co_1$, $Ti_{50}Ni_{45}Co_5$ and $Ti_{50}Ni_{40}Co_{10}$ alloy respectively exhibit the surface topographical analysis at lower values of outputs while Fig. 5.8 b, d and f $Ti_{50}Ni_{49}Co_1$, $Ti_{50}Ni_{45}Co_5$ and $Ti_{50}Ni_{40}Co_{10}$ alloy respectively shows surface topographical analysis at higher values of MRR and SR. The microstructures at lower values of outputs (Fig. 5.8 a, c and e) shows better surface when compared to microstructures at higher values of outputs (Fig. 5.8 b, d and f) however these values are presented in Table 5.3 for each alloy. Higher values of outputs achieved while machining at higher pulse on time (125μs) and lower servo voltage (20V). 11.51 mm^3/min MRR for $Ti_{50}Ni_{49}Co_1$, 9.43 mm^3/min MRR for $Ti_{50}Ni_{45}Co_5$ and 9.06 mm^3/min MRR for $Ti_{50}Ni_{40}Co_{10}$ have been noticed as higher values of material removal rate. 4.51 μm SR for $Ti_{50}Ni_{49}Co_1$, 4.01 μm SR for $Ti_{50}Ni_{45}Co_5$ and 3.63 μm SR for $Ti_{50}Ni_{40}Co_{10}$ have been noticed as higher values of surface roughness. At high pulse on time spark intensity is large; more amount of spark is produced in the machining zone while less time is available to remove the melted materials form the machined component. This leads to the formation of micro cracks, melted drops, and micro globules on the machined surface. Also at low servo voltage, surface roughness will be higher due to more intense spark discharge on the machining surface that leads to formation of larger and abrupt crater along with faster resolidification of molten material by dielectric quenching which is also confirmed through machined surface morphology and can be seen in Fig. 4.8 c.
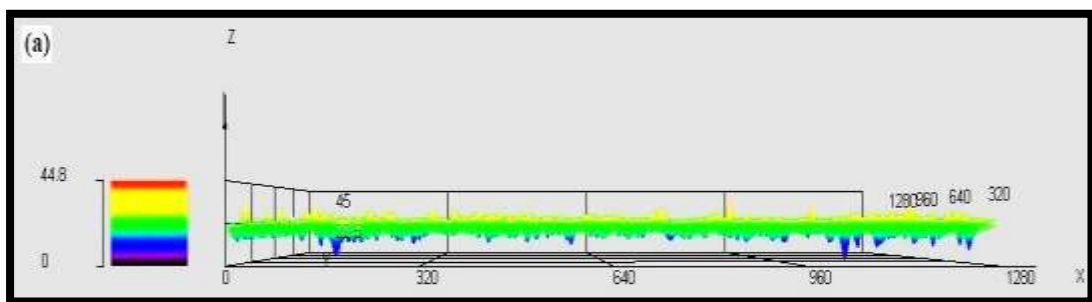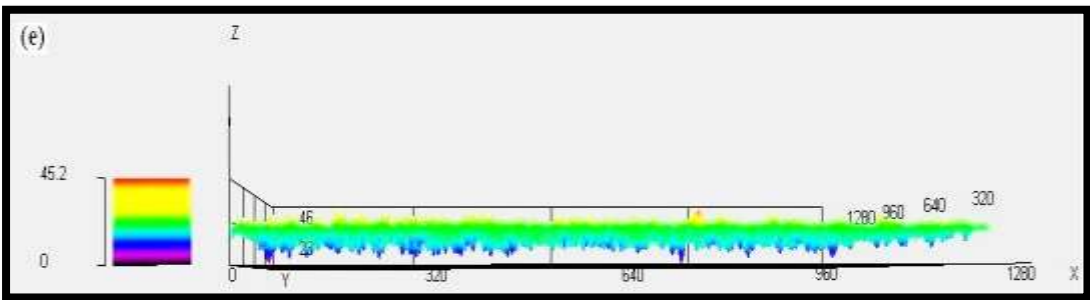
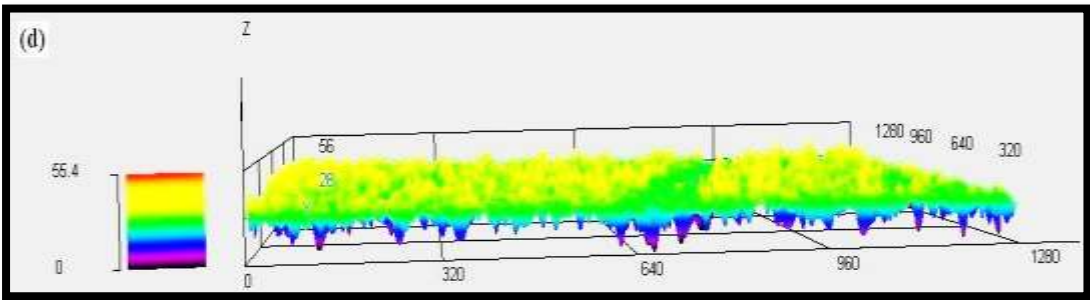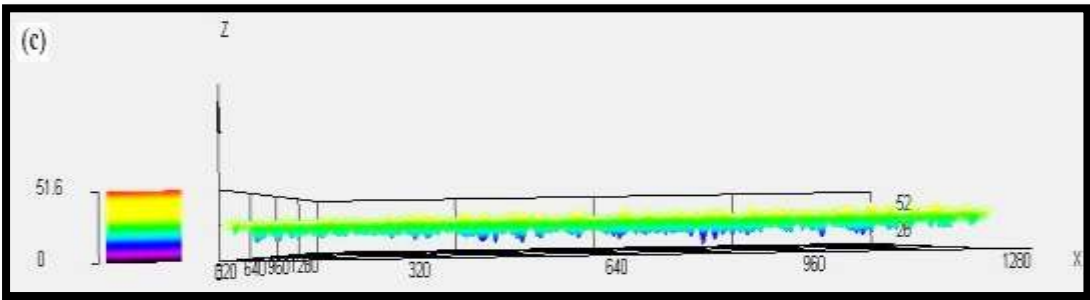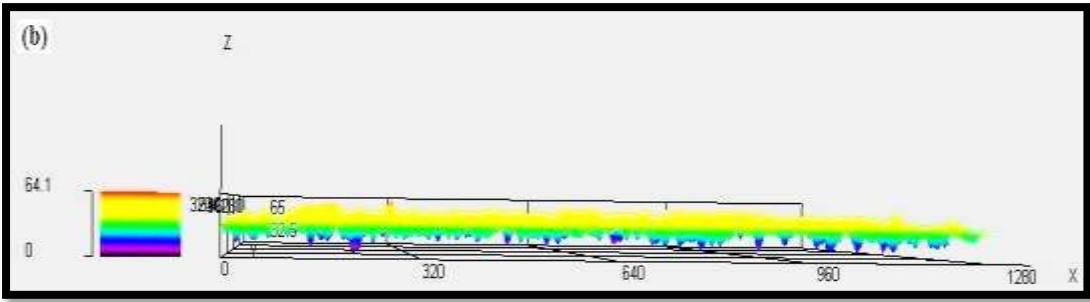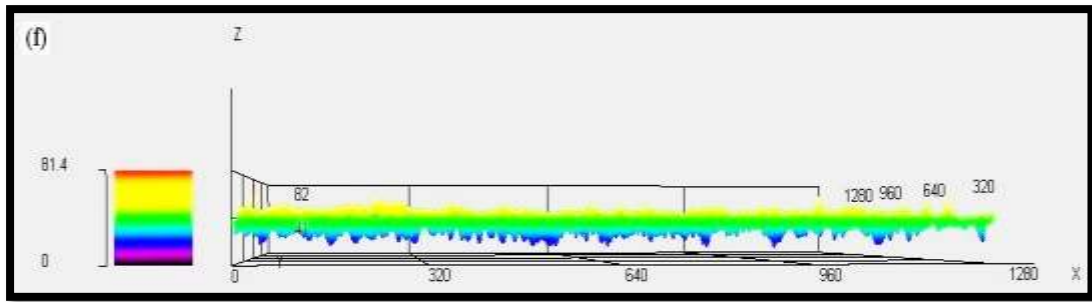Figure 5.8 Surface topography analysis of machined surface at lower values of outputs (a) $Ti_{50}Ni_{49}Co_1$ alloy, (c) $Ti_{50}Ni_{45}Co_5$ alloy and (e) $Ti_{50}Ni_{40}Co_{10}$ alloy and higher values of outputs (b) $Ti_{50}Ni_{49}Co_1$ alloy, (d) $Ti_{50}Ni_{40}Co_5$ alloy and (f) $Ti_{50}Ni_{40}Co_{10}$ alloy.

5.7 MICRO HARDNESS ANALYSIS

Microhardness analysis has been carried out at lower (1.8 mm^3/min MRR for $Ti_{50}Ni_{49}Co_1$, 1.5 mm^3/min MRR for $Ti_{50}Ni_{45}Co_5$ and 1.36 mm^3/min MRR for $Ti_{50}Ni_{40}Co_{10}$ have been noticed as lower values of material removal rate. 1.29 μm SR for $Ti_{50}Ni_{49}Co_1$, 1.11 μm SR for $Ti_{50}Ni_{45}Co_5$ and 1.04 μm SR for $Ti_{50}Ni_{40}Co_{10}$ alloy) and higher values of outputs (11.51 mm^3/min MRR for $Ti_{50}Ni_{49}Co_1$, 9.43 mm^3/min MRR for $Ti_{50}Ni_{45}Co_5$ and 9.06 mm^3/min MRR for $Ti_{50}Ni_{40}Co_{10}$ have been noticed as higher values of material removal rate. 4.51 μm SR for $Ti_{50}Ni_{49}Co_1$, 4.01 μm SR for $Ti_{50}Ni_{45}Co_5$ and 3.63 μm SR for $Ti_{50}Ni_{40}Co_{10}$ alloy). Fig. 5.9 indicates the micro hardness at lower values of outputs and Fig. 5.10 shows the microhardness at higher values of outputs. During the WEDM process three different zones are forming from the machined surface namely recast layer zone, heat affected zone and converted layer zone (Choudhary et al. 2010). Generally microhardness of converted layer zone is not affected during the WEDM process while recast layer and heat affected zone affects the microhardness of machined component. While measuring microhardness, recast layer near the cutting edge was considered as a starting point (0μm) and microhardness was measured towards the base material. From Fig. 5.9 and Fig. 5.10 it can be observed that hardness noted along the cross section of the machined surface follows a decreasing trend starting from recast layer to heat affected zone. The micro hardness of converted layer is almost equal to the hardness of base material because

converted layer is not much affected of by WEDM. The average value of micro hardness at the lower values of outputs in recast layer zone is 624 HV for $Ti_{50}Ni_{49}Co_{10}$, 602 HV for $Ti_{50}Ni_{45}Co_5$ and 580 HV for $Ti_{50}Ni_{40}Co_1$ alloy while average values of microhardness in heat affected zone is 544 HV for $Ti_{50}Ni_{49}Co_{10}$, 518 HV for $Ti_{50}Ni_{45}Co_5$ and 510 HV for $Ti_{50}Ni_{40}Co_1$ alloy. Similarly at higher values of output microhardness in recast layer zone is 601 HV for $Ti_{50}Ni_{49}Co_{10}$, 590 HV for $Ti_{50}Ni_{45}Co_5$ and 570 HV for $Ti_{50}Ni_{40}Co_1$ alloy, while micro hardness reported in heat affected zone is 519 HV for $Ti_{50}Ni_{49}Co_{10}$ 500 HV for $Ti_{50}Ni_{45}Co_5$ and 488 HV for $Ti_{50}Ni_{40}Co_1$ alloy. Moreover it is observed that by increasing percentage of Co in TiNi, resulting in decrease of micro hardness. High hardness on the machined surface is due to formation of surface oxides of TiO_2, $NiTiO_3$ and NiO Fig.4.16. The micro hardness in the heat affected zone is less than at recast layer; this may be due to phase transformation in the TiNiCo alloy which can be seen in Fig. 4.16. Similar results were reported by Hsieh et al. (2009 and 2013) during the EDM of TiNiZr and TiAlFe alloys.
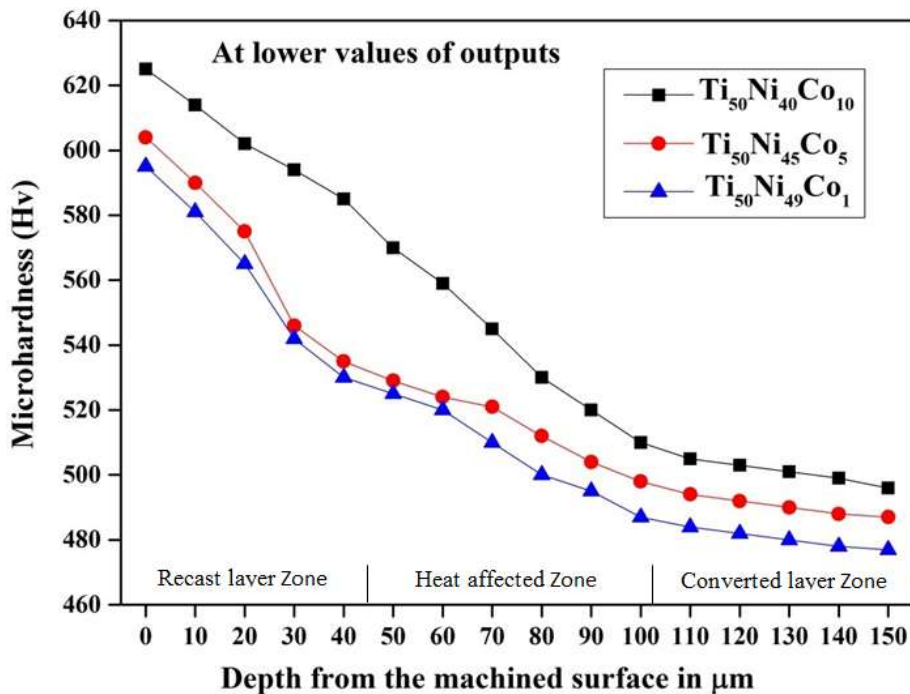
Figure 5.9 Variation of micro hardness along the cross section at the lower values of outputs.
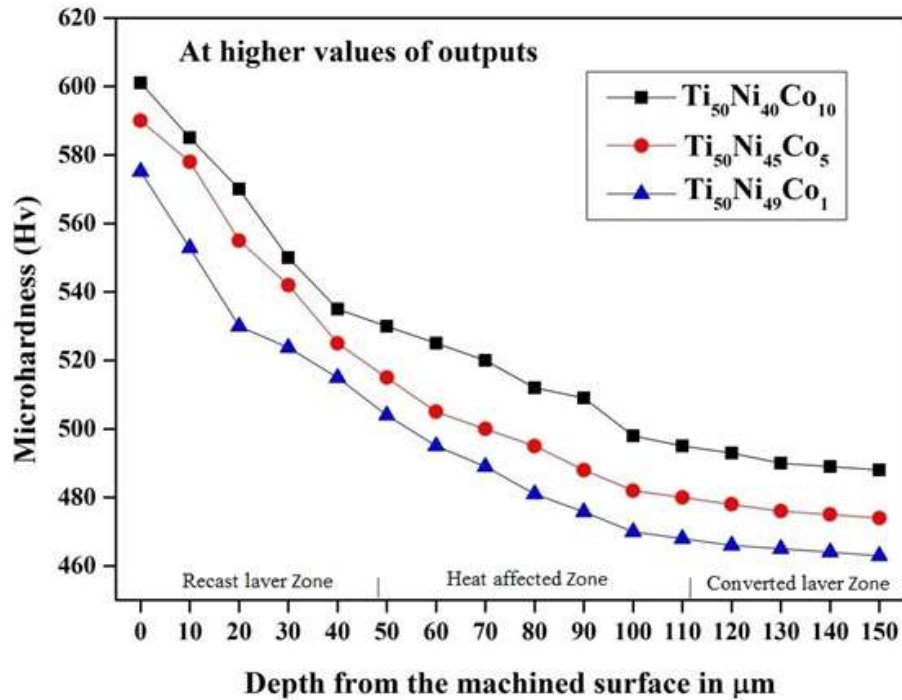
Figure 5.10 Variation of micro hardness along the cross section at the higher values of outputs.

5.8 RECAST LAYER THICKNESS

Recast layer thickness measurement has been carried out at lower and higher values of output. 1.8 mm^3/min MRR for Ti$_{50}$Ni$_{49}$Co$_1$, 1.5 mm^3/min MRR for Ti$_{50}$Ni$_{45}$Co$_5$ and 1.36 mm^3/min MRR for Ti$_{50}$Ni$_{40}$Co$_{10}$ have been noticed as lower values of material removal rate. 1.29 μm SR for Ti$_{50}$Ni$_{49}$Co$_1$, 1.11 μm SR for Ti$_{50}$Ni$_{45}$Co$_5$ and 1.04 μm SR for Ti$_{50}$Ni$_{40}$Co$_{10}$ have been noticed as lower values of surface roughness. 11.51 mm^3/min MRR for Ti$_{50}$Ni$_{49}$Co$_1$, 9.43 mm^3/min MRR for Ti$_{50}$Ni$_{45}$Co$_5$ and 9.06 mm^3/min MRR for Ti$_{50}$Ni$_{40}$Co$_{10}$ have been noticed as higher values of material removal rate. 4.51 μm SR for Ti$_{50}$Ni$_{49}$Co$_1$, 4.01 μm SR for Ti$_{50}$Ni$_{45}$Co$_5$ and 3.63 μm SR for Ti$_{50}$Ni$_{40}$Co$_{10}$ have been noticed as higher values of surface roughness. Fig. 5.11 and Fig. 5.12 indicate the recast layer thickness of machined surface. During wire electro discharge machining, rapid heating and quenching of the molten material by the dielectric fluid causes the formation of a solidified layer and gets deposited on the machined surface, which makes harder surface of machined component. The

measured values of recast layer thickness at lower values of output is 4.2 µm for $Ti_{50}Ni_{49}Co_1$, 4.6 µm for $Ti_{50}Ni_{45}Co_5$ and 4.9 µm for $Ti_{50}Ni_{40}Co_{10}$ alloy, while recast layer thickness at higher values of outputs is 30 µm for $Ti_{50}Ni_{49}Co_1$, 32 µm for $Ti_{50}Ni_{45}Co_5$ and 35 µm for $Ti_{50}Ni_{40}Co_{10}$ alloy. Thicker recast layer has been observed at the higher values of output or at input process parameters of 125µs T_{on} and 20V SV. At high pulse on time workpiece receives more spark discharge of higher intensity which leads to thicker recast layer formation. Longer pulse duration generally leads to higher discharge energy per unit cycle that melts more material and re-solidifies due to rapid quenching by constantly flowing de-ionized water on the machined surface. On the other hand, thin film of recast layer was noticed from the Fig. 5.11, Fig. 5.11b and 5.11c due to lower 105 µs pulse on time and higher servo voltage 60V. Similar results have been reported by Sharma et al. (2015) during WED machining of Inconel 706.

130
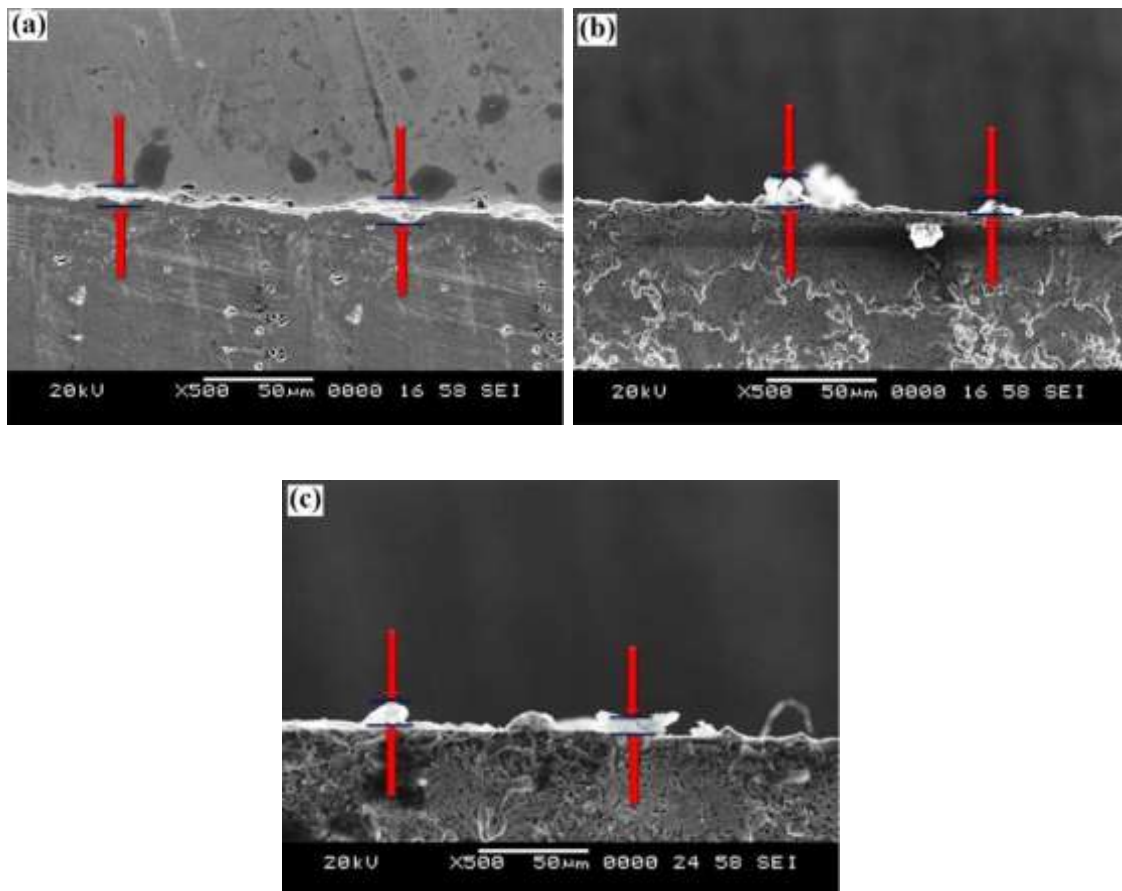
Figure 5.11 Recast layer thickness at lower values of outputs (a) $Ti_{50}Ni_{49}Co_1$ alloy, (b) $Ti_{50}Ni_{45}Co_5$ alloy and (c) $Ti_{50}Ni_{40}Co_{10}$ alloy.
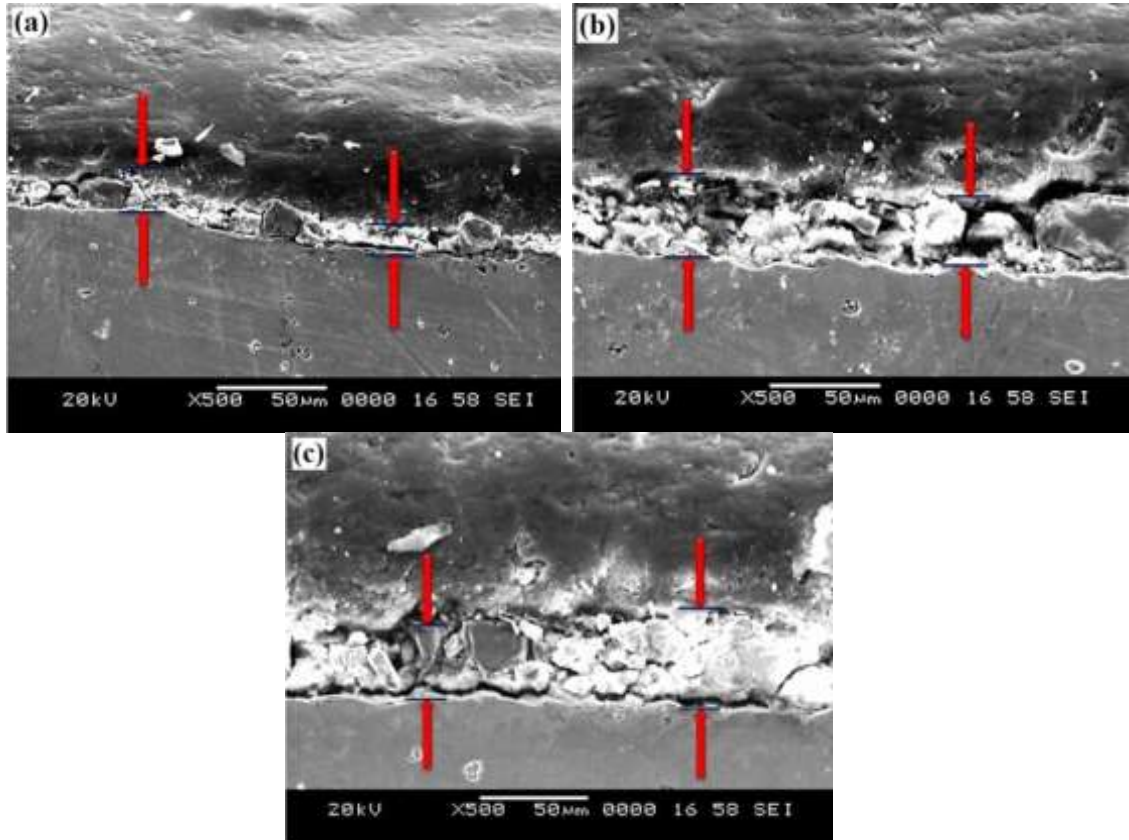
Figure 5.12 Recast layer thickness at higher values of outputs (a) $Ti_{50}Ni_{49}Co_1$ alloy, (b) $Ti_{50}Ni_{40}Co_5$ alloy and (c) $Ti_{50}Ni_{40}Co_{10}$ alloy.

5.9 RESIDUAL STRESS ANALYSIS

Residual stress exists on the machined surface is either tensile or compressive in nature. The residual stresses exist on the WED machined surface, due to non-homogeneity of heat flow, metallurgical transformations in the machining zone and plastic deformation (Ekmekci et al. 2005 and Newton et al. 2009). Plastic deformation induces the compressive residual stresses by mechanical load and tensile residual stress by thermal load (Srinivasa Rao et al. 2016). The phase transformations led to the change in volume of surface and subsurface layers, so the decrease or increase of its volume was hindered by bulk material resulting in generation of tensile or compressive residual stresses respectively. Generally, wire electro discharge

machining induced tensile residual stresses on the machined surface or in the recast layer zone further it decrease to the heat affected zone because of high spark energy involved in the machining zone. In the present study, recast layer formed on the machined surface is removed by means of polishing and residual stress measurement is made on the machined surface without recast layer. The measured values of residual stress on the machined surface at lower (1.8 mm^3/min MRR for Ti$_{50}$Ni$_{49}$Co$_1$, 1.5 mm^3/min MRR for Ti$_{50}$Ni$_{45}$Co$_5$ and 1.36 mm^3/min MRR for Ti$_{50}$Ni$_{40}$Co$_{10}$ have been noticed as lower values of material removal rate. 1.29 μm SR for Ti$_{50}$Ni$_{49}$Co$_1$, 1.11 μm SR for Ti$_{50}$Ni$_{45}$Co$_5$ and 1.04 μm SR for Ti$_{50}$Ni$_{40}$Co$_{10}$ alloy)   and higher values of outputs (11.51 mm^3/min MRR for Ti$_{50}$Ni$_{49}$Co$_1$, 9.43 mm^3/min MRR for Ti$_{50}$Ni$_{45}$Co$_5$ and 9.06 mm^3/min MRR for Ti$_{50}$Ni$_{40}$Co$_{10}$ have been noticed as higher values of material removal rate. 4.51 μm SR for Ti$_{50}$Ni$_{49}$Co$_1$, 4.01 μm SR for Ti$_{50}$Ni$_{45}$Co$_5$ and 3.63 μm SR for Ti$_{50}$Ni$_{40}$Co$_{10}$ alloy) are shown in the Fig. 5.13. Tensile residual has been found on the machined surface of all three alloys. 15 Mpa for Ti$_{50}$Ni$_{49}$Co$_1$, 10Mpa for Ti$_{50}$Ni$_{45}$Co$_5$ and 6 Mpa for Ti$_{50}$Ni$_{40}$Co$_{10}$ alloy residual stresses have been found at lower values of outputs. Mpa for 255 Ti$_{50}$Ni$_{49}$Co$_1$, 244 Mpa for Ti$_{50}$Ni$_{45}$Co$_5$ and 235 Mpa for Ti$_{50}$Ni$_{40}$Co$_{10}$ alloy residual stresses have been found at higher values of outputs. Minimum residual stress has been observed on the machined surface of Ti$_{50}$Ni$_{49}$Co$_{10}$ alloy while maximum stress has seen on the machined surface of Ti$_{50}$Ni$_{40}$Co$_1$ alloy. Also residual stresses measured at lower values of surface roughness and material removal rate is less than residual stress at the higher values of these outputs. The increase in residual stress observed at higher values of output responses is due to machining of surface under higher values of pulse on time and lower values of the servo voltage. At the higher value of pulse on time more energy of spark has been produced and at the same time lower values of servo voltage implies less spark gap, these two effects result in more melting and solidification of melted material on machined surface. Hence melting and solidification leads to higher tensile residual stresses on the machined surface. The surface morphology of machined surface is presented in Fig. 5.7 with micro cracks and thinner recast layer, formation of recast layer can be seen in Fig. 5.11 and 5.12, implies the presence of tensile residual stresses.
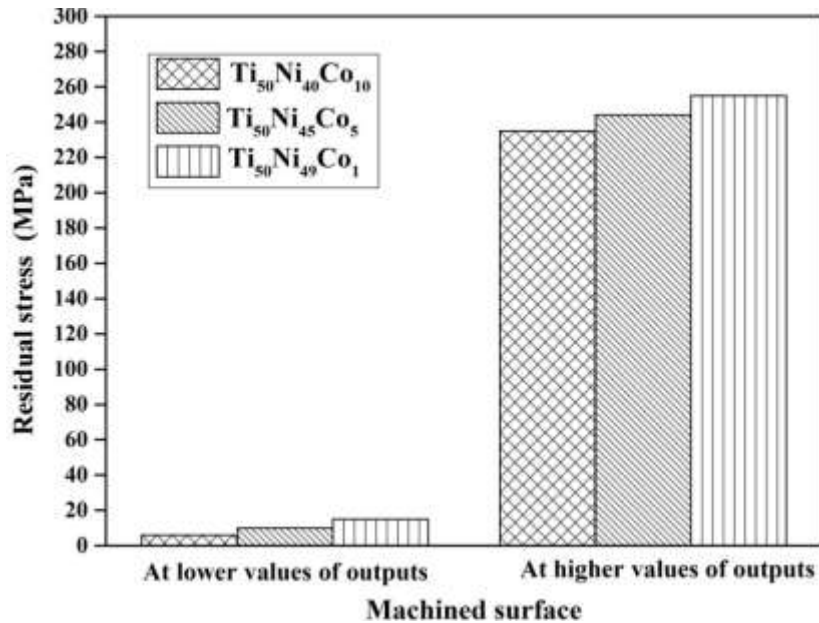
Figure 5.13 Residual stresses of machined surface.

From the above observation it has been confirmed that pulse on time and servo voltage were major affected process parameters of wire electro discharge machining process. To find the error of experimental responses and predicted responses, error analysis will be carried out in further study.

5.10 ARTIFICIAL NEURAL NETWORK

ANN is an artificial illustration of the human brain that tries to simulate its learning approach which is an interconnected pair of artificial neurons that uses a mathematical model for information processing based on a connectionist method to computation. Neural networks are non-linear mapping systems that consist of simple processors which are called neurons, linked by weighted connections. Each neuron has inputs and generates an output that can be seen as the reflection of local information that is stored in connections. Among ANN models, the feed-forward neural network based on back-propagation is the well proved general-purpose model. Hence in the present work, the network has two inputs of Ton and SV and two outputs of MRR and SR. Matlab software is used for predicting the responses. To prediction of MRR and SR 70% data was kept in training and rest of the data was test data during the prediction. To get the best regression plots which give accurate prediction 15 hidden layers were adopted during the training of the data. Developed ANN model can be seen in Fig.

3.16 and Fig. 3.17 is presented regression plots. Same procedure implemented for prediction of WEDM responses for $Ti_{50}Co_{49}Co_1$, $Ti_{50}Co_{45}Co_5$ and $Ti_{50}Co_{40}Co_{10}$ alloy. Further study has been carried out for error analysis to find the error between of experimental and predicted values. Predicted values through ANN are given in Table 5.6, Table 5.7 and Table 5.8 for $Ti_{50}Ni_{49}Co_1$ alloy, $Ti_{50}Ni_{45}Co_5$ alloy, and $Ti_{50}Ni_{40}Co_{10}$ alloy respectively. Error analysis has been carried out by using equation 5.1.

$$\text{Absolute error (\%)} = \frac{\text{Experimental Value} - \text{predicted values}}{\text{Experimental value}} \text{ x } 100 \dots.5.1$$

Table 5.6 Experimental and predicted values of responses for $Ti_{50}Ni_{49}Co_1$ alloy.

Run No.	Pulse on time	Servo voltage	Experimental MRR	Predicted MRR	Experimental SR	Predicted SR
1	105	20	4.62	4.61	1.68	1.67
2	105	30	3.64	3.63	1.61	1.59
3	105	40	2.99	2.95	1.48	1.47
4	105	50	2.6	2.57	1.27	1.25
5	105	60	1.49	1.54	1.04	1.02
6	110	20	5.27	5.20	2.1	2.09
7	110	30	5.14	5.17	2.07	1.91
8	110	40	3.58	3.57	1.89	1.86
9	110	50	2.73	2.72	1.68	1.679
10	110	60	1.83	1.93	1.18	1.17
11	115	20	7.8	7.76	2.63	2.61
12	115	30	6.18	6.14	2.51	2.49
13	115	40	4.16	4.15	2.13	2.12
14	115	50	2.99	2.97	1.85	1.86
15	115	60	2.54	2.60	1.73	1.70
16	120	20	9.23	9.22	2.82	2.81
17	120	30	7.15	7.14	2.76	2.73
18	120	40	5.97	5.96	2.4	2.39

Run No.	Pulse on time	Servo voltage	Experimental MRR	Predicted MRR	Experimental SR	Predicted SR
19	120	50	3.97	3.96	2.4	2.35
20	120	60	2.8	2.74	2.27	2.14
21	125	20	11.51	11.51	3.87	3.77
22	125	30	9.04	9.5	3.63	3.59
23	125	40	8.13	8.12	3.25	3.24
24	125	50	5.27	5.26	2.66	2.65
25	125	60	3.45	3.50	2.31	2.14

Table 5.7 Experimental and predicted values of responses for $Ti_{50}Ni_{45}Co_5$ alloy.

Run No.	Pulse on time	Servo voltage	Experimental MRR	Predicted MRR	Experimental SR	Predicted SR
1	105	20	3.71	3.40	1.51	1.60
2	105	30	3.12	3.10	1.46	1.43
3	105	40	2.28	2.27	1.33	1.36
4	105	50	1.69	1.68	1.3	1.29
5	105	60	1.11	1.10	1.02	1.02
6	110	20	4.42	4.64	2.29	2.52
7	110	30	3.19	3.18	2.2	2.19
8	110	40	2.21	2.31	2.03	2.16
9	110	50	1.69	1.67	1.96	1.94
10	110	60	1.24	1.25	1.67	1.74
11	115	20	6.18	6.14	2.72	1.64
12	115	30	5.01	5.01	2.26	2.26
13	115	40	3.71	4.19	2.15	2.18
14	115	50	2.86	2.91	2.1	2.21
15	115	60	1.82	1.74	2.05	2.10
16	120	20	8.32	8.18	2.99	3.05
17	120	30	6.31	6.30	2.77	2.76

18	120	40	5.58	5.57	2.53	2.55
19	120	50	3.58	3.43	2.53	2.18
20	120	60	2.34	2.41	2.32	2.20
21	125	20	9.43	8.65	3.42	3.2
22	125	30	8.65	8.649	3.2	3.1999
23	125	40	8.06	8.0563	3.07	3.0884
24	125	50	5.2	5.3072	2.41	2.4475
25	125	60	3.38	3.3534	2.17	2.2198

Table 5.8 Experimental and predicted values of responses for $Ti_{50}Ni_{40}Co_{10}$ alloy.

Run No.	Pulse on time	Servo voltage	Experimental MRR	Predicted MRR	Experimental SR	Predicted SR
1	105	20	3.51	3.5	1.84	1.84
2	105	30	3.06	3.24	1.72	1.57
3	105	40	2.41	2.32	1.58	1.48
4	105	50	1.69	1.69	1.26	1.26
5	105	60	1.04	1.04	1.18	1.18
6	110	20	3.71	3.66	1.98	2.05
7	110	30	3.06	3.21	1.84	1.97
8	110	40	2.28	2.40	1.67	1.80
9	110	50	1.63	1.62	1.49	1.48
10	110	60	1.11	1.10	1.2	1.20
11	115	20	5.92	5.91	2.45	2.44
12	115	30	4.81	4.75	2.31	2.49
13	115	40	3.51	3.51	2.26	2.39
14	115	50	2.41	2.40	2.15	2.15
15	115	60	1.63	1.60	1.78	1.82
16	120	20	8.78	8.77	3.41	3.40

17	120	30	6.31	6.30	3.12	3.11
18	120	40	5.04	5.20	2.2	2.33
19	120	50	3.84	3.83	2.2	2.20
20	120	60	2.47	2.47	2.17	2.1698
21	125	20	9.68	9.5049	3.63	3.6018
22	125	30	6.55	6.5514	3.3	3.3002
23	125	40	5.6	2.6704	2.45	2.7634
24	125	50	4.9	4.8999	2.26	2.2601
25	125	60	2.99	2.99	2.13	2.1298

5.11 EFFECTS OF EACH EXPERIMENTAL RUN ON MATERIAL REMOVAL RATE

An artificial neural network (ANN) approach is an effective tool to predict process parameters and can generate the outputs for a set of inputs that are within the range of the original inputs during the training phase. Shandilya et al. (2013) made an attempt to predict the WEDM response such as cutting speed. They considered response surface design and artificial neural network method to predict the cutting speed during the wire electro discharge machining of SiCp/6061 Al metal matrix composite (MMC) and found that artificial neural network method gives more accurate value than response surface method. Similarly Surya et al. (2017) also compared experimental material removal rate of wire electro discharge machining of Al7075-TiB2 in-situ composite and artificial neural network based predicated material removal rate, they found 1.31% error during their observation. The effect of each experimental run on MRR is given in the Fig. 5.14 for $Ti_{50}Ni_{49}Co_1$ alloy, Fig. 5.16 for $Ti_{50}Ni_{45}Co_5$ alloy and Fig. 5.18 for $Ti_{50}Ni_{40}Co_{10}$ alloy. It is observed from these figures that ANN based predicted values are closer to experimental values for MRR. The material removal rate decreases up to experiment no 5 because of increase in the servo voltage with a constant pulse on time. A similar trend has been noticed after every five experiments that MRR decrease with an increase in servo voltage for different values of a pulse on time. Material removal rate decreases with increase in

servo voltage because the increase in servo voltage results in larger spark gap thereby reducing the spark intensity and eventually lesser amount of material is removed from the surface of the workpiece. Sharma et al. (2013) also observed similar kind of result during the wire electro-discharge machining of High- strength low-alloy steel (HSLA). The about the effects of process parameters on material removal rate have been discussed in the section of 4.3.1.

5.12 EFFECTS OF THE EACH EXPERIMENTAL RUN ON SURFACE ROUGHNESS

As above discussed that artificial neural network prediction tool is appropriate prediction tool for prediction the output responses. Similar behaviour was observed by Karthikkeyan et al. (1999) that artificial neural network is suitable tool for better and have a higher predictive capability of surface roughness values. The values of surface roughness are predicted by artificial neural network in the present study during the wire electro discharge machining of $Ti_{50}Ni_{49}Co_1$, $Ti_{50}Ni_{45}Co_5$ and $Ti_{50}Ni_{40}Co_{10}$ alloy. Details about the developed model of artificial neural network are presented in section 3.8. The effect of each experimental run on surface roughness is given in the Fig. 5.15 for $Ti_{50}Ni_{49}Co_1$ alloy, Fig. 5.17 for $Ti_{50}Ni_{45}Co_5$ alloy and Fig. 5.19 for $Ti_{50}Ni_{40}Co_{10}$ alloy. It is observed from these figures that ANN based predicted values are more close to experimental values for SR. The surface roughness decreasing from an experiment run 1 through experiment run 5, due to increase in servo voltage with a constant pulse on time. A similar trend has been noticed after every five experiments. Surface roughness decrease with increase in servo voltage because at the higher servo voltage less amount of material is melted on the machined surface; this can be easily flushed away from the machined surface through dielectric fluid leading to low surface roughness. Details about the effect of process parameters on surface roughness have been discussed in the section of 4.3.2.
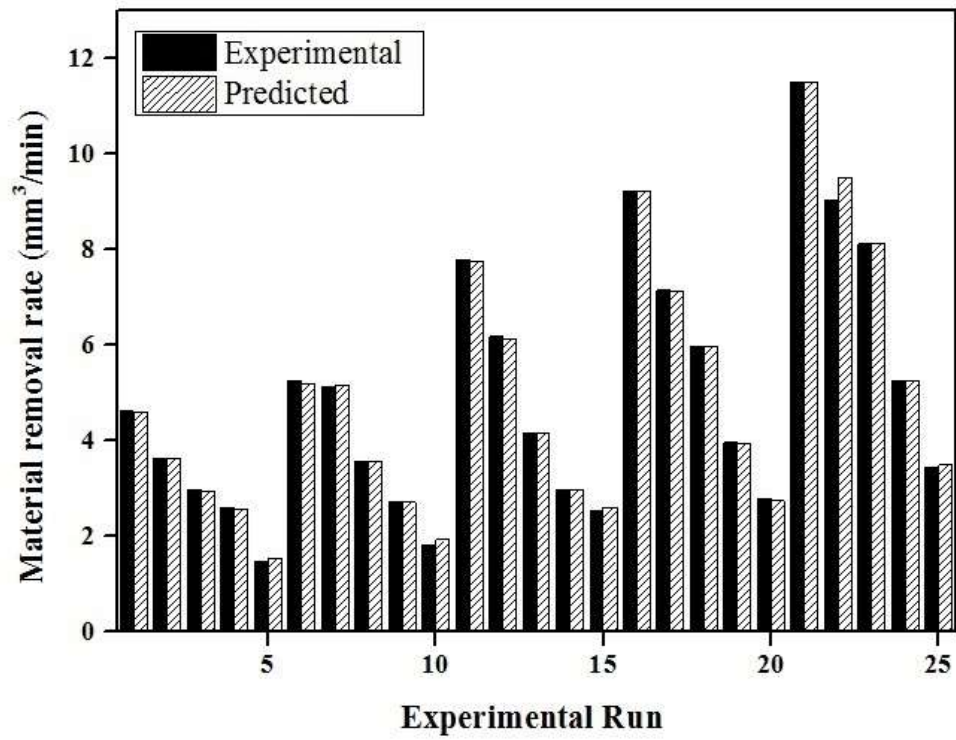
Figure 5.14 Experimental and predicted values of MRR for $Ti_{50}Ni_{49}Co_1$ alloy.
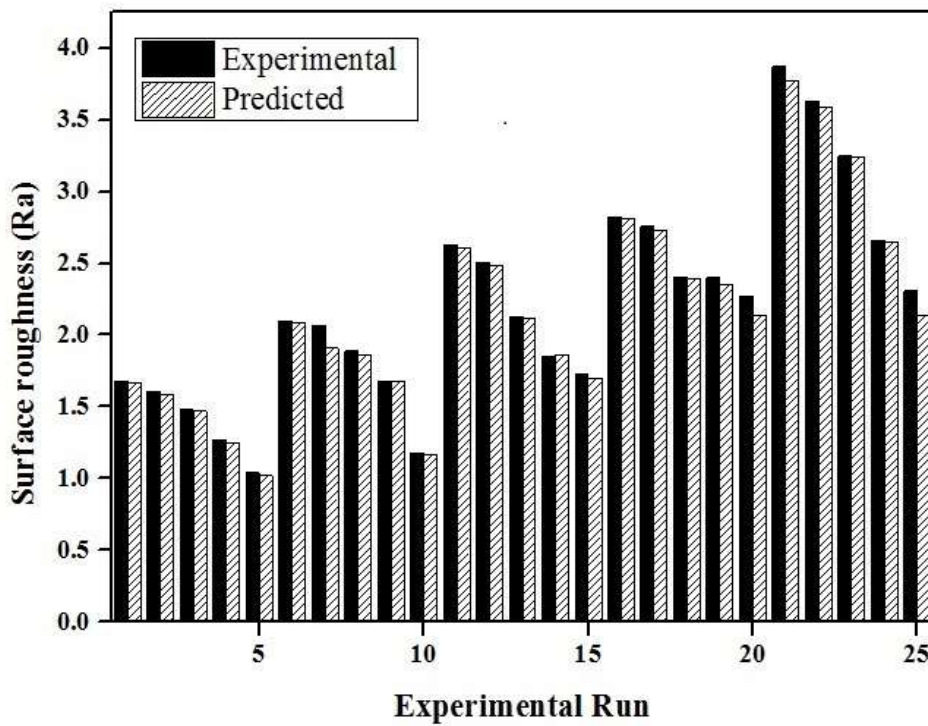
Figure 5.15 Experimental and predicted values of SR for $Ti_{50}Ni_{49}Co_1$ alloy.
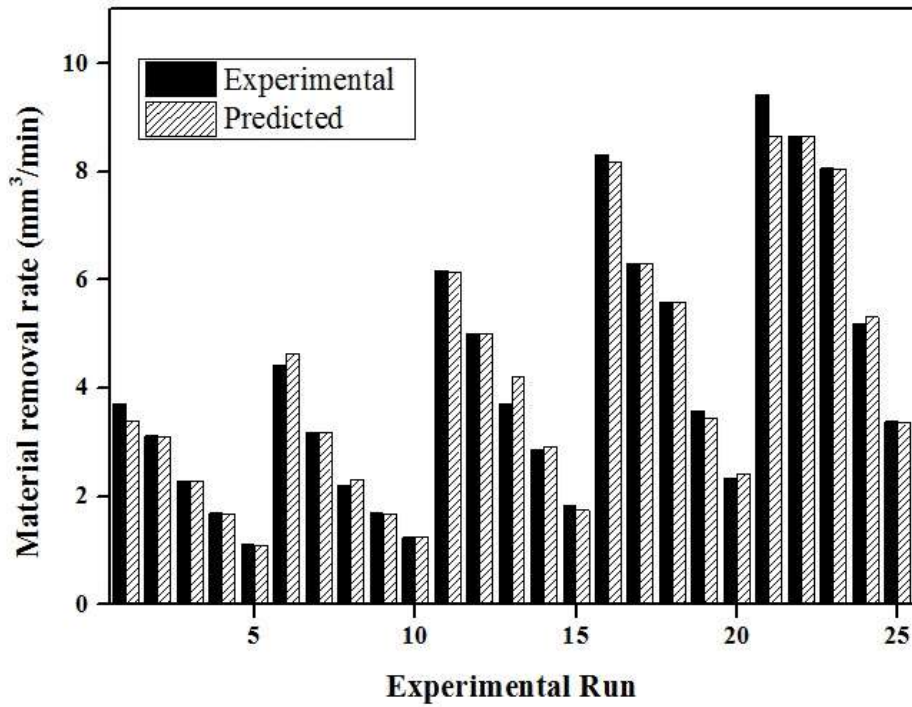
Figure 5.16 Experimental and predicted values of MRR for $Ti_{50}Ni_{45}Co_5$ alloy.
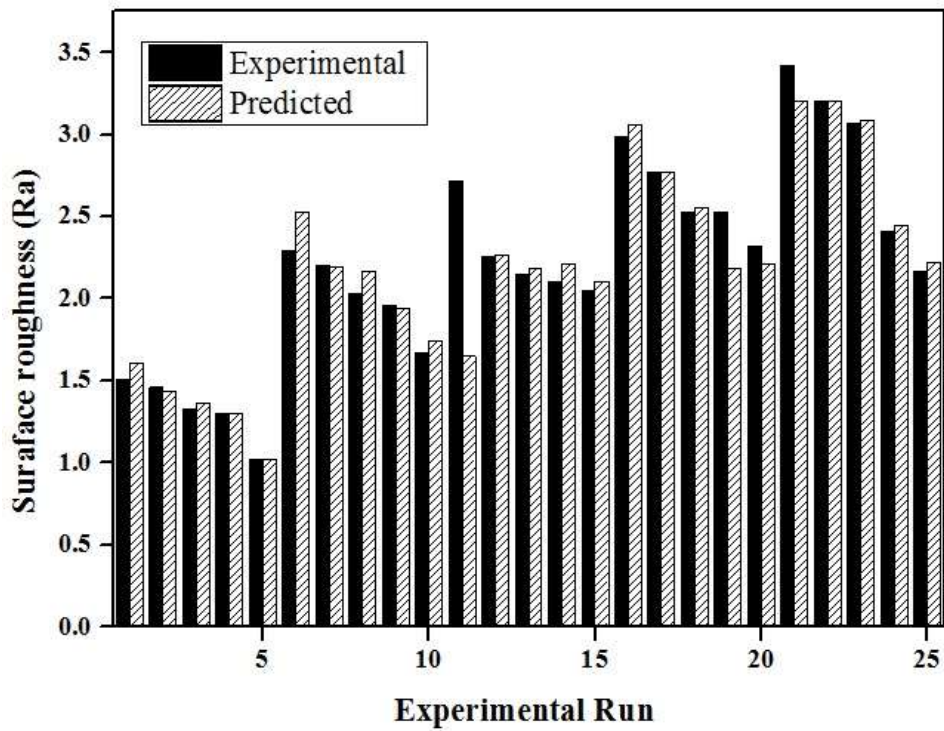
Figure 5.17 Experimental and predicted values of SR for $Ti_{50}Ni_{45}Co_5$ alloy.
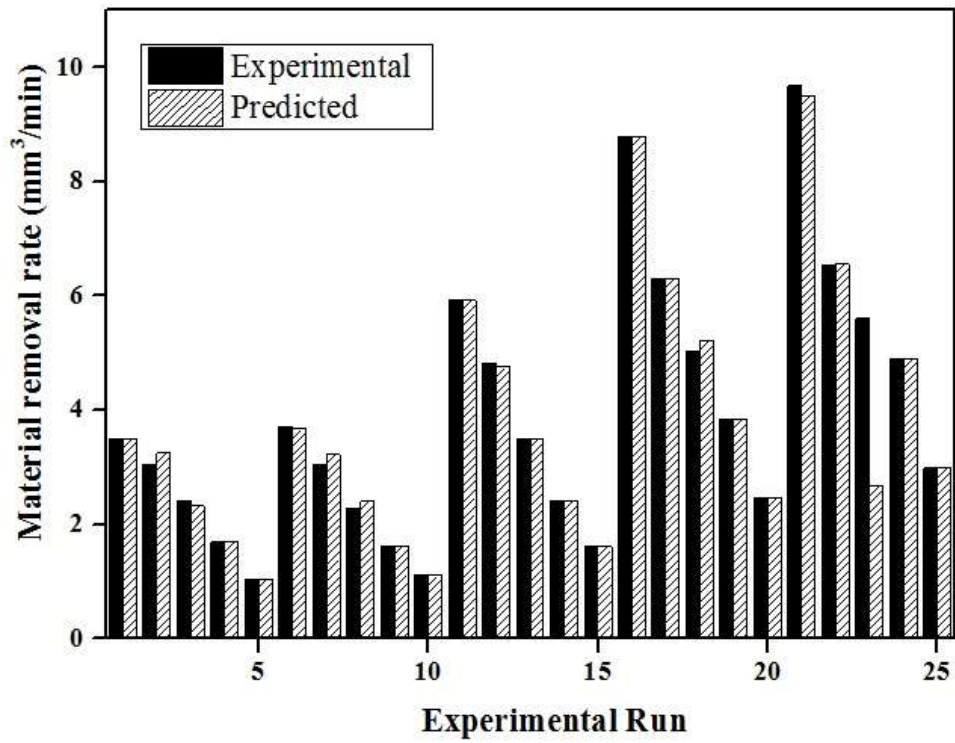
Figure 5.18 Experimental and predicted values of MRR for $Ti_{50}Ni_{40}Co_{10}$ alloy.
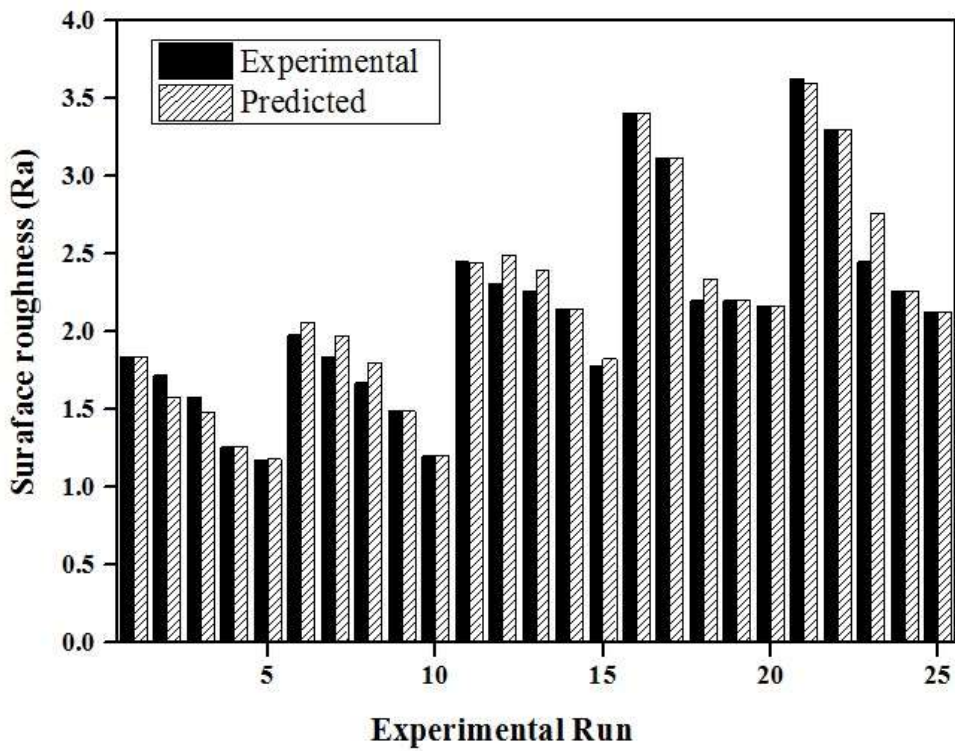
Figure 5.19 Experimental and predicted values of SR for $Ti_{50}Ni_{40}Co_{10}$ alloy.

5.13 PERCENTAGE ERROR

Fig.5.20 and Fig. 5.21 shows the percentage error for MRR and SR evaluated through ANN for all the alloys. Table 5.9 presents the maximum percentage error. It is found that the maximum percentage error is 8 percent and ANN gives accurate values. The error observed between experimental data and predicted data is small. Similar work has been reported by shandilya et al. (2013) during their comparative study on RSM and ANN based predicted values of cutting speed while machining $SiC_P/6061$ Al metal matrix composite using wire electro-discharge machine.

Table 5.9 Maximum error for all three alloys.

Alloy	Maximum Error obtained through ANN	
	MRR	SR
$Ti_{50}Ni_{49}Co_1$	6 %	8%
$Ti_{50}Ni_{45}Co_5$	5%	7%
$Ti_{50}Ni_{40}Co_{10}$	6%	8%
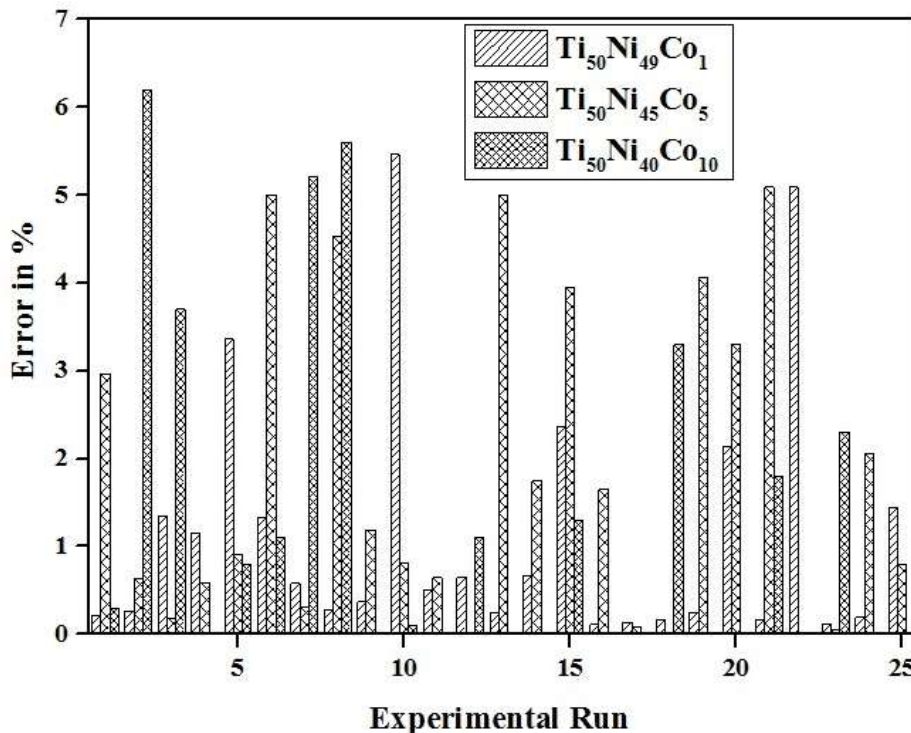
Figure 5.20 Error in % for MRR at all experimental run.
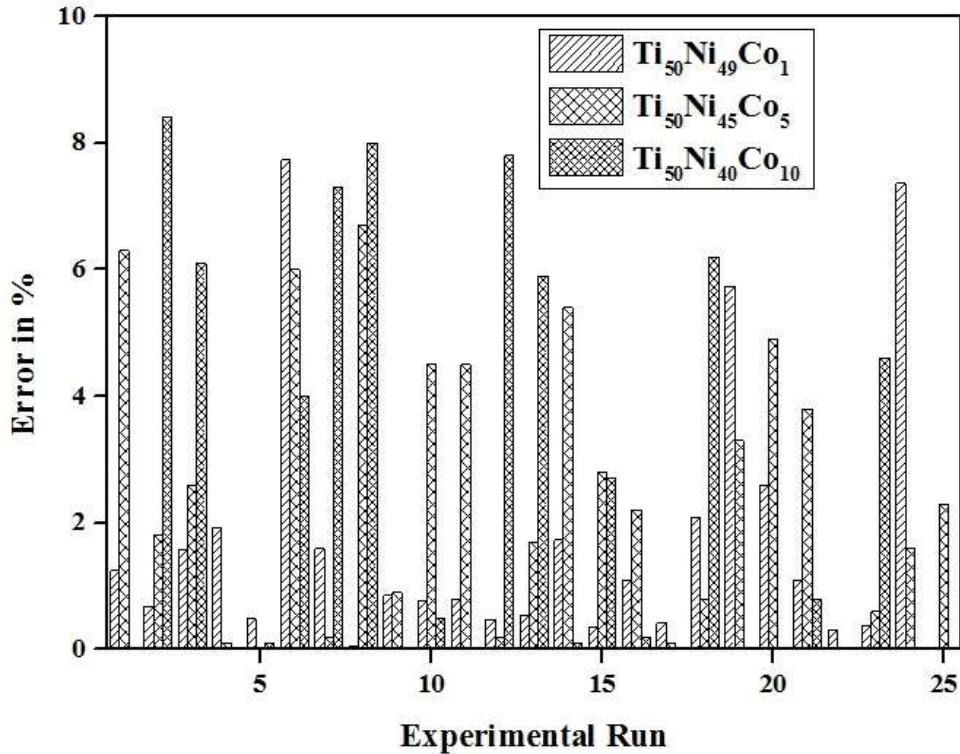
Figure 5.21 Error in % for SR at all experimental run.

5.14 SUMMARY

The effects of pulse on time and servo voltage on material removal rate and surface roughness were discussed based on the above studies following highlights are listed below-

- Lower values of material removal rate 1.8 mm^3/min for $Ti_{50}Ni_{49}Co_1$, 1.5 mm^3/min for $Ti_{50}Ni_{45}Co_5$ and 1.36 mm^3/min for $Ti_{50}Ni_{40}Co_{10}$ and surface roughness 1.29 µm for $Ti_{50}Ni_{49}Co_1$, 1.11 µm for $Ti_{50}Ni_{45}Co_5$, 1.04 µm for $Ti_{50}Ni_{40}Co_{10}$ were noticed at 60V servo voltage and 105µs pulse on time.
- Higher values of material removal rate 11.51 mm^3/min for $Ti_{50}Ni_{49}Co_1$, 9.43 mm^3/min for $Ti_{50}Ni_{45}Co_5$ and 9.06 mm^3/min for $Ti_{50}Ni_{40}Co_{10}$ and surface roughness 4.51 µm for $Ti_{50}Ni_{49}Co_1$, 4.01 µm for $Ti_{50}Ni_{45}Co_5$, 3.63 µm for $Ti_{50}Ni_{40}Co_{10}$ were noticed at 20V servo voltage and 125µs pulse on time.

- Formation of micro cracks, micro globules, micro voids are more consistent at high pulse on time 125μs and at low servo voltage 20V and therefore the machined surface offers poor surface quality.

- 624 HV for $Ti_{50}Ni_{49}Co_{10}$, 602 HV for $Ti_{50}Ni_{45}Co_5$ and 580 HV for $Ti_{50}Ni_{40}Co_1$ alloy harder surface have been found at lower values of outputs responses of WEDM.

- The recast layer thickness at lower values of outputs is 4.2 μm for $Ti_{50}Ni_{49}Co_1$, 4.6 μm for $Ti_{50}Ni_{45}Co_5$ and 4.9 μm for $Ti_{50}Ni_{40}Co_{10}$ alloy while recast layer thickness at higher values of outputs is 30 μm for $Ti_{50}Ni_{49}Co_1$, 32 μm for $Ti_{50}Ni_{45}Co_5$ and 35 μm for $Ti_{50}Ni_{40}Co_{10}$ alloy were noticed.

- At lower values of outputs responses less than 20Mpa and at higher values of outputs more than 200 Mpa residual stress have been noticed on the machined surface. Therefore the trend of residual stress is increasing with increasing the values of outputs responses; same trend has been noticed for all three alloys.

Artificial neural network (ANN) approach was adopted to predict WEDM responses after machining of $Ti_{50}Ni_{49}Co_1$, $Ti_{50}Ni_{45}Co_5$ and $Ti_{50}Ni_{40}Co_{10}$ shape memory alloys. 6% maximum error was obtained for material removal rate and 8% maximum was noticed for surface roughness.

CHAPTER 6

CONCLUSION AND SCOPE FOR FUTURE WORK

6.1 CONCLUSION

The shape memory alloys of composition $Ti_{50}Ni_{49}Co_1$, $Ti_{50}Ni_{45}Co_5$ and $Ti_{50}Ni_{40}Co_{10}$ are successfully developed using vacuum arc melting furnace and machined more effectively with WEDM process.

Wire Electro Discharge Machining Characteristics

- Machining of these shape memory alloys has been carried out by using wire electro-discharge machining as per L-33 orthogonal array. Multi-objective optimization techniques of GRA, RSM and Entropy measurement method are effectively utilised to obtain the best combination of process parameters in optimising responses of MRR and SR.

- It was found that MRR and SR increase up to 5 mm^3/min and 3.46 µm respectively with increment in pulse on time. Similarly, increase in pulse off time and servo voltage decreases MRR on an average up to 1 mm^3/min and SR 1.46 µm. The trend of servo feed and wire speed were not uniform on these output responses.

- Formation of microcracks, micro globules, microvoids are more consistent at high pulse on time of 125µs and at low servo voltage of 20V and the machined surface offers poor surface quality.

- Compressive residual stress has been noticed on the machined surface. The compressive residual stress of 252.6 Mpa for $Ti_{50}Ni_{49}Co_1$ alloy, 270.2 Mpa for $Ti_{50}Ni_{45}Co_5$ alloy and 265.9 Mpa for $Ti_{50}Ni_{40}Co_{10}$ alloy are found at optimized process parameters.

- The cross-sectional microstructure of the machined surface revealed maximum recast layer at higher pulse on time and low servo voltage. Whereas minimum recast layer thickness (4.21µm) was obtained at low pulse on time and high

servo voltage, which can be remove easily form the machined surface without affecting size of machined component.

- The harder surface is noticed near the machined surface due to formation of oxides of NiO_2 and TiO_2 which is confirmed by XRD analysis.

Parametric Study of Pulse on Time and Servo Voltage

- Pulse on time and servo voltages are identified as most influential process parameters and their effect on MRR and SR are studied using two process parameters approach. Machining as per L-25 orthogonal array has been carried out and machining performance MRR and SR are measured.

- Lower values of material removal rate and surface roughness are observed during WEDM of $Ti_{50}Ni_{49}Co_1$, $Ti_{50}Ni_{45}Co_5$ and $Ti_{50}Ni_{40}Co_{10}$ alloys at 60V servo voltage and 105µs pulse on time. Higher values of material removal rate and surface roughness are noticed at 20V servo voltage and 125µs pulse on time.

- It is observed that hardness is decreasing along the cross section from the machined surface along recast layer and heat affected zone. The micro hardness of converted layer is almost equal to the hardness of base material because converted layer is not much affected of by WEDM. The harder surface is noticed during machining of $Ti_{50}Ni_{49}Co_{10}$ alloy (624 HV) at lower values of outputs responses.

- Thin film of recast layer is noticed during machining at lower (105 µs) pulse on time and higher servo voltage (60V).The recast layer thickness at lower values of outputs is 4.2 µm for $Ti_{50}Ni_{49}Co_1$, 4.6 µm for $Ti_{50}Ni_{45}Co_5$ and 4.9 µm for $Ti_{50}Ni_{40}Co_{10}$ alloy while recast layer thickness at higher values of outputs is 30 µm for $Ti_{50}Ni_{49}Co_1$, 32 µm for $Ti_{50}Ni_{45}Co_5$ and 35 µm for $Ti_{50}Ni_{40}Co_{10}$ alloy.

- Minimum residual stress has been observed on the machined surface of $Ti_{50}Ni_{49}Co_1$ alloy while maximum stress has seen on the machined surface of $Ti_{50}Ni_{40}Co_{10}$ alloy. Also residual stresses measured at lower values of surface

roughness and material removal rate is less than residual stress at the higher values of these outputs.

- Artificial neural network (ANN) approach is adopted to predict WEDM responses of MRR and SR. The error observed between experimental data and predicted data is small and it is found that the maximum percentage error is 8 percent.

6.2 SCOPE FOR FUTURE WORK

Although the wire electro discharge machining of developed $Ti_{50}Ni_{49}Co_1$, $Ti_{50}Ni_{45}Co_5$ and $Ti_{50}Ni_{40}Co_{10}$ shape memory alloys and machined surface characterization have been carried out in the present study, still there is much scope for research in this area. The following suggestions might be consider for future work-

- Physical and mechanical properties can be improved of TiNi based shape memory alloys by adding different alloying elements such as Ag, Au etc.
- Different ternary shape memory alloys can be machined for particular applications through wire electro discharge machining at optimized process parameters.
- Physical properties can be investigate after the machining of shape memory alloys such as pseudoelastic behaviour, phase transformation temperature etc.

6.3 KEY CONTRIBUTIONS

The main contributions of present study are following -

- $Ti_{50}Ni_{49}Co_1$, $Ti_{50}Ni_{45}Co_5$ and $Ti_{50}Ni_{40}Co_{10}$ shape memory alloys developed through vacuum arc meting furnace.
- The machining of all three alloys has been carried out through wire electro discharge machining and found the optimal process parameters for higher material removal rate with better surface finish.
- Hybrid combination of optimization techniques were used to optimized the process parameters and machined surface characterization has been carried out

at optimized process parameters with respect to machined surface morphology, surface topography, recast layer thickness, microhardness, phase analysis and residual stress.

- Two process parameters approach adopted for further machining of all three alloys and detailed characterization have been carried out at the lower and higher values of material removal rate and surface roughness. Moreover Artificial neural network was implemented for prediction the WEDM responses such as material removal rate and surface roughness.

REFERENCES

A.Cladera, B.Weber, C.Leinenbach, C.Czaderski, M.Shahverdi, and M. M. (2014). "Iron-based shape memory alloys for civil engineering structures : An overview." *Constr. Build. Mater.*, 63(MAY), 281–293.

Ablyaz, T. R., and Muratov, K. R. (2017). "The Technological Quality Control of Stack Cutting By Wire Electrical Discharge Machining." *Surf. Rev. Lett.*, 24(05), 1750060.

Akkurt, A. (2013). "An ANFIS-Based Approach for Predicting the Surface Roughness of Cold Work Tool Steel in." 2(3), 234–240.

Antar, M. T., Soo, S. L., Aspinwall, D. K., Jones, D., and Perez, R. (2011). "Productivity and workpiece surface integrity when WEDM aerospace alloys using coated wires." *Procedia Eng.*, 19, 3–8.

Arikatla, S. P., Tamil Mannan, K., and Krishnaiah, A. (2017). "Surface Integrity Characteristics in Wire Electrical Discharge Machining of Titanium Alloy during Main cut and Trim cuts." *Mater. Today Proc.*, 4(2), 1500–1509.

Aspinwall, D. K., Soo, S. L., Berrisford, a. E., and Walder, G. (2008). "Workpiece surface roughness and integrity after WEDM of Ti–6Al–4V and Inconel 718 using minimum damage generator technology." *CIRP Ann. - Manuf. Technol.*, 57(1), 187–190.

Ayesta, I., Izquierdo, B., Flao, O., Snchez, J. A., Albizuri, J., and Avil??s, R. (2016). "Influence of the WEDM process on the fatigue behavior of Inconel?? 718." *Int. J. Fatigue*, 92, 220–233.

Azhiri, B., Teimouri, R., Ghasemi Baboly, M., and Leseman, Z. (2014). "Application of Taguchi, ANFIS and grey relational analysis for studying, modeling and optimization of wire EDM process while using gaseous media." *Int. J. Adv. Manuf. Technol.*, 71(1-4), 279–295.

Bijeta, B., Sankar, S., Chatterjee, S., and Abhishek, K. (2015). "Parametric Appraisal

of WEDM using Harmony Search Algorithm." *Mater. Today Proc.*, 2(4-5), 2562–2568.

Chalisgaonkar, R., and Kumar, J. (2016). "Investigation of the machining parameters and integrity of the work and wire surfaces after finish cut WEDM of commercially pure titanium." *J. Brazilian Soc. Mech. Sci. Eng.*, 38(3), 883–911.

Chen, S. L., Hsieh, S. F., Lin, H. C., Lin, M. H., and Huang, J. S. (2007). "Electrical discharge machining of TiNiCr and TiNiZr ternary shape memory alloys." *Mater. Sci. Eng. A*, 445-446, 486–492.

Chen, Z., Zhang, Y., Zhang, G., Huang, Y., and Liu, C. (2017). "Theoretical and experimental study of magnetic-assisted finish cutting ferromagnetic material in WEDM." *Int. J. Mach. Tools Manuf.*, 123(932), 36–47.

Choudhary, R., Kumar, H., and Garg, R. K. (2010). "Analysis and evaluation of heat affected zones in electric discharge machining of EN-31 die steel." *Indian J. Eng. Mater. Sci.*, 17(2), 91–98.

Dadbakhsh, S., Speirs, M., Humbeeck, J. Van, and Kruth, J.-P. (2016). "Laser additive manufacturing of bulk and porous shape-memory NiTi alloys: From processes to potential biomedical applications." *MRS Bull.*, 41(10), 765–774.

Daneshmand, S., Monfared, V., and Lotfi Neyestanak, A. A. (2017). "Effect of Tool Rotational and Al2O3 Powder in Electro Discharge Machining Characteristics of NiTi-60 Shape Memory Alloy." *Silicon*, 9(2), 273–283.

Das, A., Sarkar, S., Karanjai, M., and Sutradhar, G. (2017). "Application of Box–Behnken Design and Response Surface Methodology for Surface Roughness Prediction Model of CP-Ti Powder Metallurgy Components Through WEDM." *J. Inst. Eng. Ser. D*.

Datta, S., and Mahapatra, S. S. (2010). "Modeling, simulation and parametric optimization of wire EDM process using response surface methodology coupled with grey-Taguchi technique." *Multicr. Int. J. Eng. Sci. Technol. Ext.*, 2(5), 162–183.

Dhobe, M. M., Chopde, I. K., and Gogte, C. L. (2013). "Investigations on Surface Characteristics of Heat Treated Tool Steel after Wire Electro-Discharge Machining." *Mater. Manuf. Process.*, 28(10), 1143–1146.

El-Bagoury, N. (2014). "Microstructure and martensitic transformation and mechanical properties of cast Ni rich NiTiCo shape memory alloys." *Mater. Sci. Technol.*, 30(14), 1795–1800.

Geng, L., and Zhong, H. Y. (2010). "Evaluation of WEDM Surface Quality." *Adv. Mater. Res.*, 97-101, 4080–4083.

Ghanem, F., Fredj, N. Ben, Sidhom, H., and Braham, C. (2011). "Effects of finishing processes on the fatigue life improvements of electro-machined surfaces of tool steel." *Int. J. Adv. Manuf. Technol.*, 52(5-8), 583–595.

Ghodsiyeh, D., Golshan, A., and Shirvanehdeh, J. A. (2013). "Review on Current Research Trends in Wire Electrical Discharge Machining (WEDM)." 3(February), 154–168.

Goryczka, T., and Ochin, P. (2005). "Characterization of a Ni50Ti50 shape memory strip produced by twin roll casting technique." *J. Mater. Process. Technol.*, 162-163(SPEC. ISS.), 178–183.

Goswami, A., and Kumar, J. (2014). "Engineering Science and Technology , an International Journal Investigation of surface integrity , material removal rate and wire wear ratio for WEDM of Nimonic 80A alloy using GRA and Taguchi method." *Eng. Sci. Technol. an Int. J.*, 17(4), 173–184.

Guo, Y., Klink, A., Fu, C., and Snyder, J. (2013). "Machinability and surface integrity of Nitinol shape memory alloy." *CIRP Ann. - Manuf. Technol.*, 62(1), 83–86.

Hartl, D. J., and Lagoudas, D. C. (2007). "Aerospace applications of shape memory alloys." *Proc. Inst. Mech. Eng. Part G J. Aerosp. Eng.*, 221(4), 535–552.

Hewidy, M. S., El-Taweel, T. A., and El-Safty, M. F. (2005). "Modelling the machining parameters of wire electrical discharge machining of Inconel 601 using

RSM." *J. Mater. Process. Technol.*, 169(2), 328–336.

Ho, K. H., Newman, S. T. Ã., Rahimifard, S., and Allen, R. D. (2004). "State of the art in wire electrical discharge machining (WEDM)." 44, 1247–1259.

Hsieh, S. F., Chen, S. L., Lin, H. C., Lin, M. H., and Chiou, S. Y. (2009). "The machining characteristics and shape recovery ability of Ti-Ni-X (X=Zr, Cr) ternary shape memory alloys using the wire electro-discharge machining." *Int. J. Mach. Tools Manuf.*, 49(6), 509–514.

Hsieh, S. F., Hsue, A. W. J., Chen, S. L., Lin, M. H., Ou, K. L., and Mao, P. L. (2013). "EDM surface characteristics and shape recovery ability of Ti35.5Ni48.5Zr16 and Ni60Al24.5Fe15.5 ternary shape memory alloys." *J. Alloys Compd.*, 571, 63–68.

Ibrahim, K. M., Elbagoury, N., and Fouad, Y. (2011). "Microstructure and martensitic transformation of cast TiNiSi shape memory alloys." *J. Alloys Compd.*, 509(9), 3913–3916.

Jangra, K., Grover, S., and Aggarwal, A. (2012). "Optimization of multi machining characteristics in WEDM of WC-5.3%Co composite using integrated approach of Taguchi, GRA and entropy method." *Front. Mech. Eng.*, 7(3), 288–299.

Jiang, P. C., Zheng, Y. F., Tong, Y. X., Chen, F., Tian, B., Li, L., Gunderov, D. V., and Valiev, R. Z. (2014). "Transformation hysteresis and shape memory effect of an ultrafine-grained TiNiNb shape memory alloy." *Intermetallics*, 54, 133–135.

Karayel, D. (2009). "Prediction and control of surface roughness in CNC lathe using artificial neural network." *J. Mater. Process. Technol.*, 209(7), 3125–3137.

Karthikeyan, R., Lakshmi Narayanan, P. ., and Naagarazan, R. . (1999). "Mathematical modelling for electric discharge machining of aluminium–silicon carbide particulate composites." *J. Mater. Process. Technol.*, 87(1-3), 59–63.

Khanna, R., and Singh, H. (2016). "Comparison of optimized settings for cryogenic-treated and normal D-3 steel on WEDM using grey relational theory." *Proc. Inst. Mech. Eng. Part L J. Mater. Des. Appl.*, 230(1), 219–232.

Kim, S. W., Jo, J. W., Park, C. H., Hong, J. K., Yeom, J. T., and Kim, H. G. (2016). "Fracture toughness of TiNiHf alloys: A hybrid study using in-situ transmission electron microscopy experiments and finite element analyses." *Mater. Sci. Eng. A*, 655, 363–372.

Kong, M. C., Axinte, D., and Voice, W. (2011). "Challenges in using waterjet machining of NiTi shape memory alloys: An analysis of controlled-depth milling." *J. Mater. Process. Technol.*, 211(6), 959–971.

Kumar, A., Kumar, V., and Kumar, J. (2013). "Multi-response optimization of process parameters based on response surface methodology for pure titanium using WEDM process." *Int. J. Adv. Manuf. Technol.*, 68(9-12), 2645–2668.

Kumar, A., Kumar, V., and Kumar, J. (2016). "Surface crack density and recast layer thickness analysis in WEDM process through response surface methodology." *Mach. Sci. Technol.*, 20(2), 201–230.

Kumar, S. S., Uthayakumar, M., Kumaran, S. T., Parameswaran, P., Mohandas, E., Kempulraj, G., Babu, B. S. R., and Natarajan, S. A. (2015). "Parametric optimization of wire electrical discharge machining on aluminium based composites through grey relational analysis." *J. Manuf. Process.*, 20, 33–39.

Kumar, V., Jangra, K. K., Kumar, V., and Sharma, N. (2017). "WEDM of nickel based aerospace alloy: optimization of process parameters and modelling." *Int. J. Interact. Des. Manuf.*, 11(4), 917–929.

Kuppuswamy, R., and Yui, A. (2017). "High-speed micromachining characteristics for the NiTi shape memory alloys." *Int. J. Adv. Manuf. Technol.*, 93(1-4), 11–21.

Kuriakose, S., and Shunmugam, M. S. (2004). "Characteristics of wire-electro discharge machined Ti6Al4V surface." *Mater. Lett.*, 58(17-18), 2231–2237.

Lagoudlas, D. C. (2008). Shape Memory Alloys: Moding and Engineering Applications, Springer, ISBN 978-0-387-47685-8.

Lal, S., Kumar, S., Khan, Z., and Siddiquee, A. (2015). "Multi-response optimization

of wire electrical discharge machining process parameters for Al7075/Al $_2$ O $_3$ /SiC hybrid composite using Taguchi-based grey relational analysis." *Proc. Inst. Mech. Eng. Part B J. Eng. Manuf.*, 229(2), 229–237.

Lee, W. M., and Liao, Y. S. (2007). "Adaptive control of the WEDM process using a self-tuning fuzzy logic algorithm with grey prediction." *Int. J. Adv. Manuf. Technol.*, 34(5-6), 527–537.

Lekston, Z., Stroz, D., and Drusik-Pawlowska, M. J. (2012). "Preparation and characterization of nitinol bone staples for cranio-maxillofacial surgery." *J. Mater. Eng. Perform.*, 21(12), 2650–2656.

Liao, Y. S., Chu, Y. Y., and Yan, M. T. (1997). "Study of wire breaking process and monitoring of WEDM." *Int. J. Mach. Tools Manuf.*, 37(4), 555–567.

Liu, F., Ding, Z., Li, Y., and Xu, H. (2005). "Phase transformation behaviors and mechanical properties of TiNiMo shape memory alloys." *Intermetallics*, 13(3-4), 357–360.

Luo, G., Ming, W., Zhang, Z., Liu, M., Li, H., Li, Y., and Yin, L. (2014). "Investigating the effect of WEDM process parameters on 3D micron-scale surface topography related to fractal dimension." *Int. J. Adv. Manuf. Technol.*, 75(9-12), 1773–1786.

Manjaiah, M., Narendranath, S., and Basavarajappa, S. (2014). "Review on non-conventional machining of shape memory alloys." *Trans. Nonferrous Met. Soc. China (English Ed.*, 24(1), 12–21.

Manjaiah, M., Narendranath, S., Basavarajappa, S., and Gaitonde, V. N. (2015). "Effect of electrode material in wire electro discharge machining characteristics of Ti50Ni50−xCux shape memory alloy." *Precis. Eng.*, 41, 68–77.

McCluskey, P. J., Xiao, K., Gregoire, J. M., Dale, D., and Vlassak, J. J. (2014). "Application of in-situ nano-scanning calorimetry and X-ray diffraction to characterize Ni-Ti-Hf high-temperature shape memory alloys." *Thermochim. Acta*.

Mohd Jani, J., Leary, M., Subic, A., and Gibson, M. a. (2014). "A review of shape memory alloy research, applications and opportunities." *Mater. Des.*, 56, 1078–1113.

Mordyuk, B. N., Prokopenko, G. I., Grinkevych, K. E., Piskun, N. A., and Popova, T. V. (2017). "Effects of ultrasonic impact treatment combined with the electric discharge surface alloying by molybdenum on the surface related properties of low-carbon steel G21Mn5." *Surf. Coatings Technol.*, 309, 969–979.

Mouralova, K., Kovar, J., Klakurkova, L., Blazik, P., Kalivoda, M., and Kousal, P. (2018). "Analysis of surface and subsurface layers after WEDM for Ti-6Al-4V with heat treatment." *Measurement*, 116(April 2017), 556–564.

Mouralová, K., Kovář, J., Zahradníček, R., and Man, O. (2016). "Characterisation of 3D Topography of the Surface Machined by Finishing Technologies of WEDM and Grinding." *Mechatronika 2016*, 445–449.

Nam, T., Saburi, T., and Shimizu, K. (1990). "Cu-Content Dependence of Shape Memory Characteristics in Ti-Ni-Cu Alloys." *Mater. Trans. JIM*.

Newton, T. R., Melkote, S. N., Watkins, T. R., Trejo, R. M., and Reister, L. (2009). "Investigation of the effect of process parameters on the formation and characteristics of recast layer in wire-EDM of Inconel 718." *Mater. Sci. Eng. A*, 513-514(C), 208–215.

Ojha, K., Garg, R. K., and Singh, K. K. (2010). "MRR Improvement in Sinking Electrical Discharge Machining: A Review." *J. Miner. Mater. Charact. Eng.*, 09(08), 709–739.

Pant, P., Pandey, N., Rajesha, S., and Jain, G. (2014). "Prediction of Surface Roughness in WEDM Process Using Feed Forward Back Propagation Neural Network." 4(6), 667–674.

Petrini, L., and Migliavacca, F. (2011). "Biomedical Applications of Shape Memory Alloys." *J. Metall.*, 2011(Figure 1), 1–15.

Portillo Perez, E., Marcos, M., Cabanes, I., Zubizarreta, A., and Sánchez, J. A. (2008).

"ANN for interpolating instability trends in WEDM." *IFAC Proc. Vol.*, 17(1 PART 1), 2230–2235.

Pradhan, M. K. (2013). "Optimization of MRR, TWR and surface roughness of EDMed D2 Steel using an integrated approach of RSM, GRA and Entropy measutement method." *2013 Int. Conf. Energy Effic. Technol. Sustain. ICEETS 2013*, 865–869.

Prakash, C., Kansal, H. K., Pabla, B. S., and Puri, S. (2017). "Experimental investigations in powder mixed electric discharge machining of Ti–35Nb–7Ta–5Zrβ-titanium alloy." *Mater. Manuf. Process.*, 32(3), 274–285.

Pramanik, A. (2016). "Electrical Discharge Machining of MMCs Reinforced with Very Small Particles." *Mater. Manuf. Process.*, 31(4), 397–404.

Pramanik, A., and Basak, A. K. (2016). "Degradation of wire electrode during electrical discharge machining of metal matrix composites." *Wear*, 346-347, 124–131.

PRAMANIK, A., BASAK, A. K., ISLAM, M. N., and LITTLEFAIR, G. (2015). "Electrical discharge machining of 6061 aluminium alloy." *Trans. Nonferrous Met. Soc. China*, 25(9), 2866–2874.

Price, A. D., Jnifene, A., and Naguib, H. E. (2007). "Design and control of a shape memory alloy based dexterous robot hand." *Smart Mater. Struct.*, 16(4), 1401–1414.

Ramakrishnan, R., and Karunamoorthy, L. (2006). "Multi response optimization of wire EDM operations using robust design of experiments." *Int. J. Adv. Manuf. Technol.*, 29(1-2), 105–112.

Ramakrishnan, R., and Karunamoorthy, L. (2008). "Modeling and multi-response optimization of Inconel 718 on machining of CNC WEDM process." *J. Mater. Process. Technol.*, 207(1-3), 343–349.

Rao, P. S., Ramji, K., and Satyanarayana, B. (2010). "Prediction of Material removal rate for Aluminum BIS-24345 Alloy in wire-cut EDM." *Int. Eng. Sci. Technol.*, 2(12), 7729–7739.

Rao, R., and Ã, V. Y. (2009). "Optics & Laser Technology Multi-objective optimization of Nd : YAG laser cutting of thin superalloy sheet using grey relational analysis with entropy measurement." 41, 922–930.

Rao, R., and Yadava, V. (2009). "Multi-objective optimization of Nd:YAG laser cutting of thin superalloy sheet using grey relational analysis with entropy measurement." *Opt. Laser Technol.*, 41(8), 922–930.

Rao, S. S. M., Rao, K. V., Reddy, K. H., Ch, V., and Rao, S. P. (2017). "Prediction and optimization of process parameters in wire cut electric discharge machining for High- speed steel (HSS)." *Int. J. Comput. Appl.*, 7074(October), 1–8.

Roy, A., Narendra Nath, S., and Nedelcu, D. (2017). "Experimental investigation on variation of output responses of as cast TiNiCu shape memory alloys using wire EDM." *Int. J. Mod. Manuf. Technol.*, 9(1).

Saedon, J. B., Jaafar, N., and Azman, M. (2014). "Multi-objective optimization of titanium alloy through orthogonal array and grey relational analysis in WEDM." *Procedia Technol.*, 15, 832–840.

Saha, A., and Mondal, S. C. (2017). "Experimental investigation and modelling of WEDM process for machining nano-structured hardfacing material." *J. Brazilian Soc. Mech. Sci. Eng.*, 39(9), 3439–3455.

Saha, P., Tarafdar, D., Pal, S. K., Saha, P., Srivastava, A. K., and Das, K. (2013). "Multi-objective optimization in wire-electro-discharge machining of TiC reinforced composite through Neuro-Genetic technique." *Appl. Soft Comput. J.*, 13(4), 2065–2074.

Sarkheyli, A., Zain, A. M., and Sharif, S. (2015). "A multi-performance prediction model based on ANFIS and new modified-GA for machining processes." *J. Intell. Manuf.*, 26(4), 703–716.

Shandilya, P., Jain, P. K., and Jain, N. K. (2013). "RSM and ANN modeling approaches for predicting average cutting speed during WEDM of SiCp/6061 Al MMC." *Procedia Eng.*, 64, 767–774.

Sharma, A., Garg, M. P., and Goyal, K. K. (2014). "Prediction of Optimal Conditions for WEDM of Al 6063/ ZrSiO4(p) MMC." *Procedia Mater. Sci.*, 6(Icmpc), 1024–1033.

Sharma, N., Khanna, R., Gupta, R. D., and Sharma, R. (2013). "Modeling and multiresponse optimization on WEDM for HSLA by RSM." *Int. J. Adv. Manuf. Technol.*, 67(9-12), 2269–2281.

Sharma, P., Chakradhar, D., and Narendranath, S. (2015). "Evaluation of WEDM performance characteristics of Inconel 706 for turbine disk application." *Mater. Des.*, 88, 558–566.

Sharma, P., Chakradhar, D., and Narendranath, S. (2016). "Effect of Wire Material on Productivity and Surface Integrity of WEDM-Processed Inconel 706 for Aircraft Application." *J. Mater. Eng. Perform.*, 25(9), 3672–3681.

Shi, H., Delville, R., Srivastava, V., James, R. D., and Schryvers, D. (2014). "Microstructural dependence on middle eigenvalue in Ti–Ni–Au." *J. Alloys Compd.*, 582, 703–707.

Shivade, A. S., and Shinde, V. D. (2014). "Multi-objective optimization in WEDM of D3 tool steel using integrated approach of Taguchi method & Grey relational analysis." *J Ind Eng Int*, 10, 149–162.

Singh Nain, S., Garg, D., and Kumar, S. (2017). "Prediction of the Performance Characteristics of WEDM on Udimet-L605 Using Different Modelling Techniques." *Mater. Today Proc.*, 4(2), 546–556.

Singh, H., and Garg, R. (2009). "Effects of process parameters on material removal rate in WEDM." 32(1), 70–74.

Sivaprakasam, P., Hariharan, P., and Gowri, S. (2013). "Optimization of Micro-WEDM Process of Aluminum Matrix Composite (A413-B $_4$ C): A Response Surface Approach." *Mater. Manuf. Process.*, 28(12), 1340–1347.

Sivaprakasam, P., Hariharan, P., and Gowri, S. (2014). "Engineering Science and

Technology , an International Journal Modeling and analysis of micro-WEDM process of titanium alloy (Ti e 6Al e 4V) using response surface approach." *Eng. Sci. Technol. an Int. J.*, 17(4), 227–235.

Soni, H., Sannayellappa, N., and Motagondanahalli Rangarasaiah, R. (2017). "An experimental study of influence of wire electro discharge machining parameters on surface integrity of TiNiCo shape memory alloy." *J. Mater. Res.*, 1–9.

Soundararajan, R., Ramesh, A., Mohanraj, N., and Parthasarathi, N. (2016). "An investigation of material removal rate and surface roughness of squeeze casted A413 alloy on WEDM by multi response optimization using RSM." *J. Alloys Compd.*, 685, 533–545.

Srinivasa Rao, P., Ramji, K., and Satyanarayana, B. (2016). "Effect of wire EDM conditions on generation of residual stresses in machining of aluminum 2014 T6 alloy." *Alexandria Eng. J.*, 55(2), 1077–1084.

Sun, Y., Gong, Y., Liu, Y., Li, Q., and Zhou, Y. (2017). "Experimental study on surface characteristics and improvement of microelectrode machined by low speed wire electrical discharge turning." *Arch. Civ. Mech. Eng.*, 17(4), 964–977.

Surya, V. R., Kumar, K. M. V., Keshavamurthy, R., Ugrasen, G., and Ravindra, H. V. (2017). "Prediction of Machining Characteristics using Artificial Neural Network in Wire EDM of Al7075 based In-situ Composite." *Mater. Today Proc.*, 4(2), 203–212.

Tian, Y., Liu, X., and Qi, H. (2015). "Generation of stainless steel superhydrophobic surfaces using WEDM technique." *Proc. SPIE - Int. Soc. Opt. Eng.*, 9446, 94464G.

Tong, Y., Liu, J., Chen, F., Liang, C., Tian, B., Li, L., and Zheng, Y. (2014). "Effect of aging on martensitic transformation and superelasticity of TiNiCr shape memory alloy." *Trans. Nonferrous Met. Soc. China*, 24(8), 2598–2605.

Ugrasen, G., Ravindra, H. V., Prakash, G. V. N., and Keshavamurthy, R. (2014). "Estimation of Machining Performances Using MRA, GMDH and Artificial Neural Network in Wire EDM of EN-31." *Procedia Mater. Sci.*, 6(Icmpc), 1788–1797.

Wang, J. J., Omori, T., Sutou, Y., Kainuma, R., and Ishida, K. (2005). "Two-way shape memory effect induced by cold-rolling in Ti–Ni and Ti–Ni–Fe alloys." *Scr. Mater.*, 52(4), 311–316.

Wei, Z. G., Sandstrom, R., and Miyazaki, S. (1998). "Shape-memory materials and hybrid composites for smart systems - Part I Shape-memory materials." *J. Mater. Sci.*, 33(15), 3743–3762.

Zheng, Y. F., Zhang, B. B., Wang, B. L., Wang, Y. B., Li, L., Yang, Q. B., and Cui, L. S. (2011). "Introduction of antibacterial function into biomedical TiNi shape memory alloy by the addition of element Ag." *Acta Biomater.*, 7(6), 2758–67.

LIST OF PUBLICATIONS

Sl. No.	Title of the paper	Authors	Name of the Journal/ Conference	Month, Year of Publication	Category *
1	An experimental study of influence of wire electro discharge machining parameters on surface integrity of TiNiCo shape memory alloy	**Hargovind Soni,** Narendranath S., Ramesh M. R.	Journal of Material Research	2017 Vol.32 Issue 16 p-3100-3108	1
2	Effects of WEDM performances on microstructure, surface topography, microhardness, XRD and residual stresses on the machined surface of $Ti_{50}Ni_{45}Co_5$ shape memory alloys.	**Hargovind Soni,** Narendranath S., Ramesh M. R.	Silicon Journal	2018	1
3	Effects of Wire electro discharge machining process parameters on machined surface of $Ti_{50}Ni_{49}Co_1$ shape memory alloy.	**Hargovind Soni,** Narendranath S., Ramesh M. R.	Silicon journal Springer	2017	1
4	ANN and RSM modeling methods for predicting material removal rate and surface roughness during WEDM of $Ti_{50}Ni_{40}Co_{10}$ shape memory alloy	**Hargovind Soni,** Narendranath S., Ramesh M. R.	Advances in Modelling and Analysis A	2018	1

Sl. No.	Title of the paper	Authors	Name of the Journal/ Conference	Month, Year of Publication	Category *
5	Effect of machining process parameters on productivity rate and surface roughness of machined TiNiCo alloy	**Hargovind Soni,** Narendranath S., Ramesh M. R	Accepted in Material Today Journal Elsevier)	2018	1
6	Effect of Machining Parameters on Wire Electro Discharge Machining of Shape Memory Alloys Analyzed using Grey Entropy Method	**Hargovind Soni,** Narendranath S., Ramesh M. R.	Journal of Material Science and Mechanical Engineering	Volume 2, Issue13; Oct.-Dec., 2015 pp. 50-54.	1
7	Advanced machining of TiNiCo shape memory alloy for biomedical application.	**Hargovind Soni,** Narendranath S., Ramesh M. R.	Emerging Material Research	2017	Answer to the reviewer comments submitted awaiting for decision
8	Investigation of input process parameters of wire electro discharge machining of $Ti_{50}Ni_{50-x}Co_x$, (x=1 and 5) alloys using	**Hargovind Soni**, Narendranath S.,	Measurement Journal Elsevier	2017	Answer to the

Sl. No.	Title of the paper	Authors	Name of the Journal/ Conference	Month, Year of Publication	Category *
	hybrid combinations of multi objective optimization techniques.	Ramesh M. R., Dumitru Nedelcu.			reviewer comments submitted awaiting for decision
9	Machining of $Ti_{50}Ni_{49}Co_1$, $Ti_{50}Ni_{45}Co_5$ and $Ti_{50}Ni_{40}Co_{10}$ shape memory alloys for Bone staple application.	**Hargovind Soni,** Narendranath S., Ramesh M. R	Advances in Manufacturing	2018	Communicated
10	Investigations on Surface Characteristics of Developed TiNiCo Ternary Shape memory alloy after Wire Electro-Discharge Machining	**Hargovind Soni,** Narendranath S., Ramesh M. R.	Applied Surface Science	2018	Communicated
11	Evaluation Of Wedm Performance Characteristics Of $Ti_{50}Ni_{45}Co_5$ Shape Memory Alloys" has been	**Hargovind Soni,** Narendranath S., Ramesh M. R.	10th International Conference on Precision, Meso, Micro and Nano Engineering at IIT Madras, Chennai.	2017	3

Sl. No.	Title of the paper	Authors	Name of the Journal/ Conference	Month, Year of Publication	Category *
12	Effect of Machining Parameters on Wire Electro Discharge Machining of Shape Memory Alloys Analyzed using Grey Entropy Method	**Hargovind Soni,** Narendranath S., Ramesh M. R.	"Advances in Mechanical, Material Science, Manufacturing, Automobile, Aerospace Engineering and Applied Physics"	2015	3

*Category: 1: Journal paper, full paper reviewed   2: Journal paper, Abstract reviews   3: Conference/Symposium paper, full paper reviewed
4: Conference/Symposium paper, abstract reviewed   5: Others (including papers in Workshops, NITK Research Bulletins, Short notes etc.)

Hargovind Soni
Research Scholar
Name & Signature, with Date

Prof. Narendranath S.
Research Guide
Name & Signature, with Date

Dr. Ramesh M R
Research Guide
Name & Signature, with Date

BIO-DATA

Hargovind Soni
PhD research scholar
Department of mechanical Engineering
National Institute of Technology Karnataka India- 575025

Present Address	Department of Mechanical Engineering NITK, Surathkal-575025, Mangalore Karnataka India.
Permanent address	Jeron Road Bus stand Prithvipur – 472338, Dist. Tikamgarh M.P. India.
Phone No.	+91-9993706033, +91-9449556033
Email Id:	hargovindsoni2002@gmail.com
Date of Birth	**20-02-1988**

<div align="center">

Academic details

</div>

Degree	Subject/ specialization	% / CGPA	Division	Passing Year	Board / university
PhD	Advanced machining of smart materials	Pursuing			National Institute of Technology Karnataka
M. Tech	Advanced production system	7.29 CGPA	First	2014	RGPV Bhopal & NIT Bhopal (research work)
B.E./B. Tech	Industrial and production	67.12 %	First	2010	RGPV Bhopal
Intermediate	PCM	60 %	First	2005	M. P. Board
High School	ALL	72.6 %	First	2003	M. P. Board

<div align="center">

Experience

JRF – 01-08-2014 to 06-01-2015 at Department of Mechanical Engineering NITK Karnataka India

</div>

I declare that above information is true and correct to best of my knowledge.

(Hargovind Soni)